A Theoretical Perspective on Streaming Noisy Data with Distribution Shift

Wenshui Luo, Shuo Chen, Tao Zhou, *Member, IEEE,* Chen Gong, *Senior Member, IEEE*

Abstract—Intelligent systems typically need to continually learn from streaming data subject to distribution shift, where a key requirement is that they cannot catastrophically forget the historical knowledge learned from previous data. More seriously, streaming data often contain substantial label noise, which can exacerbate catastrophic forgetting and lead to performance degradation on forthcoming data. To address these problems, Continual Noisy Label Learning (CNLL) has been proposed. However, existing CNLL methods still fall short of the ability in addressing catastrophic forgetting because they adopted heuristic strategies in handling label noise and did not explicitly characterize the distributional shift across time, which hinders effective knowledge transfer from historical data to new data. To tackle these challenges, we theoretically analyze the problem of learning from streaming noisy data with distribution shift and propose a unified framework called **C**ontinual **N**oisy **L**abel Learning on **D**rifting **D**ata Streams (CNLDD). Specifically, we theoretically explore, for the first time, the upper bound of cumulative generalization error for CNLL problem, which reveals three factors leading to forgetting, namely selection bias of buffered data, distribution shift, and label noise. To alleviate the selection bias of buffered data, we design a two-step buffer update strategy to narrow the distribution gap between the original historical data and the selected representative data in buffer. To address distribution shift, our CNLDD explicitly characterizes the distribution discrepancies between buffered data and incoming data, prioritizing historical data with minimal discrepancies to enhance knowledge transfer. To tackle noisy labels, CNLDD estimates the importance weight of each example with the instance-dependent noise transition matrix, thereby avoiding the data bias and knowledge forgetting arising from noisy labels. Empirically, due to the unified modeling of the aforementioned issues, our CNLDD achieves superior classification performance when compared with state-of-the-art CNLL methods on both synthetic and real-world datasets.

Index Terms—Continual learning, Streaming data, Distribution shift, Label noise, Generalization error.

1 Introduction

Learning is foundational for intelligent systems to accommodate dynamic environments. To handle external changes, continual learners should have strong adaptability to continually acquire, update, accumulate, and utilize knowledge from streaming data with distribution shift [40], [41]. In this scenario, catastrophic forgetting of prior knowledge contained in historical data is a significant challenge [43]. More seriously, in many practical situations, the accurate labels of streaming data may be difficult to obtain due to various subjective or objective factors such as unavoidable human fatigue, limitation of human knowledge, unreliable automatic labeling process, *etc* [13]. The existence of noisy labels may exacerbate knowledge forgetting and degrade model performance on upcoming data [1], [20]. Therefore, **C**ontinual **N**oisy **L**abel **L**earning (CNLL) [3], [20], [21] has been proposed to address noisy labels in continual learning scenarios.

To the best of our knowledge, there are only a handful of existing works focusing on the CNLL problem, and they usually combine **C**ontinual **L**earning (CL) techniques with **L**abel **N**oise **L**earning (LNL) approaches [3], [20], [21] in a direct way, where clean sample selection is commonly employed to establish a memory buffer to store useful historical patterns, so that catastrophic forgetting can be avoided. For example, Self-Purified Replay (SPR) [21] demonstrates that noisy labels can accelerate forgetting and severely degrade performance on learned tasks. Therefore, to effectively maintain the purity of memory buffer, SPR introduces a self-supervised replay technique combined with a self-centered filter. In addition to prioritizing the purity of buffered data, Purity and Diversity aware Episode Replay (PuriDivER) [3] emphasizes the significance of data diversity. To this end, PuriDivER defines a scoring function to promote diversity by aligning the distribution of buffered data with that of the original noisy data. Moreover, inspired by DivideMix [27], Karim et al. [20] additionally adopt a noisy memory buffer and employ semi-supervised learning techniques to enhance the training of robust classifiers. In a word, existing CNLL methods usually focus on selecting clean representative data to reduce forgetting.

However, these CNLL methods often adopt heuristic data selection strategies to mitigate catastrophic forgetting, and they also did not consider the CNLL problem in a holistic view. In this paper, we theoretically identify that

- *This research is supported by National Natural Science Fund of China (Nos: 62336003, 12371510, 62576153, 62506155), Shanghai Municipal Science and Technology Major Project (No: 2025SHZDZX025G12), Provincial Natural Science Fund of Jiangsu (No: BK20251985), and Suzhou Municipal Leading Talents Fund (2025).*
- *W. Luo and C. Gong are with the School of Automation and Intelligent Sensing, Shanghai Jiao Tong University, Shanghai, P. R. China.*
E-mail: randylo@sjtu.edu.cn; chen.gong@sjtu.edu.cn
- *S. Chen is with the School of Intelligence Science and Technology, Nanjing University, P. R. China, and is also with Center for Advanced Intelligence Project, RIKEN, Japan.*
E-mail: shuo.chen@nju.edu.cn
- *T. Zhou is with the School of Computer Science and Engineering, Nanjing University of Science and Technology, P. R. China.*
E-mail: taozhou.ai@gmail.com
- *Corresponding author: C. Gong.*

forgetting can be attributed to three critical factors, namely selection bias of buffered data, distribution shift, and label noise. Among them, the distribution shift over time has also not been explicitly modeled by existing CNLL methods. Therefore, we simultaneously consider the three factors in a single framework, and formally refer to the problem studied in this paper as "learning from streaming noisy data with distribution shift".

Actually, distribution shift is ubiquitous in various applications of CNLL. For example, in the task of financial fraud detection [15], the distribution of transaction data may change over time due to the factors such as evolving fraud patterns, shifts in user behavior, different economic conditions, *etc*. Given the need for quick detection responses, the labels of most incoming transaction data are typically generated by historical models, inevitably introducing noisy labels. Therefore, the continual detector should adapt to the dynamic changes, retain previous knowledge on fraud, and also maintain robustness against noisy labels. Moreover, CNLL is also crucial in machine-aided medical diagnosis. A typical application is the tumor detection task [24], where tumor images may exhibit distribution shift due to the variations in imaging techniques, patient demographics, *etc*. Additionally, there is a continuous need for incremental learning as new tumor types, imaging techniques, or clinical knowledge emerge over time. Meanwhile, inexperienced experts may annotate noisy labels for medical images due to a lack of sufficient expertise. This highlights the importance of developing robust and adaptive tumor detectors capable of handling catastrophic forgetting caused by distribution shift and label noise.

To address the problem of learning from streaming noisy data with distribution shift, we theoretically explore, for the first time, the upper bound of the cumulative generalization error, which can be regarded as a sum of learning plasticity and memory stability [43]. Here, learning plasticity refers to the model ability to learn from new data, while memory stability pertains to its capacity to retain previously acquired knowledge. To achieve an optimal balance between plasticity and stability, we focus on exploring a minimizable upper bound for the cumulative generalization error and propose a new method termed "**C**ontinual **N**oisy **L**abel learning on **D**rifting **D**ata streams (CNLDD)".

Guided by the upper bound, we propose a new update strategy for the memory buffer aimed at minimizing the distribution gap between buffered data in memory and the data seen so far. To update the memory buffer, we select representative examples in a two-step manner, where at each step CNLDD selects a subset with a minimum covering radius, allowing a minimum selection bias of the buffered data. Additionally, we explicitly characterize the distribution discrepancy between buffered data and new incoming data, and prioritize historical data with small discrepancy to ensure effective knowledge transfer, which alleviates catastrophic forgetting arising from distribution shift. Finally, to address label noise, we employ the instance-dependent noise transition matrix to determine the importance weight of each example, thereby mitigating the negative impact of directly replaying noisy examples.

The main contributions of our paper can be highlighted in three folds:

- Theoretically, we are the first to study the upper bound of the cumulative generalization error for the problem of learning from streaming noisy data with distribution shift.
- Algorithmically, we propose CNLDD, a unified framework that simultaneously addresses the three critical factors leading to catastrophic forgetting, namely selection bias of buffered data, distribution shift, and label noise.
- Empirically, we conducted intensive experiments on synthetic and real-world datasets with distribution shift and label noise, which demonstrate the superiority of CNLDD over existing continual noisy label learning methods.

The rest of this paper is organized as follows. In Section 2, we review related works on continual learning and label noise learning. In Section 3, we introduce useful preliminary knowledge, which is followed by Section 4 that presents a theoretical study on the generalization error. Subsequently, the CNLDD method is introduced thoroughly in Section 5. After that, theoretical justifications of CNLDD are detailed in Section 6. Experimental results are provided in Section 7. Finally, we conclude our paper in Section 8.

2 Related Work

Since the main focus of this paper is continual learning on streaming noisy data with distribution shift, here we briefly review some related works on continual learning and label noise learning.

2.1 Continual Learning

Existing continual learning methods can be roughly classified into three categories, namely regularization-based methods, optimization-based methods, and replay-based methods [12], [43].

Regularization-based methods are characterized by the addition of explicit regularization terms to balance old and new data, with weight regularization and function regularization as the two main branches. Here, weight regularization methods usually add a quadratic term to the loss function, penalizing the variation of each parameter based on its contribution or "importance" to the old task. Representative approaches include Elastic Weights Consolidation (EWC) [23], which leverages the Fisher Information Matrix (FIM) to characterize parametric importance, and Synaptic Intelligence (SI) [49], which approximates the parameter importance by its contribution to the loss variation over the entire training trajectory. In contrast, function regularization methods often treat the previously learned model as a teacher and the currently trained model as a student. These methods then use knowledge distillation [39] to maintain historical knowledge. For example, Learning without Forgetting (LwF) [43] encourages output consistency on new data between the fine-tuned model and the old model. Furthermore, to directly distill from historical data, Functional-Regularization of Memorable Past (FROMP) [34] employs buffered data to regularize the functional behavior of the model within a Bayesian framework.

Since the estimation of the importance matrix in regularization-based methods often incurs additional computational overhead, and they may face challenges in modeling parametric importance for complex network architectures, their generalizability to complicated scenarios becomes limited. Consequently, the second line of research, namely optimization-based method, aims to address the forgetting problem via optimization techniques such as gradient projection and meta-learning [41]. Representative methods include Adam-NSCL [44], which projects gradients onto the null space of the feature covariance, and Layerwise Proximal Replay (LPR) [48], which constraints the gradient variation of hidden layers to ensure that the direction of the gradient update lies in the orthogonal complement of the subspace spanned by the gradients of historical data [11].

Due to the lack of access to historical data, the above two types of methods may struggle to effectively alleviate catastrophic forgetting, which frequently results in suboptimal performance. Therefore, the third line of research focuses on the explicit storage and replay of historical examples by using a small memory buffer. Typical types of replayed data in this direction include historical examples [5], [40], generated examples [37], and transformed examples [29]. Moreover, to further account for noisy labels, many methods intend to replay potentially clean examples. For example, Self-Purified Replay (SPR) [21] identifies that noisy labels can exacerbate catastrophic forgetting and significantly degrade performance on previously learned tasks. To ensure the purity of memory buffer, SPR combines a self-supervised replay mechanism with a self-centered filter, and selects clean examples via Beta Mixture Models [19]. Beyond emphasizing the purity of buffered data, Purity and Diversity aware Episode Replay (PuriDivER) [3] highlights the critical role of diversity. That is to say, PuriDivER proposes a scoring function to enhance the diversity of data in buffer by aligning the distribution of buffered data with the overall distribution of the original noisy data. Furthermore, inspired by DivideMix [27], Karim et al. [20] proposed Continual Noisy Label Learning (CNLL), which introduces a separate noisy memory buffer and leverages semi-supervised learning techniques to facilitate the training of robust classifiers.

However, these replay-based methods often rely on heuristic strategies to identify potential clean examples, which may result in a biased memory buffer and significantly mislead the continual learner. Furthermore, they are unable to explicitly characterize the distribution discrepancy between buffered data and new data, making it more challenging to transfer knowledge from historical data to new data. In light of these issues, we propose a unified framework that simultaneously addresses the critical factors contributing to forgetting, *i.e.*, selection bias of buffered data, distribution shift, and label noise.

2.2 Label Noise Learning

Existing methods for handling label noise can be classified into three categories, namely sample selection-based methods, robust loss function design-based methods, and statistic estimation-based methods.

TABLE 1
Summary of main mathematical notations.

Notation	Interpretation
$(X_t, Y_t),\ (X_t, \widetilde{Y}_t)$	A pair of input random variables and the observed contaminated counterpart at the t-th timestep. Here $X_t \in \mathcal{X} \subseteq \mathbb{R}^d$ represents the feature and $Y_t \in \mathcal{Y} = \{0,1\}^C$ represents the one-hot label, where d is the dimension of the feature space and C denotes the number of classes.
$\mathbb{D}_t,\ \widetilde{\mathbb{D}}_t$	The joint probability distribution of X_t and Y_t, and its noisy counterpart, respectively. Their density functions are $P_t(X_t, Y_t)$ and $\widetilde{P}_t(X_t, \widetilde{Y}_t)$, respectively.
$\mathcal{S}_t = \{(\mathbf{x}_i, \mathbf{y}_i)\}_{i=1}^{n_t}$	The unobservable clean sample of $\mathbb{D}_t$ with n_t data points.
$\widetilde{\mathcal{S}}_t = \{(\mathbf{x}_i, \widetilde{\mathbf{y}}_i)\}_{i=1}^{n_t}$	The observed noisy sample of $\widetilde{\mathbb{D}}_t$ with n_t possibly mislabeled training data.
$[\![C]\!]$	The shorthand for the set $\{1, 2, \cdots, C\}$.
$\widetilde{\mathcal{M}}_{1:t}$	The memory buffer up to the t-th timestep.
$\beta_{\mathbb{P}}(\cdot, \cdot)$	The density ratio function with respect to the distribution $\mathbb{P}$, defined as $\beta_{\mathbb{P}}(\mathbf{x}, \widetilde{\mathbf{y}}) := {}^{P(\mathbf{x},\widetilde{\mathbf{y}})}/_{\widetilde{P}(\mathbf{x},\widetilde{\mathbf{y}})} = {}^{P(\widetilde{\mathbf{y}} \mid \mathbf{x})}/_{\widetilde{P}(\widetilde{\mathbf{y}} \mid \mathbf{x})}$.
$\overline{L},\ \overline{\beta}$	The upper bounds of the loss function and the density ratio function, respectively.
$\lambda^P,\ \lambda^\ell$	The Lipschitz constants of $P_t(Y_t \mid X_t)$ and the loss function $\ell(f_{\boldsymbol{\theta}}(\cdot), \cdot)$, respectively.
$\Vert\mathbf{x}\Vert_p$	The ℓ_p-norm of a given vector $\mathbf{x}$, with $p \in \{1, 2, \infty\}$.
$\Vert\mathbf{A}\Vert_p,\ \Vert\mathbf{A}\Vert_{\mathrm{F}}$	The matrix norms induced by the corresponding vector norms $\Vert \cdot \Vert_p$, and by the Frobenius norm.

Sample selection-based methods focus on identifying clean examples or removing noisy examples from the original training dataset. Leveraging the memorization effect [1] of deep neural networks, these methods typically consider the examples with small loss values as clean ones during training. Representative methods in this category include Co-teaching [16] and CoDis [45]. However, a major limitation of most sample selection-based methods is their inability to theoretically guarantee the correctness of the labels for the selected examples, which undermines their stability and effectiveness in practical applications. As an alternative, a second strand of research emphasizes the development of robust loss functions to address noisy labels. Representative approaches include ϵ-Softmax [42] and Regularly Truncated M-Estimators (RTME) [46]. Nevertheless, the above two types of methods do not explicitly characterize the generation process of the label noise, so they inevitably become weak in some complicated noisy scenarios [8].

The third strand of research is to estimate some critical statistics of clean or noisy data. These methods can be further categorized based on the estimated statistics, such as the label noise transition matrix [28], the dataset centroid [13], and the mean/covariance of data [30]. However, the aforementioned label noise learning methods cannot be directly applied to tackle noisy labels in continual learning scenarios, as they often assume a fixed data distribution, which makes them less effective in scenarios with shifting distribution. Moreover, the absence of mechanisms to retain and integrate previously learned knowledge poses additional challenges for continual learning.

3 Preliminaries

In this section, we present the detailed definition and the related mathematical notations for our setting, *i.e.*, learning from streaming noisy data with distribution shift. Additionally, we provide a brief introduction to the noise transition matrix estimation utilized by our CNLDD method.

3.1 Problem Definition

We first introduce some mathematical notations which will be used in this paper. Specifically, the superscript "$\sim$" indicates that the variable is calculated based on noisy observations, and the variable with a superscript "$\wedge$" is the corresponding empirical estimation. Note that a statistic value accompanied by the term "clean" means that this statistic is calculated by using underlying clean labels, whereas a statistic accompanied by the term "noisy" implies that it is calculated by using observed noisy labels. We use the notation $[\![K]\!]$ to represent the set $\{1, 2, \cdots, K\}$ for any $K \in \mathbb{Z}$. Besides, the one-hot vector with a value of 1 in its j-th element is denoted by $\mathbf{e}_j$. The mathematical expectation is denoted by $\mathbb{E}[\cdot]$. Moreover, we use $\mathbf{A} = (A_{ij})_{1\le i\le m}^{1\le j\le n} \in \mathbb{R}^{m\times n}$ to denote an $m \times n$ matrix $\mathbf{A}$ of which the (i, j)-th element is A_{ij}. We also use "$\bigotimes$" to represent the Cartesian product of distributions. For clarity, the main mathematical notations that will be later used for algorithm description are listed in Tab. 1.

We now formally define the setting considered in this paper. Specifically, we focus on a C-way classification task on streaming noisy data with time-varying distribution shift. Let $X_t \in \mathcal{X} \subseteq \mathbb{R}^d$ and $Y_t \in \mathcal{Y} = \{\mathbf{e}_1, \mathbf{e}_2, \cdots, \mathbf{e}_C\}$ denote the random variables of the feature and label at the t-th timestep, respectively. The joint probability distribution for (X_t, Y_t) and its noisy counterpart are denoted by $\mathbb{D}_t$ and $\widetilde{\mathbb{D}}_t$, respectively, with the corresponding density functions being $P_t(X_t, Y_t)$ and $\widetilde{P}_t(X_t, \widetilde{Y}_t)$. In the following, we use $\mathbb{D}_{1:t}$ to denote the cumulative distribution up to timestep t, and any quantity with a subscript $1 : t$ indicates a cumulative quantity. At timestep t, the clean sample set $\mathcal{S}_t = \{(\mathbf{x}_i, \mathbf{y}_i)\}_{i=1}^{n_t}$ contains n_t independent and identically distributed (i.i.d.) examples from $\mathbb{D}_t$. However, due to the existence of noisy labels, we are only accessible to a sample $\widetilde{\mathcal{S}}_t = \{(\mathbf{x}_i, \widetilde{\mathbf{y}}_i)\}_{i=1}^{n_t}$ from a noisy distribution $\widetilde{\mathbb{D}}_t$. In line with existing CNLL methods [3], [20], [21], we also assume the existence of a small memory buffer to store historical data. At timestep t, the updated memory buffer with capacity M is denoted by $\widetilde{\mathcal{M}}_{1:t}$, while $\mathcal{M}_{1:t}$ represents the buffer with all labels replaced by the corresponding clean ones.

In this paper, we consider the instance-dependent label noise [6], which closely aligns with the real-world label noise. In this setting, the observed noisy label for each $\mathbf{x} \in \mathcal{X}$ depends not only on its underlying clean label, but also on the feature itself. To be more specific, for any $\mathbf{x} \in \mathcal{X}$, the transition probability of class i to class j is given by $P(\widetilde{Y} = \mathbf{e}_j | Y = \mathbf{e}_i, X = \mathbf{x}) = T_{ij}(\mathbf{x}), \forall i, j \in [\![C]\!]$, where $\mathbf{T}(\mathbf{x}) := (T_{ij}(\mathbf{x}))_{1\le i,j\le C} \in \mathbb{R}^{C\times C}$ is the noise transition matrix for $\mathbf{x}$, and C is the number of classes.

3.2 Estimation of Noise Transition Matrix for Instance-Dependent Label Noise

In this section, we briefly introduce the High-Order Consensuses (HOC) [52] algorithm, which can be adopted to estimate the instance-dependent transition matrix $\mathbf{T}(\mathbf{x})$ for any example $\mathbf{x}$ in the training set.

The key observation of HOC is that noisy data can still induce good representations, even though label noise makes the model generalize poorly [26]. Based on this, HOC assumes the "2-NN label clusterability", *i.e.*, for any example $\mathbf{x}$ in a dataset $\mathcal{D}$, its two nearest neighbors belong to the same class as $\mathbf{x}$. Under this condition, the joint probability distributions of noisy labels for one, two, and three adjacent examples can be modeled accordingly. The transition matrix and class prior can then be jointly estimated by using up to the third-order consensus of the label distribution. In the following, we first present the estimation procedure for class-dependent label noise, which means that the generation of label noise is independent to feature $\mathbf{x}$, so $\mathbf{T}(\mathbf{x})$ degenerates to a fixed matrix $\mathbf{T}$ for any input $\mathbf{x}$. Subsequently, we introduce the extension to the instance-dependent case with noise transition matrix strictly being $\mathbf{T}(\mathbf{x})$.

For the class-dependent case, let X and Y denote the random variables representing the feature and the label, respectively. We define the class prior distribution as $\mathbf{p} := [P(Y = \mathbf{e}_1), P(Y = \mathbf{e}_2), \cdots, P(Y = \mathbf{e}_C)]^\top$. To facilitate the derivation of three orders of consensus, we define the transition matrices with column permutation as:

$$\mathbf{T}_r := \mathbf{T}\mathbf{S}_r, \quad \forall\, r \in [\![C]\!], \tag{1}$$

where $\mathbf{S}_r := [\mathbf{e}_{r+1}, \mathbf{e}_{r+2}, \cdots, \mathbf{e}_C, \mathbf{e}_1, \mathbf{e}_2, \cdots, \mathbf{e}_r]$ is a permutation matrix. Let $(i+r)_C := [(i+r-1) \bmod C]+1$, and the first-, second-, and third-order consensuses of noisy labels can then be denoted in vector forms, namely,

$$\begin{aligned}
&\mathbf{c}^{[1]} = [P(\widetilde{Y} = \mathbf{e}_i), i \in [\![C]\!]]^\top,\\
&\mathbf{c}^{[2]}_r = [P(\widetilde{Y} = \mathbf{e}_i, \widetilde{Y}_1 = \mathbf{e}_{(i+r)_C}), i \in [\![C]\!]]^\top,\\
&\mathbf{c}^{[3]}_{r,s} = [P(\widetilde{Y} = \mathbf{e}_i, \widetilde{Y}_1 = \mathbf{e}_{(i+r)_C}, \widetilde{Y}_2 = \mathbf{e}_{(i+s)_C}), i \in [\![C]\!]]^\top,
\end{aligned} \tag{2}$$

where $\widetilde{Y}_1$ and $\widetilde{Y}_2$ are the random variables corresponding to the noisy labels of the two nearest neighbors, respectively. To empirically estimate quantities in Eq. (2), a subset of the noisy dataset is sampled, and the corresponding estimated values are denoted by $\widehat{\mathbf{c}}^{[1]}$, $\widehat{\mathbf{c}}^{[2]}_r$, and $\widehat{\mathbf{c}}^{[3]}_{r,s}$, respectively.

Furthermore, the three orders of consensuses can also be formally defined as functions of $(\mathbf{T}, \mathbf{p})$, respectively, namely,

$$\begin{aligned}
&\mathbf{c}^{[1]}(\mathbf{T}, \mathbf{p}) := \mathbf{T}^\top \mathbf{p},\\
&\mathbf{c}^{[2]}_r(\mathbf{T}, \mathbf{p}) := (\mathbf{T} \circ \mathbf{T}_r)^\top \mathbf{p},\ \forall\, r \in [\![C]\!],\\
&\mathbf{c}^{[3]}_{r,s}(\mathbf{T}, \mathbf{p}) := (\mathbf{T} \circ \mathbf{T}_r \circ \mathbf{T}_s)^\top \mathbf{p},\ \forall\, r, s \in [\![C]\!],
\end{aligned} \tag{3}$$

where $\circ$ denotes the element-wise matrix product. For brevity, we compactly define $\mathbf{c}^{[2]}(\mathbf{T}, \mathbf{p}) := [\mathbf{c}^{[2]}_r(\mathbf{T}, \mathbf{p}), \forall\, r \in [\![C]\!]]$ and $\mathbf{c}^{[3]}(\mathbf{T}, \mathbf{p}) := [\mathbf{c}^{[3]}_{r,s}(\mathbf{T}, \mathbf{p}), \forall\, r, s \in [\![C]\!]]$. The estimated quantities $\widehat{\mathbf{c}}^{[2]}$ and $\widehat{\mathbf{c}}^{[3]}$ are defined analogously to $\mathbf{c}^{[2]}(\mathbf{T}, \mathbf{p})$ and $\mathbf{c}^{[3]}(\mathbf{T}, \mathbf{p})$. Based on these quantities, the noise transition matrix $\mathbf{T}$ and the class prior $\mathbf{p}$ in Eq. (3) can then be estimated by leveraging the consensus between the expected values $\mathbf{c}^{[z]}(\mathbf{T}, \mathbf{p})$ and their empirical counterparts $\widehat{\mathbf{c}}^{[z]}$ for all $z \in \{1, 2, 3\}$. More specifically, estimating $\mathbf{T} = (T_{ij})_{1\le i,j\le C}$ and $\mathbf{p} = (p_i)_{1\le i\le C}$ can be formulated as the following constrained optimization problem:

$$\begin{aligned}
\min_{\mathbf{T},\mathbf{p}} \sum_{z=1}^{3} &\left\| \widehat{\mathbf{c}}^{[z]} - \mathbf{c}^{[z]}(\mathbf{T}, \mathbf{p}) \right\|_2^2\\
\text{s.t.}\quad & p_i \ge 0,\ T_{ij} \ge 0,\ \forall\, i, j \in [\![C]\!]\\
& \sum_{i=1}^{C} p_i = 1,\ \sum_{j=1}^{C} T_{ij} = 1,\ \forall\, i \in [\![C]\!].
\end{aligned} \tag{4}$$

Building upon the estimation method for the class-dependent noise transition matrix $\mathbf{T}$ in Eq. (4), HOC extends this framework to address the instance-dependent case. To this end, HOC assumes that the entire dataset can be partitioned into U disjoint subsets, with each subset characterized by a shared noise transition matrix. Then, to estimate the shared matrix for a single subset, HOC algorithm developed for the class-dependent scenario is employed. Formally, let $q(\mathbf{x})$ denote the index of the subset to which feature $\mathbf{x}$ belongs, and the estimated transition matrices for the U subsets are $\{\widehat{\mathbf{T}}^u\}_{u=1}^U$. Based on these quantities, the transition matrix for $\mathbf{x}$ is expressed as $\mathbf{T}(\mathbf{x}) = \widehat{\mathbf{T}}^{q(\mathbf{x})}$.

4 Theoretical Study

In this section, we study the problem of learning from streaming noisy data with distribution shift from a theoretical perspective and present a comprehensive evaluation on the cumulative generalization error in our setting. Due to space limitations, all proofs of theorems are deferred to the supplementary materials.

4.1 A General Upper Bound for Cumulative Generalization Error

According to the aforementioned problem definition, a small memory buffer $\widetilde{\mathcal{M}}_{1:t}$ is accessible at timestep t. Representative CNLL methods often update this buffer with the consideration of purity [21] or diversity [3]. However, these heuristic strategies cannot be directly applied to balance memory stability and learning plasticity [43]. Moreover, the updated buffer may still be biased, primarily due to the inclusion of noisy labels, which can result in toxic replay [20]. In view of this, we directly study the cumulative generalization error defined on the data distributions seen so far, namely $\mathbb{E}_{\mathbb{D}_{1:t}}[\ell(f_{\boldsymbol{\theta}}(\mathbf{x}), \mathbf{y})]$, where $\ell(\cdot,\cdot)$ is a loss function, and $f_{\boldsymbol{\theta}} \in \mathcal{F}_\Theta$ represents a certain hypothesis in the hypothesis space $\mathcal{F}_\Theta = \{f_{\boldsymbol{\theta}} : \mathcal{X} \to \Delta^K, \boldsymbol{\theta} \in \Theta\}$. Here, Δ^C is a C-dimensional probability simplex, and Θ is the parameter space. Since the generalization error is difficult to estimate in a direct way with data in memory buffer, an optimizable upper bound for this error naturally serves as a practical alternative. As shown later, the cumulative generalization error can be expressed as a convex combination of two components, representing memory stability and learning plasticity, respectively. Therefore, minimizing the upper bound for this error is directly related to the performance of a continual learner.

Before formally deriving the upper bound of the cumulative generalization error, we first need to define two key concepts, namely distribution discrepancy (Definition 1) and density ratio (Definition 2):

Definition 1. *(**Distribution Discrepancy**) For a loss function $\ell(\cdot,\cdot)$ and two distributions $\mathbb{P}$ and $\mathbb{Q}$, the distribution discrepancy between $\mathbb{P}$ and $\mathbb{Q}$ is defined as: $disc_{\mathcal{F}_\Theta}(\mathbb{P}, \mathbb{Q}) := \sup_{f_{\boldsymbol{\theta}} \in \mathcal{F}_\Theta} \left|\mathbb{E}_{(\mathbf{x},\mathbf{y})\sim\mathbb{P}}[\ell(f_{\boldsymbol{\theta}}(\mathbf{x}), \mathbf{y})] - \mathbb{E}_{(\mathbf{x},\mathbf{y})\sim\mathbb{Q}}[\ell(f_{\boldsymbol{\theta}}(\mathbf{x}), \mathbf{y})]\right|$.*

Definition 2. *(**Density Ratio**) For a distribution $\mathbb{P}$ and its corresponding noisy distribution $\widetilde{\mathbb{P}}$, assuming their probability density functions are $P(\cdot,\cdot)$ and $\widetilde{P}(\cdot,\cdot)$, respectively, the density ratio between the posterior probability distributions $\mathbb{P}$ and $\widetilde{\mathbb{P}}$ is defined as: $\beta_{\mathbb{P}}(\mathbf{x}, \widetilde{\mathbf{y}}) := {P(\widetilde{\mathbf{y}}|\mathbf{x})}/{\widetilde{P}(\widetilde{\mathbf{y}}|\mathbf{x})}$, $\forall\, (\mathbf{x}, \widetilde{\mathbf{y}}) \in supp(\widetilde{\mathbb{P}})$.*

The two definitions are useful for strictly characterizing the discrepancies between data distributions. In the following, unless otherwise stated, we use $\mathbb{E}_{\mathbb{Q}}[\cdot]$ to denote the expectation over $(\mathbf{x}, \mathbf{y}) \sim \mathbb{Q}$, *i.e.*, $\mathbb{E}_{(\mathbf{x},\mathbf{y})\sim\mathbb{Q}}[\cdot]$. Moreover, to decompose the generalization error over the first t timesteps, we make the Assumption 1, wherein it is assumed that the cumulative distribution $\mathbb{D}_{1:t}$ can be expressed as a weighted sum of $\mathbb{D}_{1:t-1}$ and $\mathbb{D}_t$ with weight α_t.

Assumption 1. *(**Mixture of Distributions**) Assume that for any t, there exists $0 < \alpha_t < 1$, such that $\mathbb{D}_{1:t} = (1-\alpha_t)\mathbb{D}_{1:t-1} + \alpha_t \mathbb{D}_t$. For example, if $\mathbb{D}_{1:t} = \frac{1}{t}\sum_{i=1}^t \mathbb{D}_i$, then $\alpha_t = {1}/{t}$.*

Assumption 1 is widely adopted in machine learning research [31]. By the factorization in this assumption, it can be observed that the cumulative error consists of two factors associated with memory stability and learning plasticity [43]. The former pertains to the model capacity to retain acquired knowledge (namely $\mathbb{D}_{1:t-1}$), while the latter refers to its ability to learn from new data (namely $\mathbb{D}_t$). Additionally, we follow [28], [35] and assume the existence of upper bounds for the adopted loss function as well as the density ratio functions, as described in Assumption 2:

Assumption 2. *(**Boundedness of** $\ell(\cdot,\cdot)$ **and** $\beta_{\mathbb{P}}(\cdot,\cdot)$) Assume that the loss function and the density ratio function are respectively bounded above by $\overline{L} > 0$ and $\overline{\beta} > 0$, namely $\overline{L} = \sup_{f_{\boldsymbol{\theta}} \in \mathcal{F}_\Theta, \mathbf{x} \in \mathcal{X}, 1 \le i \le C} \ell(f_{\boldsymbol{\theta}}(\mathbf{x}), \mathbf{e}_i)$ and $\overline{\beta} = \sup_{(\mathbf{x}, \widetilde{\mathbf{y}}) \in supp(\widetilde{\mathbb{P}})} \beta_{\mathbb{P}}(\mathbf{x}, \widetilde{\mathbf{y}})$ for all measurable distributions $\mathbb{P}$.*

This assumption will be leveraged to establish the upper bound of the cumulative generalization error. To justify these assumptions, we present detailed analyses in Section A of the supplementary material.

Based on the definitions and assumptions above, we proceed to analyze the cumulative generalization error over the first t timesteps. The empirical distribution for examples in $\mathcal{M}_{1:t-1}$, *i.e.*, the buffer containing examples with clean but unobservable labels, is given by

$$\mathbb{P}^{\mathcal{M}}_{1:t-1} = \frac{1}{|\mathcal{M}_{1:t-1}|} \sum_{\mathbf{z}=(\mathbf{x},\mathbf{y}) \in \mathcal{M}_{1:t-1}} \delta(\mathbf{z}), \tag{5}$$

where $\delta(\cdot)$ denotes the Dirac delta function. Similarly, the data distribution corresponding to the noisy buffer is $\widetilde{\mathbb{P}}^{\mathcal{M}}_{1:t-1}$. By considering the approximation error between buffered data distribution and cumulative distribution $\mathbb{D}_{1:t-1}$, we provide in Theorem 1 a preliminary upper bound for the cumulative generalization error.

Theorem 1. *(**Preliminary Sketch of Cumulative Generalization Error Bound**) Based on Assumption 1, we define the density ratio functions corresponding to buffered data distribution and clean data distribution at timestep t as $\beta_1 = \beta_{\mathbb{P}^{\mathcal{M}}_{1:t-1}}$ and $\beta_2 = \beta_{\mathbb{D}_t}$, respectively. Then, the generalization error is upper-bounded as:*

$$\begin{aligned}\mathbb{E}_{\mathbb{D}_{1:t}}[\ell(f_{\boldsymbol{\theta}}(\mathbf{x}), \mathbf{y})] \le \underbrace{(1-\alpha_t)\mathbb{E}_{\widetilde{\mathbb{P}}^{\mathcal{M}}_{1:t-1}}[\beta_1(\mathbf{x}, \widetilde{\mathbf{y}})\ell(f_{\boldsymbol{\theta}}(\mathbf{x}), \widetilde{\mathbf{y}})]}_{\textit{Term 1}} + \\ \underbrace{(1-\alpha_t)Gap(\mathbb{P}^{\mathcal{M}}_{1:t-1}, \mathbb{D}_{1:t-1})}_{\textit{Term 2}} + \underbrace{\alpha_t \mathbb{E}_{\widetilde{\mathbb{D}}_t}[\beta_2(\mathbf{x}, \widetilde{\mathbf{y}})\ell(f_{\boldsymbol{\theta}}(\mathbf{x}), \widetilde{\mathbf{y}})]}_{\textit{Term 3}},\end{aligned} \tag{6}$$

where Term 2 contains the distribution gap between $\mathbb{P}^{\mathcal{M}}_{1:t-1}$ and $\mathbb{D}_{1:t-1}$, which is defined as

$$\begin{aligned} &Gap(\mathbb{P}^{\mathcal{M}}_{1:t-1}, \mathbb{D}_{1:t-1}) \\ &:= \Big|\mathbb{E}_{\mathbb{P}^{\mathcal{M}}_{1:t-1}}[\ell(f_{\boldsymbol{\theta}}(\mathbf{x}), \mathbf{y})] - \mathbb{E}_{\mathbb{D}_{1:t-1}}[\ell(f_{\boldsymbol{\theta}}(\mathbf{x}), \mathbf{y})]\Big|. \end{aligned} \tag{7}$$

From Theorem 1, we observe that for any timestep t, the upper bound of generalization error can be decomposed into three parts. Specifically, Term 1 at the right-hand side of Eq. (6) represents the empirical risk defined on the buffered data, Term 2 characterizes the gap between the distribution of buffered data and the distribution of clean cumulative data, and Term 3 accounts for the generalization error defined on the data distribution $\mathbb{D}_t$. Here, Term 1 in the upper bound can be estimated by using a finite number of noisy examples in the buffer. However, Term 2, namely the selection bias of buffered data, cannot be minimized directly, because it lacks a concrete measure that quantifies the closeness between $\mathbb{P}^{\mathcal{M}}_{1:t-1}$ and $\mathbb{D}_{1:t-1}$. We will show later in Section 5.1 a theoretically solid method to minimize this term. Moreover, the bound in Theorem 1 is coarse-grained, because it cannot incorporate the distribution shift across time. Therefore, in the following section, we particularly consider such shift and propose to transfer knowledge based on distribution discrepancy.

4.2 Discrepancy-Based Knowledge Transfer

In this section, we thoroughly analyze Term 3 in Theorem 1, where distribution discrepancy-based knowledge transfer between buffered data and new data is considered.

Since the examples in $\widetilde{\mathcal{M}}_{1:t}$ are drawn from various distributions that may differ significantly from $\mathbb{D}_t$ at timestep t, directly optimizing both the first and third terms in the error upper bound of Eq. (6) poses substantial optimization challenges. Moreover, the examples in the memory buffer may be beneficial for the improvement of learning plasticity [43], *i.e.*, the ability to learn from $\mathbb{D}_t$. However, the aforementioned generalization error bound does not explicitly capture the process of knowledge transfer from buffered data to new data at timestep t.

Inspired by the theory of batch distribution drift [2], we derive an upper bound for $\mathbb{E}_{\widetilde{\mathbb{D}}_t}[\beta_2(\mathbf{x}, \widetilde{\mathbf{y}})\ell(f_{\boldsymbol{\theta}}(\mathbf{x}), \widetilde{\mathbf{y}})]$, which incorporates knowledge transfer across distinct distributions. To facilitate this discussion, we first define the weighted Rademacher complexity, which quantifies the expressiveness of a given hypothesis space [32], [36]. Let $\widetilde{\mathcal{S}}$ denote a dataset of m examples drawn from the distribution $\widetilde{\mathbb{P}}$. The weighted Rademacher complexity of the hypothesis space $\mathcal{F}_\Theta$ is then defined as:

$$\begin{aligned} &\mathfrak{R}_{\mathbf{q}}(\beta_{\mathbb{P}} \circ \ell \circ \mathcal{F}_\Theta) \\ &:= \mathbb{E}_{\widetilde{\mathcal{S}} \sim \widetilde{\mathbb{P}}} \mathbb{E}_{\boldsymbol{\sigma}}\Big[\sup_{f_{\boldsymbol{\theta}} \in \mathcal{F}_\Theta} \sum_{i=1}^{m} \sigma_i q_i \beta_{\mathbb{P}}(\mathbf{x}_i, \widetilde{\mathbf{y}}_i)\ell(f_{\boldsymbol{\theta}}(\mathbf{x}_i), \widetilde{\mathbf{y}}_i)\Big]. \end{aligned} \tag{8}$$

Here, we use $\boldsymbol{\sigma} = (\sigma_i)_{1 \le i \le m} \in \{-1, +1\}^m$ to represent a Rademacher random vector, where $P(\sigma_i = +1) = P(\sigma_i = -1) = 1/2, \forall\, i \in [\![m]\!]$. The density ratio function $\beta_{\mathbb{P}}(\cdot, \cdot)$ is defined in Definition 2. Additionally, the vector $\mathbf{q} = (q_i)_{1 \le i \le m}$ satisfies $0 < q_i < 1, \forall\, i \in [\![m]\!]$ and $\|\mathbf{q}\|_1 = 1$.

Since buffered data are sampled from distinct distributions (*i.e.*, $\widetilde{\mathbb{D}}_1$ to $\widetilde{\mathbb{D}}_{t-1}$), they may not be equally useful for the learning of $\widetilde{\mathbb{D}}_t$. However, historical examples similar to new data should hold greater importance in facilitating the learning of the latest model. Therefore, we can cluster buffered data into K clusters, namely $\{\mathcal{M}^{(k)}_{1:t-1}\}_{k=1}^K$ and dynamically determine importance values according to distribution discrepancies. To this end, we incorporate the discrepancies into the upper bound of $\mathbb{E}_{\widetilde{\mathbb{D}}_t}[\beta_2(\mathbf{x}, \widetilde{\mathbf{y}})\ell(f_{\boldsymbol{\theta}}(\mathbf{x}), \widetilde{\mathbf{y}})]$. Let $\mathbb{P}_k$ denote the empirical distribution on $\mathcal{M}^{(k)}_{1:t-1}$ for all $k \in [\![K]\!]$, with m_k denoting the number of examples in the k-th cluster. The noisy counterparts of the K clusters and the empirical distributions are given by $\{\widetilde{\mathcal{M}}^{(k)}_{1:t-1}\}_{k=1}^K$ and $\{\widetilde{\mathbb{P}}_k\}_{k=1}^K$, respectively. The empirical distribution of $\widetilde{\mathcal{S}}_t$ is denoted by $\mathbb{P}_{\mathcal{S}_t}$. Based on the aforementioned definitions, Theorem 2 presents an upper bound for Term 3 in Theorem 1, which is:

Theorem 2. *Under Assumption 2, when the dataset $\{\widetilde{\mathcal{M}}^{(k)}_{1:t-1}\}_{k=1}^K \cup \widetilde{\mathcal{S}}_t$ is sampled from $\widetilde{\mathbb{P}} = \widetilde{\mathbb{P}}_1^{m_1} \otimes \widetilde{\mathbb{P}}_2^{m_2} \otimes \cdots \otimes \widetilde{\mathbb{P}}_K^{m_K} \otimes \widetilde{\mathbb{D}}_t^{n_t}$ with $\mathbb{P}$ denoting the corresponding clean distribution, for any $f_{\boldsymbol{\theta}} \in \mathcal{F}_\Theta$, with probability at least $1 - \delta$, it holds that:*

$$\begin{aligned} &\mathbb{E}_{\widetilde{\mathbb{D}}_t}[\beta_{\mathbb{D}_t}(\mathbf{x}, \widetilde{\mathbf{y}})\ell(f_{\boldsymbol{\theta}}(\mathbf{x}), \widetilde{\mathbf{y}})] \\ &\le \sum_{(\mathbf{x}_i, \widetilde{\mathbf{y}}_i) \in \widetilde{\mathcal{M}}_{1:t-1} \cup \widetilde{\mathcal{S}}_t} q_i \cdot \beta_{\mathbb{P}}(\mathbf{x}_i, \widetilde{\mathbf{y}}_i)\ell(f_{\boldsymbol{\theta}}(\mathbf{x}_i), \widetilde{\mathbf{y}}_i) \\ &+ \sum_{k=1}^{K} \overline{q}_k \cdot disc_{\mathcal{F}_\Theta}(\mathbb{P}_k, \mathbb{P}_{\mathcal{S}_t}) + \mathcal{O}\left(\frac{1}{\sqrt{|\widetilde{\mathcal{S}}_t|}}\right) \\ &+ 2\mathfrak{R}_{\mathbf{q}}(\beta_{\mathbb{P}} \circ \ell \circ \mathcal{F}_\Theta) + \|\mathbf{q}\|_2 \overline{L}\sqrt{\frac{\log(2/\delta)}{2}}, \end{aligned} \tag{9}$$

where $\mathbf{q} = (q_i)_{i=1}^{|\widetilde{\mathcal{M}}_{1:t-1}| + |\widetilde{\mathcal{S}}_t|}$ satisfies $q_i > 0$ and $\|\mathbf{q}\|_1 = 1$. Moreover, $\overline{q}_k = \sum_{(\mathbf{x}_i, \widetilde{\mathbf{y}}_i) \in \widetilde{\mathcal{M}}^{(k)}_{1:t-1}} q_i$ represents the sum of the weights assigned to all the examples in the k-th cluster $\widetilde{\mathcal{M}}^{(k)}_{1:t-1}$.

Theorem 2 indicates that the generalization error on the data distribution $\mathbb{D}_t$ is bounded above by the weighted loss computed over both buffered data and newly observed data. For a specific subset $\widetilde{\mathcal{M}}^{(k)}_{1:t-1}$ of the memory buffer, if its distribution substantially deviates from that of the current data $\widetilde{\mathcal{S}}_t$, the corresponding distribution discrepancy term $disc_{\mathcal{F}_\Theta}(\mathbb{P}_k, \mathbb{P}_{\mathcal{S}_t})$ becomes large. Consequently, the weight sum $\overline{q}_k$ of this subset should be reduced to maintain a tight upper bound on the generalization error. Since uniform weights can be assigned to new data and zero weights to buffered data, it is evident that this bound is no worse than the empirical error bound computed solely on $\widetilde{\mathcal{S}}_t$.

It is observed that the distribution discrepancy term $disc_{\mathcal{F}_\Theta}(\mathbb{P}_k, \mathbb{P}_{\mathcal{S}_t})$ in Theorem 2 depends on the clean data $\mathcal{M}^{(k)}_{1:t-1}$ and $\mathcal{S}_t$, which are inaccessible in our setting. Therefore, we can further estimate this term by using the noisy counterparts, namely $\widetilde{\mathcal{M}}^{(k)}_{1:t-1}$ and $\widetilde{\mathcal{S}}_t$. For clarity, the estimation algorithm is derived for two distributions $\mathbb{P}$ and $\mathbb{Q}$. The corresponding empirical distributions, composed of n and m examples, are denoted as $\mathbb{P}_n$ and $\mathbb{Q}_m$, respectively. Similarly, the noisy distributions are defined as $\widetilde{\mathbb{P}}$, $\widetilde{\mathbb{Q}}$, $\widetilde{\mathbb{P}}_n$, and $\widetilde{\mathbb{Q}}_m$, respectively. Given above notational definitions, we can instead estimate the empirical value of $disc_{\mathcal{F}_\Theta}(\mathbb{P}, \mathbb{Q})$ via importance reweighting on noisy data [28] by introducing density ratio functions $\beta_{\mathbb{P}}(\cdot,\cdot)$ and $\beta_{\mathbb{Q}}(\cdot,\cdot)$, namely

$$\begin{aligned} &\widehat{disc}_{\mathcal{F}_\Theta}(\widetilde{\mathbb{P}}_n, \widetilde{\mathbb{Q}}_m) \\ &= \sup_{f_{\boldsymbol{\theta}} \in \mathcal{F}_\Theta} \left| \mathbb{E}_{\widetilde{\mathbb{P}}_n} \left[\beta_{\mathbb{P}}(\mathbf{x}, \widetilde{\mathbf{y}}) \ell(f_{\boldsymbol{\theta}}(\mathbf{x}), \widetilde{\mathbf{y}})\right] - \mathbb{E}_{\widetilde{\mathbb{Q}}_m} \left[\beta_{\mathbb{Q}}(\mathbf{x}, \widetilde{\mathbf{y}}) \ell(f_{\boldsymbol{\theta}}(\mathbf{x}), \widetilde{\mathbf{y}})\right] \right|. \end{aligned} \tag{10}$$

4.3 Critical Factors Leading to Catastrophic Forgetting

Based on the analysis of three terms in Theorem 1 from Section 4.1∼4.2, we provide the main result in Theorem 3 below, namely

Theorem 3. ***(Main Theorem of Cumulative Generalization Error Bound)*** *Under Assumptions 1∼2, when the dataset $\{\widetilde{\mathcal{M}}_{1:t-1}^{(k)}\}_{k=1}^K \cup \widetilde{\mathcal{S}}_t$ is sampled from the distribution $\widetilde{\mathbb{P}}_1^{m_1} \otimes \widetilde{\mathbb{P}}_2^{m_2} \otimes \cdots \otimes \widetilde{\mathbb{P}}_K^{m_K} \otimes \widetilde{\mathbb{D}}_t^{|\widetilde{\mathcal{S}}_t|}$, with probability at least $1-\delta$, the final cumulative generalization error bound for any $f_{\boldsymbol{\theta}} \in \mathcal{F}_\Theta$ is:*

$$\begin{aligned} &\mathbb{E}_{\mathbb{D}_{1:t}}[\ell(f_{\boldsymbol{\theta}}(\mathbf{x}), \mathbf{y})] \\ &\le \underbrace{\sum_{(\mathbf{x}_i, \widetilde{\mathbf{y}}_i) \in \widetilde{\mathcal{M}}_{1:t-1}} \left(\tfrac{1-\alpha_t}{|\widetilde{\mathcal{M}}_{1:t-1}|} + \alpha_t q_i \right) \beta_{\mathbb{P}_{1:t-1}^{\mathcal{M}}}(\mathbf{x}_i, \widetilde{\mathbf{y}}_i) \ell(f_{\boldsymbol{\theta}}(\mathbf{x}_i), \widetilde{\mathbf{y}}_i)}_{\textit{Weighted loss on buffered data}} \\ &\underbrace{+ \alpha_t \cdot \sum_{(\mathbf{x}_j, \widetilde{\mathbf{y}}_j) \in \widetilde{\mathcal{S}}_t} q_j \beta_{\mathbb{D}_t}(\mathbf{x}_j, \widetilde{\mathbf{y}}_j) \ell(f_{\boldsymbol{\theta}}(\mathbf{x}_j), \widetilde{\mathbf{y}}_j)}_{\textit{Weighted loss on new data}} + \underbrace{O(1)}_{\textit{Approximation error}} \\ &\underbrace{+ \alpha_t \sum_{k=1}^K \overline{q}_k \widehat{disc}_{\mathcal{F}_\Theta}(\widetilde{\mathbb{P}}_k, \widetilde{\mathbb{P}}_{\mathcal{S}_t})}_{\textit{Distribution shift}} + \underbrace{(1-\alpha_t) Gap(\mathbb{P}_{1:t-1}^{\mathcal{M}}, \mathbb{D}_{1:t-1})}_{\textit{Buffered data selection bias}}, \end{aligned} \tag{11}$$

where q_i is the i-th element of $\mathbf{q}$, which satisfies $q_i > 0$ and $\|\mathbf{q}\|_1 = 1$, and $\overline{q}_k$ represents the sum of the weights assigned to the examples in the k-th cluster.

Theorem 3 reveals that catastrophic forgetting is fundamentally influenced by the three critical factors below, namely

- **Buffered data selection bias**. The selection bias term contains $Gap(\mathbb{P}_{1:t-1}^{\mathcal{M}}, \mathbb{D}_{1:t-1})$, which quantifies the distribution gap between buffered data and the data seen so far, and a smaller bias can contribute to a tighter bound.
- **Distribution shift**. The K clusters $\{\mathcal{M}_{1:t-1}^{(k)}\}_{k=1}^K$ may exhibit distribution shift relative to $\widetilde{\mathcal{S}}_t$, and the discrepancies among their distributions (*e.g.*, $\widetilde{\mathbb{P}}_k$ and $\widetilde{\mathbb{P}}_{\mathcal{S}_t}$) are characterized by the terms $\widehat{disc}_{\mathcal{F}_\Theta}(\widetilde{\mathbb{P}}_k, \widetilde{\mathbb{P}}_{\mathcal{S}_t}), \forall\, k \in [\![K]\!]$. Therefore, for a larger discrepancy value, a smaller weight $\overline{q}_k$ can lead to a tighter bound.
- **Label noise**. The density ratio functions (*i.e.*, $\beta_{\mathbb{P}_{1:t-1}^{\mathcal{M}}}(\cdot,\cdot)$ and $\beta_{\mathbb{D}_t}(\cdot,\cdot)$) appearing in the right-hand side of Eq. (11) serve as measures of importance for examples. Consequently, incorrectly labeled examples, which typically incur large loss values, should be assigned low importance values to ensure a tight bound.

5 The Proposed CNLDD Method

In this section, we design practical algorithms to tackle the three challenging factors revealed by Theorem 3. After that, the overall optimization method is introduced to minimize the upper bound of cumulative generalization error.

Algorithm 1 Greedy Algorithm for the k-Center Problem : cover($\mathcal{S}$, k)

```
Input: Dataset $\mathcal{S} = \{(\mathbf{x}_i, \mathbf{y}_i)\}_{i=1}^n$; and the number of selected examples $k$.
$\mathcal{M} \leftarrow \{$a random integer $j$ sampled from $\{1, 2, \cdots, n\}\}$;
Initialize a distance matrix $D^{min}$ with size $n$;
$D_i^{min} \leftarrow \|\mathbf{x}_i - \mathbf{x}_j\|_2, \forall\, i \in [\![n]\!]$;
while $|\mathcal{M}| < k$ do
    $u \in \arg\max_{i \in [\![n]\!] \setminus \mathcal{M}} D_i^{min}$;
    $\mathcal{M} \leftarrow \mathcal{M} \cup \{u\}$;
    $D_i^{min} \leftarrow \min\{D_i^{min}, \|\mathbf{x}_i - \mathbf{x}_u\|_2\}, \forall\, i \in [\![n]\!]$.
end while
Output: Selected subset $\mathcal{M}$.
```

5.1 A Two-Step Buffer Update Strategy

To ensure a minimum selection bias of buffered data, we propose a two-step buffer update strategy. To introduce this strategy, we need some additional definitions. We begin by presenting the concept of "covering radius" [35]. Intuitively, we draw spheres of uniform size centered at arbitrary points within a subset of data. The smallest radius needed to encompass all the data is then referred to as the covering radius. Formally, for a set $\mathcal{U}$ and its subset $\mathcal{U}^{\text{sub}}$, the covering radius γ of $\mathcal{U}^{\text{sub}}$ w.r.t. $\mathcal{U}$ is defined as:

$$\gamma := \max_{\mathbf{u} \in \mathcal{U}} \min_{\mathbf{u}' \in \mathcal{U}^{\text{sub}}} \|\mathbf{u} - \mathbf{u}'\|_2. \tag{12}$$

Furthermore, we refer to $\mathcal{U}^{\text{sub}}$ as a γ-cover of set $\mathcal{U}$.

Identifying a subset that has a minimum covering radius γ with k points is known as the k-center problem [14]. The k-center problem assumes that the original set is $\mathcal{V}$, and the subset is $\mathcal{C}$. The goal is to identify an optimal subset $\mathcal{C}^*$ of size k that minimizes the covering radius, *i.e.*,

$$\mathcal{C}^* \in \arg \min_{|\mathcal{C}|=k,\, \mathcal{C} \subset \mathcal{V}} \max_{\mathbf{v} \in \mathcal{V}} \min_{\mathbf{c} \in \mathcal{C}} \|\mathbf{v} - \mathbf{c}\|_2. \tag{13}$$

However, the k-center problem is NP-hard [7], making it computationally expensive to find an exact solution for large-scale datasets. In light of this, several "2-opt" approximation algorithms have been proposed [38]. In particular, these algorithms guarantee that if the optimal covering radius is r^*, the approximation algorithm yields a solution with a covering radius no greater than $2r^*$. Among them, the simple greedy algorithm (summarized in Algorithm 1) is widely recognized for its effectiveness as a 2-opt method.

By the definition of covering radius in Eq. (12), the subset with a minimum covering radius typically contains the most representative examples in $\mathcal{U}$. Motivated by this observation, we design a two-step buffer update strategy to ensure that the buffered examples are the most representative data seen so far. Specifically, at timestep t, if the memory buffer is not full, all newly received examples are directly added to it. If the memory buffer is full, we first select a subset from new data $\widetilde{\mathcal{S}}_t$ with a minimal covering radius, which is denoted by $\widetilde{\mathcal{M}}_t$. In practice, we use the ratio ρ to represent the proportion of examples selected from the new data $\widetilde{\mathcal{S}}_t$, such that $\widetilde{\mathcal{M}}_t$ has a size of $|\widetilde{\mathcal{S}}_t| \cdot \rho$. Subsequently, the ultimate memory buffer for timestep-t (*i.e.*, $\widetilde{\mathcal{M}}_{1:t}$) is constructed by selecting M examples from the union $\widetilde{\mathcal{M}}_{1:t-1} \cup \widetilde{\mathcal{M}}_t$ with a minimal covering radius, where M is the size of memory buffer. Since Algorithm 1 is easy to implement and can already produce satisfactory performance, it is employed at each step of the proposed two-step buffer update strategy.

As a 2-opt approximation algorithm, the greedy method adopted in our buffer update strategy keeps the covering radius close to the optimal value, which means that the buffered data are sufficiently representative of the data seen so far. Furthermore, as demonstrated in the post-hoc theoretical justification (Section 6), our strategy effectively leads to a small selection bias $Gap(\mathbb{P}^{\mathcal{M}}_{1:t-1}, \mathbb{D}_{1:t-1})$. Therefore, by employing our strategy, a tight upper bound on the generalization error in Theorem 3 can be achieved, which alleviates catastrophic forgetting in a principled manner.

5.2 The Estimation of Density Ratio Functions

In Theorem 3, several density ratio functions must be estimated, namely $\beta_{\mathbb{P}^{\mathcal{M}}_{1:t-1}}(\cdot,\cdot)$, $\beta_{\mathbb{D}_t}(\cdot,\cdot)$, $\beta_{\mathbb{P}_k}(\cdot,\cdot)$, and $\beta_{\mathbb{P}_{\mathcal{S}_t}}(\cdot,\cdot)$, which play a crucial role in mitigating label noise in both buffered data and new data. Since estimating each of these density ratios individually may result in significant estimation error due to the limited number of buffered data and incoming data, we instead propose a unified procedure to estimate all density ratios simultaneously.

To this end, we employ the HOC algorithm introduced in Section 3. To apply HOC algorithm, we merge the data from the memory buffer $\widetilde{\mathcal{M}}_{1:t-1}$ with the data for timestep-t (*i.e.*, $\widetilde{\mathcal{S}}_t$). Given each example $(\mathbf{x}, \widetilde{\mathbf{y}})$ in the combined dataset, the transition matrix $\mathbf{T}(\mathbf{x})$ and the corresponding noisy posterior $\widetilde{P}(\mathbf{e}_k|\mathbf{x}) = \sum_{j=1}^{C} T_{jk}(\mathbf{x}) \cdot P(\mathbf{e}_j|\mathbf{x})$ are estimated. Consequently, by Definition 2, for any example $(\mathbf{x}, \widetilde{\mathbf{y}}) \in \widetilde{\mathcal{M}}_{1:t-1}$, its density ratio can be expressed as:

$$\beta_{\mathbb{P}^{\mathcal{M}}_{1:t-1}}(\mathbf{x}, \widetilde{\mathbf{y}}) = \frac{\widehat{p}(Y = \widetilde{\mathbf{y}}|X = \mathbf{x})}{\widetilde{\mathbf{y}}^{\top}\mathbf{T}^{\top}(\mathbf{x})\widehat{\mathbf{p}}(Y|X = \mathbf{x})}, \qquad (14)$$

where $\widehat{\mathbf{p}}(Y|X = \mathbf{x}) = [\widehat{p}(Y = \mathbf{e}_1|X = \mathbf{x}), \widehat{p}(Y = \mathbf{e}_2|X = \mathbf{x}), \cdots, \widehat{p}(Y = \mathbf{e}_C|X = \mathbf{x})]^{\top} =: f_{\boldsymbol{\theta}}(\mathbf{x})$ represents the output probability vector of the hypothesis $f_{\boldsymbol{\theta}}$. Likewise, for any example $(\mathbf{x}, \widetilde{\mathbf{y}})$ sampled from $\mathbb{D}_t$, $\mathbb{P}_k$, and $\mathbb{P}_{\mathcal{S}_t}$, its density ratio can also be estimated via Eq. (14). For simplicity, we use the abbreviated symbol $\beta(\mathbf{x}, \widetilde{\mathbf{y}})$ to represent one of the four density ratio functions according to the related distribution that the specific example $(\mathbf{x}, \widetilde{\mathbf{y}})$ falls into.

5.3 The Estimation of Distribution Discrepancy

In addition to the factors of buffered data selection bias and label noise, it is also necessary to design an algorithm for computing the terms regarding distribution shift in Theorem 3. To achieve this, we propose a practical approach to estimate distribution discrepancy terms.

First of all, K clusters of buffered data must be identified. In this paper, we directly employ the K-Means method to obtain the clusters $\{\mathcal{M}^{(k)}_{1:t-1}\}_{k=1}^{K}$, due to its simplicity and its demonstrated effectiveness in our experiments. Moreover, since the hypothesis space $\mathcal{F}_\Theta$ can be highly complicated (such as the neural networks used in this paper), the term regarding distribution shift, *i.e.*, $\widehat{disc}_{\mathcal{F}_\Theta}(\widetilde{\mathbb{P}}_k, \widetilde{\mathbb{P}}_{\mathcal{S}_t})$, is difficult to compute directly. To address this issue, we propose to employ a linear hypothesis space with a fixed latent representation as a simplified alternative to $\mathcal{F}_\Theta$, namely

$$\mathcal{F}^{\text{lin}}_{\Theta} = \left\{ f_{\boldsymbol{\theta}} : f_{\boldsymbol{\theta}}(\mathbf{x}) = \boldsymbol{\theta}^{\top}\phi(\mathbf{x}), \boldsymbol{\theta} \in \Theta \subset \mathbb{R}^{d_\phi \times C} \right\}, \qquad (15)$$

where $\phi(\mathbf{x}) \in \mathbb{R}^{d_\phi}$ represents the latent representation of $\mathbf{x}$, and d_ϕ denotes its dimensionality.

Algorithm 2 Continual **N**oisy **L**abel Learning on **D**rifting **D**ata Streams (CNLDD)

```
Input: New data $\widetilde{\mathcal{S}}_t = \{(\mathbf{x}_i, \widetilde{\mathbf{y}}_i)\}_{i=1}^{n_t}$; the memory buffer $\widetilde{\mathcal{M}}_{1:t-1}$; selection ratio $\rho$; the capacity $M$ of memory buffer; number of clusters $K$; number of iterations $I$; and the parameter $\boldsymbol{\theta}_{t-1,I+1}$ learned at the $t-1$-th timestep.
Estimate the noise transition matrix $\mathbf{T}(\mathbf{x})$ for $\forall\,(\mathbf{x}, \widetilde{\mathbf{y}}) \in \widetilde{\mathcal{M}}_{1:t-1} \cup \widetilde{\mathcal{S}}_t$ using the HOC algorithm [52];
Calculate the density ratio $\beta(\mathbf{x}, \widetilde{\mathbf{y}})$ for $\forall\,(\mathbf{x}, \widetilde{\mathbf{y}}) \in \widetilde{\mathcal{M}}_{1:t-1} \cup \widetilde{\mathcal{S}}_t$ using Eq. (14);
Partition $\widetilde{\mathcal{M}}_{1:t-1}$ into $K$ clusters $\{\widetilde{\mathcal{M}}^{(k)}_{1:t-1}\}_{k=1}^{K}$ using $K$-Means clustering;
for $k = 1$ to $K$ do
    Estimate $\widehat{disc}_{\mathcal{F}^{\text{lin}}_{\Theta}}(\widetilde{\mathbb{P}}_k, \widetilde{\mathbb{P}}_{\mathcal{S}_t})$ via Eq. (16);
end for
$\mathbf{q}_{t,1} \leftarrow$ Uniform Distribution;
$\boldsymbol{\theta}_{t,1} \leftarrow \boldsymbol{\theta}_{t-1,I+1}$;
for $j = 1$ to $I$ do
    Compute the updated parameters $\boldsymbol{\theta}_{t,j+1}$ and $\mathbf{q}_{t,j+1}$ via Eq. (18);
end for
$\widetilde{\mathcal{M}}_t \leftarrow \text{cover}(\widetilde{\mathcal{S}}_t, \rho \cdot |\widetilde{\mathcal{S}}_t|)$;
$\widetilde{\mathcal{M}}_{1:t} \leftarrow \text{cover}(\widetilde{\mathcal{M}}_{1:t-1} \cup \widetilde{\mathcal{M}}_t, M)$.
Output: The predictive model $f_{\boldsymbol{\theta}_{t,I+1}}$ and the updated memory buffer $\widetilde{\mathcal{M}}_{1:t}$ for $t$ timesteps.
```

Next, we briefly outline the estimation of distribution discrepancy based on $\mathcal{F}^{\text{lin}}_{\Theta}$. For clarity, we denote the two underlying distributions as $\mathbb{P}$ and $\mathbb{Q}$. The corresponding density ratio vectors are represented as $\boldsymbol{\beta}_1 = (\beta_{\mathbb{P}}(\mathbf{x}_i, \widetilde{\mathbf{y}}_i))_{1 \le i \le n}$ and $\boldsymbol{\beta}_2 = (\beta_{\mathbb{Q}}(\mathbf{x}_j, \widetilde{\mathbf{y}}_j))_{1 \le j \le m}$, respectively. Subsequently, the optimal hypothesis $f_{\boldsymbol{\theta}^*}$ can be obtained by solving the following problem:

$$\min_{f_{\boldsymbol{\theta}} \in \mathcal{F}^{\text{lin}}_{\Theta}} \left\{ \frac{1}{n} \sum_{i=1}^{n} \beta_{1i} \ell(f_{\boldsymbol{\theta}}(\mathbf{x}_i), \widetilde{\mathbf{y}}_i) - \frac{1}{m} \sum_{j=1}^{m} \beta_{2j} \ell(f_{\boldsymbol{\theta}}(\mathbf{x}_j), \widetilde{\mathbf{y}}_j) \right\}. \qquad (16)$$

The procedure for solving this problem is detailed in Section C.1 of supplementary material, where the Cross-Entropy loss is adopted as the loss function. The optimal hypothesis $f_{\boldsymbol{\theta}^*}$, once obtained, is then utilized to compute the empirical discrepancy in Eq. (10). It is also proven in Section B.3 of supplementary material that the empirical estimation $\widehat{disc}_{\mathcal{F}^{\text{lin}}_{\Theta}}(\widetilde{\mathbb{P}}_n, \widetilde{\mathbb{Q}}_m)$ achieves an approximation error of $\mathcal{O}(\sqrt{1/m + 1/n})$ to $disc_{\mathcal{F}^{\text{lin}}_{\Theta}}(\mathbb{P}, \mathbb{Q})$ under mild conditions.

5.4 The Overall Optimization Problem

So far, we have thoroughly investigated each term in the upper bound of cumulative generalization error in Theorem 3. In this section, we present the optimization procedure designed to minimize this bound.

To obtain a tight upper bound for the generalization error, we propose to alternatively optimize over the hypothesis $f_{\boldsymbol{\theta}}$ and the weight vector $\mathbf{q}$ in Theorem 3. The approximation error is negligible as it does not depend on $f_{\boldsymbol{\theta}}$ or $\mathbf{q}$. To further regularize the optimization of $\mathbf{q}$, we add two terms to the objective function, namely $\|\mathbf{q}-\mathbf{p}^0\|_1$ and $\|\mathbf{q}\|_2$, where $\mathbf{p}^0$ is a prior for $\mathbf{q}$. By appending the two terms, prior knowledge can be leveraged, namely, we can assign more weight to historical data if they are more important than newly arrived data, and vice versa. Here, we set $\mathbf{p}^0$ as a uniform vector, which ensures the full utilization of data while preventing the collapse of $\mathbf{q}$. Finally, by considering all relevant factors, the upper bound of generalization error forms the following objective function:

$$\begin{aligned}\mathcal{L}_t(\boldsymbol{\theta},\mathbf{q}) := &\underbrace{\sum_{i=1}^{|\widetilde{\mathcal{M}}_{1:t-1}|}\left(\alpha_t q_i + \frac{1-\alpha_t}{|\widetilde{\mathcal{M}}_{1:t-1}|}\right)\beta(\mathbf{x}_i,\widetilde{\mathbf{y}}_i)\ell(f_{\boldsymbol{\theta}}(\mathbf{x}_i),\widetilde{\mathbf{y}}_i)}_{\text{Term 1}} \\ &+ \underbrace{\alpha_t\sum_{j=1}^{|\widetilde{\mathcal{S}}_t|} q_j\beta(\mathbf{x}_j,\widetilde{\mathbf{y}}_j)\ell(f_{\boldsymbol{\theta}}(\mathbf{x}_j),\widetilde{\mathbf{y}}_j)}_{\text{Term 2}} + \underbrace{\lambda_1\|\mathbf{q}-\mathbf{p}^0\|_1}_{\text{Term 3}} + \underbrace{\lambda_2\|\mathbf{q}\|_2}_{\text{Term 4}} \\ &+ \underbrace{\sum_{k=1}^{K}\overline{q}_k\widehat{disc}_{\mathcal{F}_{\Theta}^{\text{lin}}}(\widetilde{\mathbb{P}}_k,\widetilde{\mathbb{P}}_{\mathcal{S}_t})}_{\text{Term 5}},\end{aligned} \tag{17}$$

where the density ratio $\beta(\cdot,\cdot)$ can be estimated via Eq. (14). Moreover, λ_1 and λ_2 are two non-negative hyperparameters. In Eq. (17), Term 1 and Term 2 correspond to the losses on buffered data and new data, respectively. Term 3 and Term 4 serve as regularizers for $\mathbf{q}$. Additionally, Term 5 captures the discrepancy between the distributions of the K clusters and the data distribution at timestep t.

Subsequently, we present the detailed procedure for the optimization over $f_{\boldsymbol{\theta}}$ and $\mathbf{q}$ in the objective function $\mathcal{L}_t(\boldsymbol{\theta},\mathbf{q})$. Let I denote the number of iterations performed at each timestep. We denote by $\boldsymbol{\theta}_{t,j}$ and $\mathbf{q}_{t,j}$ the parameters after j iterations at timestep t. The parameter $\boldsymbol{\theta}$ and the weight vector $\mathbf{q}$ are updated iteratively according to Eq. (18):

$$\left\{\begin{array}{l}\boldsymbol{\theta}_{t,j+1} = \boldsymbol{\theta}_{t,j} - \eta\nabla_{\boldsymbol{\theta}}\mathcal{L}_t(\boldsymbol{\theta},\mathbf{q}_{t,j})\big|_{\boldsymbol{\theta}_{t,j}} \\ \mathbf{q}_{t,j+1} = \text{Proj}\big(\mathbf{q}_{t,j} - \eta\nabla_{\mathbf{q}}\mathcal{L}_t\left(\boldsymbol{\theta}_{t,j+1},\mathbf{q}\right)\big|_{\mathbf{q}_{t,j}}\big)\end{array}\right., \tag{18}$$

where $\text{Proj}(\cdot)$ denotes a projection operator onto the probability simplex, and η is the learning rate. For a p-dimensional vector $\boldsymbol{\nu} = (\nu_i)_{1\le i\le p} \in \mathbb{R}^p$, this operator is defined as $\text{Proj}(\boldsymbol{\nu}) = ([\nu_i - \mu^*]_+)_{1\le i\le p}$, where μ^* is the unique solution to the equation $\mathbf{1}^\top[\mathbf{q}-\mu^*\mathbf{1}]_+ = 1$ [4]. Here, $\mathbf{1}\in\mathbb{R}^p$ is an all-one vector, and $[a]_+ = \max\{a,0\}$ for any scalar a.

The main steps of the proposed CNLDD method are summarized in Algorithm 2, where $\text{cover}(\cdot,\cdot)$ denotes the greedy k-center approach described in Algorithm 1. For this algorithm, we provide a detailed computational complexity analysis in Section D of the supplementary material. In Section E, we further present a per-step runtime analysis and compare the computational cost of CNLDD with those of representative continual noisy label learning methods in memory update and model training. The results demonstrate that, although our method involves multiple optimization steps, its overall runtime remains acceptable.

6 Theoretical Analysis of CNLDD Method

In this section, we provide supplementary justifications to our specifically designed CNLDD method.

First, we present rigorous theoretical support for our buffer update strategy, demonstrating its close relationship to the minimization of $Gap(\mathbb{P}^{\mathcal{M}}_{1:t-1},\mathbb{D}_{1:t-1})$ in Theorem 3. Our analysis is mainly based on the following lemma:

Lemma 1. *Under Assumption 2, we further assume that the class posterior probability $P_t(Y_t=\mathbf{y}|X_t=\mathbf{x})$ is λ^P-Lipschitz continuous at any timestep, and the loss function $\ell(f(\cdot),\mathbf{y})$ is λ^ℓ-Lipschitz continuous for all $\mathbf{y}$. At timestep $t-1$, we assume the following: the memory buffer $\widetilde{\mathcal{M}}_{1:t-2}$ with size k_1 is a γ-cover of the entire dataset $\widetilde{\mathcal{S}}_{1:t-2}$; the temporary buffer $\widetilde{\mathcal{M}}_{t-1}$ with size k_2 is a γ'-cover of the data $\widetilde{\mathcal{S}}_{t-1}$; and the updated memory buffer $\widetilde{\mathcal{M}}_{1:t-1}$ with size k_3 at timestep $t-1$ is a γ''-cover of $\widetilde{\mathcal{M}}_{1:t-2}\cup\widetilde{\mathcal{M}}_{t-1}$. If the loss on buffered data is sufficiently small, i.e., $\mathbb{E}_{\mathbb{P}^{\mathcal{M}}_{1:t-1}}[\ell(f(\mathbf{x}),\mathbf{y})] < \epsilon$ with ϵ being a very small positive value, then with probability at least $1-\delta$, we have:*

$$\begin{aligned}&Gap(\mathbb{P}^{\mathcal{M}}_{1:t-1},\mathbb{D}_{1:t-1}) < 2\epsilon \\ &+ (\max\{\gamma,\gamma'\}+\gamma'')(\lambda^\ell+\lambda^P\overline{L}C) + 2\overline{L}\sqrt{\frac{\log(2/\delta)}{2|\widetilde{\mathcal{S}}_{1:t-1}|}}.\end{aligned} \tag{19}$$

The above lemma demonstrates that an appropriate selection of data will lead to small values of γ, γ' and γ'', which further result in a lower upper bound for $Gap(\mathbb{P}^{\mathcal{M}}_{1:t-1},\mathbb{D}_{1:t-1})$. In view of this, by applying Lemma 1, we show in Theorem 4 that the two-step buffer update strategy proposed in Section 5.1 can induce an upper bound characterized by a single covering radius γ.

Theorem 4. *Based on Lemma 1, if the update strategy for the memory buffer at timestep $t-1$ is designed as follows: first, a $\frac{\gamma}{t}$-cover of $\widetilde{\mathcal{S}}_{t-1}$, denoted by $\widetilde{\mathcal{M}}_{t-1}$, is selected; then, a $\frac{\gamma}{t}$-cover of $\widetilde{\mathcal{M}}_{1:t-2}\cup\widetilde{\mathcal{M}}_{t-1}$, denoted by $\widetilde{\mathcal{M}}_{1:t-1}$, is further selected. The resulting $\widetilde{\mathcal{M}}_{1:t-1}$ serves as the final memory buffer at timestep $t-1$. Based on this strategy, if the loss on buffered data is sufficiently small, i.e., $\mathbb{E}_{\mathbb{P}^{\mathcal{M}}_{1:t-1}}[\ell(f(\mathbf{x}),\mathbf{y})] < \epsilon$ with ϵ being a very small positive value, then with probability at least $1-\delta$, it holds that*

$$\begin{aligned}&Gap(\mathbb{P}^{\mathcal{M}}_{1:t-1},\mathbb{D}_{1:t-1}) < \gamma\log(t+1)(\lambda^\ell+\lambda^P\overline{L}C)+2\epsilon \\ &+ 2\overline{L}\sqrt{\frac{\log(2/\delta)}{2|\widetilde{\mathcal{S}}_{1:t-1}|}} = \widetilde{\mathcal{O}}(\gamma)+\mathcal{O}\left(\sqrt{\frac{1}{\sum_{i=1}^{t-1}n_i}}+\epsilon\right),\end{aligned} \tag{20}$$

where $\widetilde{\mathcal{O}}(\cdot)$ denotes the big-$\mathcal{O}$ that hides all logarithmic factors.

Theorem 4 establishes an upper bound on the distribution gap term $Gap(\mathbb{P}^{\mathcal{M}}_{1:t-1},\mathbb{D}_{1:t-1})$, which includes a term $\widetilde{\mathcal{O}}(\gamma)$ that explicitly depends on the covering radius γ in each step of our update strategy. By substituting this bound into Theorem 3, we can readily derive the upper bound of cumulative generalization error specific to our CNLDD method. Recalling our two-step buffer update strategy in Section 5.1, we ensure a minimum covering radius in each step of our strategy, and thus γ in Eq. (20) is minimized. Consequently, our buffer update strategy reduces the selection bias term in Theorem 3. In contrast to existing CNLL methods [3], [20], [21], which typically rely on heuristic selection strategies for memory buffer maintenance, our theoretical framework demonstrates that the proposed update strategy is intrinsically linked to the minimization of cumulative generalization error, contributing to improved performance in a principled manner.

Moreover, we demonstrate in supplementary material (Section B.7) that a prior $\mathbf{p}_0$ can also be introduced for the weight vector $\mathbf{q}$ in Theorem 3, and the corresponding upper bound exhibits a structure similar to that of Eq. (17). Disregarding the approximation error, the objective $\mathcal{L}_t(\boldsymbol{\theta}, \mathbf{q})$ serves as an exact upper bound for cumulative generalization error. Consequently, minimizing $\mathcal{L}_t(\boldsymbol{\theta}, \mathbf{q})$ can lead to a reduction in generalization error, and thus the proposed CNLDD method can effectively mitigate catastrophic forgetting induced by distribution shift and label noise.

7 Experimental Results

To validate the effectiveness of the proposed CNLDD algorithm, we conducted extensive experiments on representative synthetic and real-world datasets. The parametric sensitivity and contribution of various modules in our CNLDD method are also investigated.

In this paper, we investigate three common types of label noise [6], [13] on both synthetic and real-world datasets, namely 1) symmetric noise, which means that for each example, we uniformly select a label different from its ground-truth label with probability $\epsilon/C-1$, where ϵ is the noise rate; 2) pairflip noise, where we flip the label of each example cyclically to the next class with a probability of ϵ; and 3) instance-dependent noise, where the noise rate of a certain example depends on its feature and here we adopt the noise generation strategy proposed in prior work [6]. Additionally, two levels of label noise, namely 20% and 40%, are considered in our experiments. For simplicity, “sym. ϵ”, “asym. ϵ” and “inst. ϵ” are used to denote the symmetric noise, pairflip noise, and instance-dependent noise with the noise rate of ϵ, respectively. Furthermore, we also consider the noise-free case, which is denoted as “clean. 0%”.

The baseline methods adopted in our experiments are Finetune, ER [40], PuriDivER [3], SPR [21], CNLL [20], Meta-DR [41], Online EWC [23], AdaStreams [50], Co-teaching [16], ϵ-Softmax [42], ContinualCRUST [33], STAR [10], and WSC [51]. In detail, Finetune refers to a naive method that does not employ any strategy to combat label noise or catastrophic forgetting. It simply finetunes the trained model with new data at each timestep without preserving historical models or examples. ER is a classical replay-based paradigm in continual learning. Moreover, online EWC and STAR are representative regularization-based CL approaches, whereas Meta-DR serves as a typical CL method built upon meta-learning principles. PuriDivER, SPR, CNLL, and ContinualCRUST are methods specifically designed for continual noisy label learning, with their key differences lying in the mechanisms adopted for buffer update. Additionally, AdaStreams, Co-teaching, and ϵ-Softmax are typical LNL approaches based on statistic estimation, sample selection, and robust loss function design, respectively. WSC is a recently proposed method that aims to learn a robust representation space even in the presence of imprecise supervision. In accordance with the common practice in continual noisy label learning [20], a noisy memory buffer is incorporated in AdaStreams, Co-teaching, ϵ-Softmax, and WSC. During training, the reservoir sampling technique [40] is leveraged to sample and replay historical data, enabling these LNL methods to mitigate the problem of catastrophic forgetting to some extent. Notably, PuriDivER, SPR, CNLL, and WSC incorporate auxiliary strategies, such as data augmentation, self-supervised learning, and semi-supervised learning, to improve their robustness and generalization capability. Therefore, to ensure fairness, all compared methods employ AugMix data augmentation [18]. Overall, the selected methods include existing continual noisy label learning methods as well as continual learning and label noise learning methods based on different strategies, ensuring a comprehensive evaluation of the proposed CNLDD method.

7.1 Experiments on Synthetic Datasets

In this section, we use different domains or datasets to simulate the distribution shift in our setting. Inspired by the study of continual domain adaptation [41], we start by conducting experiments on two synthetic datasets, namely *PACS* [25] and *Digits* [41], which are broadly adopted by the computer vision community. Here, *Digits* comprises four digit datasets with different styles, namely, *MNIST*, *MNIST-M*, *SYN*, and *SVHN* [41].

The *PACS* dataset, widely utilized in image classification tasks, consists of 9,991 images across four distinct styles, namely Sketch, Cartoon, Art Painting, and Photo. In our setting, different styles in *PACS* refer to different data distributions, and the same type and level of label noise are applied to all styles. The training data derived from *PACS* is illustrated in Fig. 1. It can be seen that the style of images evolves over time from the most abstract to the most realistic. At each timestep, the model receives noisy examples from a certain style without being informed of the exact type of the style. Moreover, 80% of the data from each style in *PACS* is used for model training, while the rest is reserved for testing. The size of new data $\widetilde{\mathcal{S}}_t$ received by the model is set to 200. Additionally, in prior work [41], 100∼300 examples are buffered for each style. Since style information is unknown in our setting, here we set the size M of memory buffer as 200, resulting in a total of 40 timesteps.

For *Digits* dataset, by following previous study [41], we adopt two distinct protocols to organize the four data subsets, namely $P1$: *MNIST*→*MNIST-M*→*SYN*→*SVHN* and $P2$: *SVHN*→*SYN*→*MNIST-M*→*MNIST*. Here, the two protocols allow the evaluation of model performance from easy datasets to hard datasets and vice versa. The two protocols are shown in Fig. 2. For compatibility, the size of each image in *Digits* is adjusted to 28×28 pixels beforehand. Consistent with the setting of Meta-DR [41], 10,000 examples are randomly selected from each data subset for model training, and additional 2,000 noise-free examples from each dataset are selected for testing. In our experiments, the size of new data $\widetilde{\mathcal{S}}_t$ received by the model at each time step t is set to 500, and the size of the memory buffer M is set to 1,000, with 80 timesteps in total.

For *PACS* and *Digits* datasets, the adopted backbone network is ResNet-18 [17] and the network is pretrained on ImageNet [9] for *PACS*. On *PACS* dataset, we train the network for 20 iterations at each timestep with a batch size

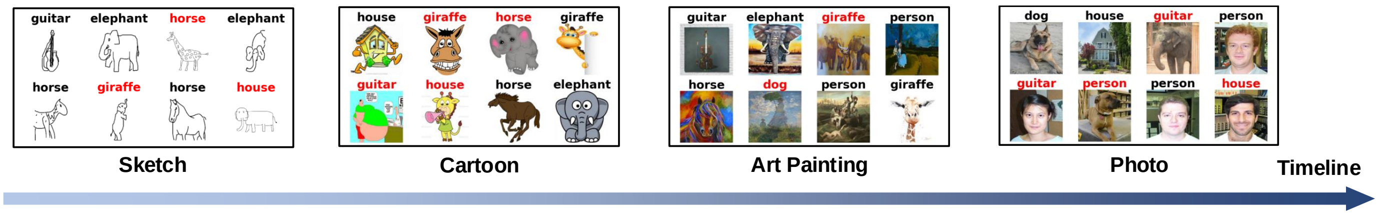

Fig. 1. The streaming training data constructed from *PACS* dataset. Each image is labeled with its observed class (one of seven categories), where black labels denote correct annotations while red labels indicate incorrect ones. Additionally, the image styles vary at certain timesteps, which is model-agnostic. The goal is to accurately predict the class of test images across all styles along the entire timeline after training.

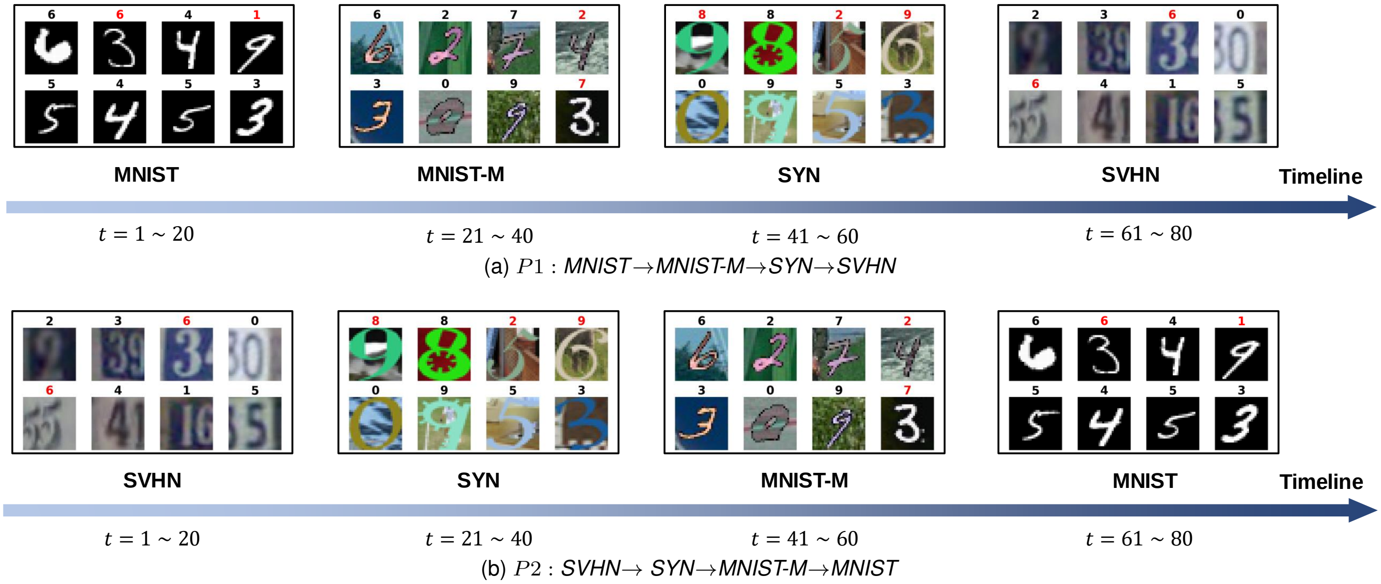

(a) $P1$: *MNIST*→*MNIST-M*→*SYN*→*SVHN*

(b) $P2$: *SVHN*→ *SYN*→*MNIST-M*→*MNIST*

Fig. 2. Two arrangement protocols for *Digits*, where (a) and (b) illustrate protocol 1 (easy to difficult) and protocol 2 (difficult to easy), respectively. The number above each image indicates the observed class (one of ten categories), with black labels signifying correct annotations and red labels indicating incorrect ones. The objective is to accurately recognize the ten digits "0∼9" across various data subsets along the entire timeline.

TABLE 2
Average test accuracies (%) of various approaches on *PACS* dataset. The two best records under each noise setting are highlighted in red and blue, respectively.

Method	clean. 0%	sym. 20%	sym. 40%	asym. 20%	asym. 40%	inst. 20%	inst. 40%
Finetune	39.69 ± 0.24	34.77 ± 0.34	27.89 ± 1.02	45.24 ± 0.91	37.04 ± 0.21	33.38 ± 0.41	26.92 ± 1.02
ER [5]	67.43 ± 0.53	53.39 ± 0.22	38.76 ± 1.09	50.43 ± 0.23	43.49 ± 0.51	50.96 ± 0.52	34.30 ± 0.14
Online EWC [23]	44.36 ± 0.11	36.98 ± 0.14	29.01 ± 0.72	38.03 ± 0.25	30.09 ± 2.52	33.28 ± 0.51	28.89 ± 0.62
AdaStreams [50]	86.85 ± 0.09	76.12 ± 0.24	61.70 ± 0.91	72.75 ± 0.71	52.66 ± 0.51	68.87 ± 0.63	27.94 ± 0.24
CNLL [20]	61.09 ± 0.27	54.34 ± 0.91	47.45 ± 0.55	57.98 ± 0.42	44.00 ± 0.61	53.50 ± 0.69	27.95 ± 0.90
Meta-DR [41]	78.02 ± 0.35	62.37 ± 0.13	46.40 ± 2.05	61.87 ± 0.45	50.78 ± 1.29	62.64 ± 0.10	51.36 ± 2.88
SPR [21]	58.99 ± 0.25	50.73 ± 0.22	42.29 ± 0.25	60.47 ± 0.52	47.10 ± 0.96	49.99 ± 0.81	39.90 ± 0.25
PuriDivER [3]	54.49 ± 0.18	45.72 ± 0.45	34.57 ± 0.99	53.34 ± 0.61	43.10 ± 0.14	45.86 ± 0.91	32.98 ± 0.61
Co-teaching [16]	82.77 ± 0.11	77.10 ± 0.29	60.07 ± 0.71	71.30 ± 0.81	57.16 ± 0.62	74.18 ± 0.90	43.52 ± 1.24
ϵ-Softmax [42]	71.99 ± 0.10	65.31 ± 0.25	53.13 ± 0.44	63.30 ± 0.88	45.87 ± 0.86	57.04 ± 0.05	25.47 ± 0.91
ContinualCRUST [33]	83.04 ± 0.23	64.00 ± 0.18	47.50 ± 1.81	64.61 ± 0.23	50.22 ± 2.41	67.48 ± 1.72	52.44 ± 1.67
STAR [10]	85.54 ± 0.90	67.28 ± 0.99	51.06 ± 1.29	68.66 ± 1.34	49.79 ± 3.92	64.04 ± 1.70	48.39 ± 3.09
WSC [51]	85.35 ± 0.25	76.21 ± 0.08	55.15 ± 1.73	73.68 ± 1.12	53.22 ± 0.70	72.24 ± 1.80	52.78 ± 0.25
CNLDD	85.75 ± 0.28	77.72 ± 0.24	62.22 ± 0.51	75.08 ± 0.82	58.80 ± 0.41	75.68 ± 0.34	60.85 ± 0.55

of 32. For our CNLDD, α_t is set to 0.2, because small α_t facilitates memory stability. The number of clusters K is set to 6, and the selection ratio ρ is set to 0.3, which are tuned on a noisy validation set. The sensitivity analysis in Section 7.3 also demonstrates that $5 \leq K \leq 8$ and $\rho \in \{0.2, 0.3\}$ typically yield satisfactory performance. Additionally, in all experiments, the coefficients λ_1 and λ_2 are set to 10.0 and 0.01, respectively, since this configuration often leads to satisfactory performance across all datasets. For *Digits* dataset, the batch size is 128 for all the compared methods. For our CNLDD, the coefficient α_t is set to 0.1, the ratio ρ is set to 0.3, the number of clusters is set to $K = 2$. For all compared methods, the Adam optimizer [22] is employed. We record the highest test accuracy from the last five timesteps of each experiment and report the mean and standard deviation of accuracies from three independent trials [3], [20], [21].

The experimental results on *PACS* dataset are shown in Tab. 2. As shown in this table, our CNLDD consistently ranks among the top two places across all noise settings. Particularly, in the "inst. 40%" noise setting, CNLDD

TABLE 3
Average test accuracies (%) of various approaches on *Digits* dataset. The two best records under each noise setting are highlighted in red and blue, respectively.

Protocol	Method	clean. 0%	sym. 20%	sym. 40%	asym. 20%	asym. 40%	inst. 20%	inst. 40%
$P1$	Finetune	60.30 ± 0.11	51.09 ± 0.23	45.60 ± 4.26	59.77 ± 0.27	43.05 ± 0.33	48.38 ± 0.52	42.11 ± 0.54
	ER [5]	86.11 ± 0.42	67.44 ± 0.14	42.15 ± 0.55	74.06 ± 0.25	51.24 ± 0.66	71.48 ± 0.24	44.62 ± 0.91
	Online EWC [23]	58.59 ± 0.32	54.18 ± 0.14	45.77 ± 0.34	53.39 ± 0.55	45.43 ± 0.72	51.25 ± 0.13	43.21 ± 0.44
	AdaStreams [50]	74.81 ± 0.14	69.58 ± 0.20	52.22 ± 0.31	63.03 ± 0.23	44.05 ± 0.50	61.16 ± 0.15	30.90 ± 0.33
	CNLL [20]	78.42 ± 0.34	84.66 ± 0.32	65.95 ± 0.91	82.49 ± 0.55	60.66 ± 0.66	79.65 ± 0.11	58.22 ± 0.55
	Meta-DR [41]	91.41 ± 0.12	73.29 ± 0.33	48.20 ± 0.54	77.98 ± 0.20	54.71 ± 0.55	69.38 ± 1.00	51.89 ± 1.01
	SPR [21]	69.72 ± 0.23	60.14 ± 0.28	50.45 ± 1.05	62.11 ± 0.08	46.55 ± 0.05	60.12 ± 0.23	47.88 ± 0.99
	PuriDivER [3]	88.17 ± 0.06	73.12 ± 0.31	49.41 ± 1.22	76.20 ± 0.21	55.44 ± 1.02	72.50 ± 1.01	49.10 ± 1.55
	Co-teaching [16]	87.09 ± 0.42	82.45 ± 0.29	66.00 ± 0.82	83.53 ± 0.43	64.26 ± 0.22	80.94 ± 0.65	57.15 ± 0.39
	ϵ-Softmax [42]	80.28 ± 0.23	79.62 ± 0.25	66.06 ± 0.23	75.65 ± 0.35	53.92 ± 0.25	75.70 ± 0.24	49.24 ± 0.17
	ContinualCRUST [33]	91.88 ± 0.00	65.32 ± 1.32	45.68 ± 0.80	71.30 ± 1.62	51.04 ± 2.65	67.76 ± 0.56	53.80 ± 1.84
	STAR [10]	89.65 ± 0.16	72.46 ± 4.84	46.74 ± 0.64	74.56 ± 1.25	49.28 ± 4.67	72.98 ± 5.88	47.32 ± 3.21
	WSC [51]	88.56 ± 0.50	84.79 ± 0.08	64.71 ± 3.25	84.04 ± 0.59	51.57 ± 2.08	78.78 ± 3.10	50.69 ± 1.39
	CNLDD	92.05 ± 0.19	85.01 ± 0.18	67.05 ± 0.72	85.60 ± 0.65	67.84 ± 0.95	81.04 ± 0.13	61.69 ± 0.85
$P2$	Finetune	69.60 ± 0.24	56.02 ± 0.10	39.24 ± 0.99	59.62 ± 0.23	47.24 ± 0.77	63.24 ± 0.57	49.83 ± 0.30
	ER [5]	90.06 ± 0.14	76.06 ± 0.24	44.83 ± 0.45	76.11 ± 0.43	50.69 ± 0.23	72.74 ± 0.72	51.86 ± 1.02
	Online EWC [23]	67.00 ± 0.72	57.69 ± 0.19	38.59 ± 0.24	61.12 ± 0.91	49.29 ± 1.87	63.16 ± 0.39	47.26 ± 2.03
	AdaStreams [50]	78.95 ± 0.25	71.23 ± 0.07	55.67 ± 0.56	67.92 ± 0.23	49.25 ± 1.03	62.42 ± 0.53	40.24 ± 2.01
	CNLL [20]	81.24 ± 0.36	67.60 ± 0.90	53.56 ± 1.02	75.45 ± 0.34	64.39 ± 1.03	56.40 ± 0.32	38.89 ± 2.12
	Meta-DR [41]	73.19 ± 0.29	57.14 ± 0.02	44.67 ± 0.34	58.65 ± 1.01	45.27 ± 0.29	59.67 ± 0.25	48.15 ± 0.34
	SPR [21]	61.26 ± 0.10	48.44 ± 0.16	40.42 ± 0.26	50.40 ± 0.92	33.95 ± 2.94	47.06 ± 0.21	39.55 ± 2.24
	PuriDivER [3]	90.39 ± 0.23	77.91 ± 0.23	47.50 ± 1.02	78.69 ± 0.44	55.01 ± 0.32	77.19 ± 0.42	55.93 ± 0.35
	Co-teaching [16]	89.67 ± 0.08	81.05 ± 0.25	54.51 ± 0.23	77.27 ± 0.32	55.26 ± 1.02	76.94 ± 0.29	60.60 ± 1.29
	ϵ-Softmax [42]	85.38 ± 0.35	81.31 ± 0.56	53.71 ± 0.43	77.79 ± 0.42	53.01 ± 0.23	76.60 ± 0.19	50.52 ± 0.42
	ContinualCRUST [33]	92.24 ± 1.12	68.35 ± 1.62	43.97 ± 1.02	74.43 ± 2.95	53.16 ± 1.75	69.50 ± 1.85	56.46 ± 3.29
	STAR [10]	94.32 ± 0.65	73.97 ± 0.28	48.48 ± 5.51	78.04 ± 0.01	54.32 ± 1.38	76.50 ± 1.21	50.64 ± 0.64
	WSC [51]	92.05 ± 0.78	80.54 ± 0.23	61.51 ± 2.14	78.16 ± 0.71	51.05 ± 2.25	77.39 ± 1.84	57.30 ± 0.78
	CNLDD	93.49 ± 0.11	81.88 ± 0.23	63.65 ± 0.29	79.74 ± 0.23	62.08 ± 0.38	78.75 ± 0.48	61.34 ± 0.66

outperforms Meta-DR by nearly 9% in average accuracy. This highlights the advantage of explicitly modeling the instance-dependent transition matrix over clean sample selection. Moreover, although CNLL is specifically designed for continual noisy label learning, its performance suffers due to its failure to mitigate the impact of distribution shift. In contrast, our CNLDD evaluates the importance of buffered data based on distribution discrepancy, and thus it achieves superior performance when compared with CNLL. Additionally, when comparing label noise learning methods (*e.g.*, Co-teaching and ϵ-Softmax) with continual learning methods (*e.g.*, ER and Online EWC) which lack explicit noise-handling strategies, it reflects that label noise significantly exacerbates model forgetting and hinders the memorization of new data. Consequently, typical continual learning methods often perform poorly.

The experimental results on *Digits* dataset using two distinct protocols are presented in Tab. 3. It can be seen that, under the “inst. 40%” noise condition, the accuracy of CNLDD surpasses ϵ-Softmax by approximately 12%, indicating that robust loss functions designed without explicitly modeling the noise generation process often perform poorly in complex noise scenarios. Furthermore, under the setting of “asym. 40%”, the test accuracy of CNLDD exceeds that of the second-best method, *i.e.*, Co-teaching, by 3.58%. This suggests that the theoretically grounded CNLDD method is more effective than the experience-driven LNL method based on the technique of sample selection.

7.2 Experiments on Real-World Datasets with Natural Distribution shift

In addition to evaluating the effectiveness of our CNLDD over baseline methods on synthetic datasets, we also conduct experiments on two real-world datasets with temporal distribution shift and label noise.

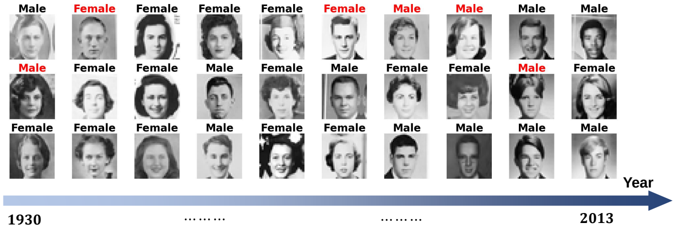

Fig. 3. The streaming noisy data constructed from the *Yearbook* dataset for model training. Each image is labeled with the observed class (one of two categories), where black labels represent correct annotations while red labels indicate incorrect ones. Due to the changes in societal norms, fashion styles, and demographics over time, the styles of images, hairstyles, and other features evolve over time. The goal is to accurately predict the gender of each face across all the time periods.

The real-world classification datasets utilized are *Yearbook* and *FMoW* (Functional Map of the World) from the Wild-Time benchmark [47]. The *Yearbook* dataset contains 33,431 annotated frontal-view yearbook photographs of American high school students spanning 1930∼2013. Each image is a single-channel grayscale image with the resolution of 32×32. The dataset provides a correct label for each face image to indicate the gender. Due to the changes in societal norms, fashion styles, and demographics, the styles of the images, clothing, and other features in *Yearbook* dataset also change over time, resulting in natural distribution shift [47]. Fig. 3 demonstrates some training examples sampled from different time periods in *Yearbook* dataset. This figure illustrates the subtle shift in data distribution over time, which differs from the abrupt distribution shift observed in *PACS* and *Digits* datasets introduced in the previous section. To adapt the *Yearbook* dataset to the setting studied in this paper, 20% of the images and their correct

TABLE 4
Average test accuracies (%) of various approaches on *Yearbook* and *FMoW* datasets. The two best records under each noise setting are highlighted in red and blue, respectively.

Dataset	Method	clean. 0%	sym. 20%	sym. 40%	asym. 20%	asym. 40%	inst. 20%	inst. 40%
Yearbook	Finetune	83.26 ± 0.23	74.59 ± 0.35	57.61 ± 0.36	-	-	71.47 ± 0.12	55.54 ± 0.21
	ER [5]	94.01 ± 0.56	78.45 ± 1.23	59.50 ± 0.14	-	-	79.70 ± 0.31	61.68 ± 1.19
	Online EWC [23]	87.20 ± 0.41	72.33 ± 0.57	57.11 ± 1.32	-	-	71.87 ± 1.00	61.87 ± 0.43
	AdaStreams [50]	92.58 ± 0.90	84.73 ± 1.09	62.53 ± 1.34	-	-	86.14 ± 0.52	66.39 ± 0.44
	CNLL [20]	88.19 ± 0.42	87.52 ± 0.48	75.15 ± 0.23	-	-	87.33 ± 0.34	73.23 ± 0.08
	Meta-DR [41]	85.07 ± 0.36	81.16 ± 0.91	70.20 ± 0.32	-	-	81.16 ± 0.23	70.65 ± 0.55
	SPR [21]	84.57 ± 0.45	82.57 ± 0.28	70.49 ± 0.46	-	-	79.27 ± 1.21	67.19 ± 1.01
	PuriDivER [3]	92.95 ± 0.89	80.76 ± 1.43	69.88 ± 1.19	-	-	82.70 ± 1.03	68.87 ± 1.05
	Co-teaching [16]	91.27 ± 0.66	85.42 ± 0.45	70.62 ± 0.24	-	-	87.60 ± 0.29	70.62 ± 0.27
	ϵ-Softmax [42]	91.56 ± 0.43	86.35 ± 0.12	53.19 ± 0.22	-	-	87.04 ± 0.30	71.65 ± 0.45
	ContinualCRUST [33]	95.07 ± 0.99	75.96 ± 1.98	52.39 ± 0.66	-	-	75.18 ± 1.85	52.05 ± 3.95
	STAR [10]	96.22 ± 0.39	85.99 ± 0.21	66.32 ± 0.26	-	-	85.72 ± 2.76	60.28 ± 2.20
	WSC [51]	95.04 ± 1.15	83.18 ± 1.99	63.69 ± 0.35	-	-	80.24 ± 0.89	58.46 ± 2.00
	CNLDD	94.49 ± 0.23	89.17 ± 0.55	76.24 ± 0.78	-	-	88.11 ± 0.28	73.44 ± 1.21
FMoW	Finetune	55.81 ± 0.65	38.69 ± 1.03	33.35 ± 1.32	42.51 ± 1.55	33.80 ± 0.60	40.77 ± 1.18	31.56 ± 1.04
	ER [5]	59.53 ± 1.13	40.77 ± 1.39	34.91 ± 0.82	45.09 ± 0.71	35.01 ± 1.22	42.65 ± 1.31	32.56 ± 0.71
	Online EWC [23]	58.19 ± 1.43	39.15 ± 1.59	33.89 ± 1.31	42.79 ± 1.76	32.35 ± 0.72	39.39 ± 1.27	30.51 ± 1.11
	AdaStreams [50]	58.76 ± 0.93	55.16 ± 1.58	47.32 ± 1.08	53.19 ± 0.69	38.51 ± 0.24	48.53 ± 1.10	29.15 ± 8.23
	CNLL [20]	55.95 ± 2.09	48.26 ± 0.39	42.78 ± 1.36	53.15 ± 0.32	42.81 ± 0.25	49.12 ± 0.78	36.47 ± 1.11
	Meta-DR [41]	70.77 ± 0.91	51.63 ± 0.67	37.81 ± 0.78	53.69 ± 1.32	38.40 ± 1.21	52.36 ± 1.94	36.36 ± 1.44
	SPR [21]	46.50 ± 0.00	39.49 ± 0.00	31.89 ± 0.00	39.13 ± 1.43	29.48 ± 0.00	39.35 ± 0.00	25.75 ± 0.00
	PuriDivER [3]	62.52 ± 1.14	45.74 ± 0.65	36.05 ± 0.89	48.50 ± 1.13	36.99 ± 1.78	45.98 ± 3.56	33.13 ± 3.74
	Co-teaching [16]	51.95 ± 1.47	41.00 ± 1.15	31.72 ± 0.94	44.80 ± 2.23	32.92 ± 2.19	42.82 ± 0.68	30.88 ± 1.18
	ϵ-Softmax [42]	53.35 ± 2.17	49.94 ± 0.49	42.66 ± 0.68	48.41 ± 1.57	36.99 ± 0.89	46.98 ± 1.74	26.43 ± 1.05
	ContinualCRUST [33]	69.61 ± 2.16	54.00 ± 0.69	42.07 ± 0.59	57.47 ± 2.80	44.40 ± 1.29	55.84 ± 1.94	45.15 ± 0.64
	STAR [10]	74.56 ± 0.25	61.45 ± 1.37	45.88 ± 4.04	60.88 ± 0.35	44.38 ± 0.33	59.18 ± 4.77	41.48 ± 9.39
	WSC [51]	74.73 ± 0.33	63.94 ± 0.42	44.90 ± 1.34	62.17 ± 0.45	43.01 ± 0.69	64.46 ± 0.20	48.44 ± 0.49
	CNLDD	75.16 ± 0.28	67.42 ± 0.52	54.85 ± 0.81	64.84 ± 0.71	46.23 ± 0.75	65.22 ± 0.13	50.45 ± 1.50

labels are randomly selected from each year as the test set, while the remaining examples are used as the training set.

The *FMoW* dataset, comprising satellite imagery from 2002 to 2017, is initially designed to support humanitarian and policy efforts by monitoring croplands and predicting poverty levels. Due to human activity, temporal shift inevitably exists in the distribution of satellite imagery, making *FMoW* a suitable real-world dataset for studying distribution shift. In our experiments, we use the examples from the ten categories of this dataset with the most examples to mitigate the impact of minority categories on model training, resulting in 51,946 training examples and 6,432 test examples. Here, test examples are drawn uniformly from 2002 to 2017. During training, each input image is resized to 224×224×3, the size of new data at each timestep is set to 5,000, and the size of memory buffer is set to 2,000.

To align with the experiments in the previous section, we also investigate three noise settings, namely symmetric noise, pairflip noise and instance-dependent noise. It is important to note that the pairflip noise is not studied on *Yearbook* dataset due to its equivalence to symmetric label noise in binary classification. The backbone network employed in both datasets is ResNet-18 [17]. For our CNLDD method, α_t and ρ should be small to maintain historical knowledge and the number of clusters K should be set to a moderate value to ensure an effective knowledge transfer. The sensitivity analysis in Section 7.3 also provides justifications on the choices of hyperparameters. Therefore, hyperparameters on *Yearbook* are set as $\rho = 0.25$, $K = 5$, and $\alpha_t = 0.1$, while for *FMoW* dataset they are $\rho = 0.20$, $K = 5$, and $\alpha_t = 0.2$.

The experimental results on *Yearbook* and *FMoW* datasets are presented in Tab. 4. As shown in this table, our CNLDD method achieves the highest classification accuracies across almost all the noise cases, except for the clean. 0% setting on *Yearbook* dataset. This is due to the sophisticated weight perturbation technique adopted in ContinualCRUST, which facilitates the learning of a stable parameter space in noise-free scenarios. On *Yearbook* dataset, CNLDD consistently outperforms AdaStreams under instance-dependent noise scenarios, which can be attributed to the fact that AdaStreams only models the class-conditional noise transition matrix, while the proposed CNLDD explicitly characterizes the instance-dependent noise transition matrix with the HOC [52] algorithm. On *FMoW* dataset, the methods relying on heuristic sample selection strategies, such as PuriDivER and Co-teaching, fail to achieve satisfactory performance. Additionally, the proposed CNLDD method outperforms the second-best method, *i.e.*, WSC, by a margin of 2.01% under the most challenging setting (namely "inst. 40%"). This result implies that WSC exhibits limited capability in learning discriminative representations when exposed to severe label noise.

In a word, the classification results on real-world datasets clearly verify that CNLDD is also effective in handling classification tasks with temporal distribution shift.

7.3 Sensitivity Analysis

In this section, we perform detailed experiments to evaluate the sensitivity of the performance of our CNLDD to parameter variations. Specifically, the analysis focuses on the distribution combination coefficient α_t, the ratio ρ for the first-step subset selection in the buffer update strategy, the number of clusters K in the clustering algorithm, and the weight coefficients λ_1 and λ_2 in the objective function. To ensure generality, experiments are conducted on *PACS*, *Digits*, *Yearbook*, and *FMoW* datasets with the most challenging noise setting (namely "inst. 40%").

The experimental results for the distribution combina-

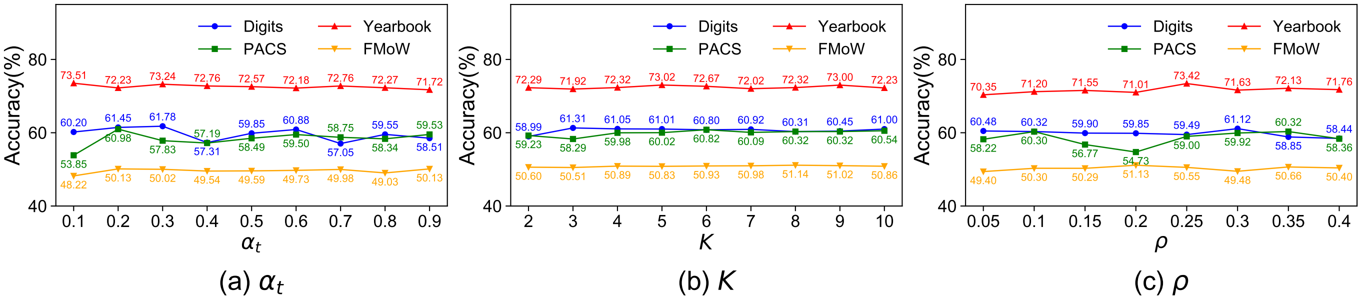

(a) α_t (b) K (c) ρ

Fig. 4. Parametric sensitivity under different values of (a) α_t, (b) K, and (c) ρ. The experiments are conducted on *Digits*, *PACS*, *Yearbook*, and *FMoW* datasets.

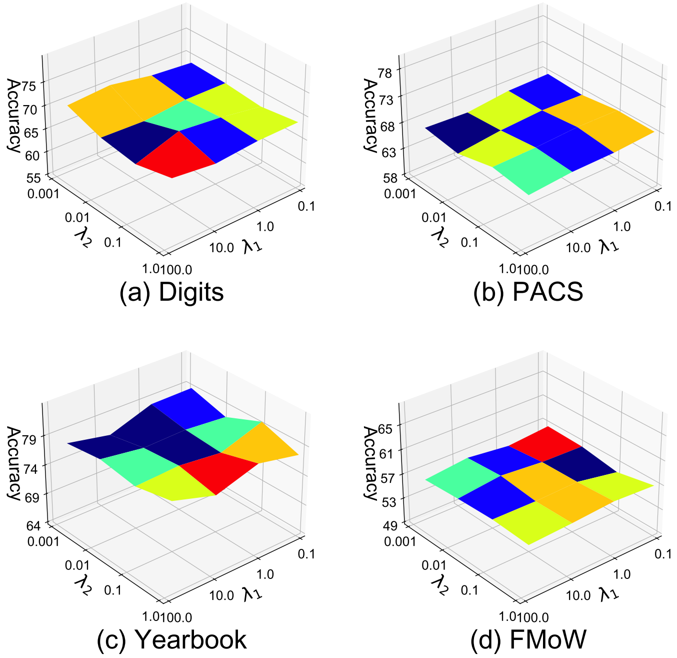

(a) Digits (b) PACS

(c) Yearbook (d) FMoW

Fig. 5. Parametric sensitivity of the CNLDD method with different values of λ_1 and λ_2. The experiments are conducted on *Digits*, *PACS*, *Yearbook*, and *FMoW* datasets.

TABLE 5
Average test accuracies (%) under three ablation settings, namely: (I) w/o the two-step buffer update strategy, (II) w/o the selective transfer mechanism, and (III) w/o the density ratio reweighting. The best record on each dataset is highlighted in **bold**.

Setting	*Digits*	*PACS*	*Yearbook*	*FMoW*
(I)	57.14	57.09	71.10	44.11
(II)	50.85	54.88	72.09	49.60
(III)	48.29	51.68	70.80	46.18
CNLDD	**61.69**	**60.85**	**73.44**	**50.45**

tion coefficient α_t, the selection ratio ρ, and the number of clusters K are shown in Fig. 4. As shown in Fig. 4(a), small values of α_t generally result in satisfactory classification accuracies. For instance, on *Digits* dataset, when α_t is set to 0.2, the classification accuracy is 61.45%, and it improves to 61.78% when α_t is set to 0.3. On *PACS* dataset, a value of $\alpha_t = 0.2$ achieves an accuracy of 60.98%, and on *Yearbook* dataset, a smaller value of α_t also corresponds to relatively higher accuracy. Therefore, setting α_t within the range of $(0.1, 0.3)$ yields the encouraging results overall. Additionally, the evaluation of the number of clusters K in K-Means algorithm (Fig. 4(b)) reveals that moderate values of K, such as 5 or 6, generally yield better results. For example, on *PACS* dataset, $K = 6$ results in the highest accuracy of 60.82%. Lastly, Fig. 4(c) shows that the CNLDD algorithm shows sensitivity to the selection ratio ρ. The best performance is observed when $\rho \in \{0.20, 0.30\}$.

For the weight coefficients λ_1 and λ_2 in the objective function (*i.e.*, Eq. (17)), the classification accuracies under various combinations are shown in Fig. 5. Here, the range of λ_1 is $\{0.1, 1.0, 10.0, 100.0\}$, and λ_2 is varied over $\{0.001, 0.01, 0.1, 1.0\}$. The experimental results reveal that the classification performance of CNLDD is not sensitive to the selection of (λ_1, λ_2). In general, large values of λ_1 and small values of λ_2 tend to yield consistently better results.

7.4 Ablation Study

In this section, we conduct ablative experiments to evaluate the contribution of each component in our CNLDD.

Our theoretical analysis in Section 4 reveals three critical factors that lead to catastrophic forgetting, namely selection bias of buffered data, distribution shift, and label noise. Therefore, we examine the effectiveness of the three techniques introduced in Section 5, each of which targets one of these challenging factors. Specifically, to evaluate the effectiveness of CNLDD in mitigating selection bias of buffered data, we replace the proposed two-step buffer update strategy (Section 5.1) with the commonly employed reservoir sampling strategy [5], [40], [43]. Moreover, regarding the factor of distribution shift, we eliminate the discrepancy-based selective transfer mechanism (Section 5.4) by setting the weight vector $\mathbf{q}$ to a uniform vector. Additionally, to evaluate the robustness of CNLDD against label noise, we remove the density ratios from the objective function, *i.e.*, $\beta(\cdot, \cdot)$ in Eq. (17). The three ablation settings are respectively referred to as (I), (II), and (III) in Tab. 5. Consistent with the experiments in Section 7.3, the noise setting utilized here is the most challenging case, namely “inst. 40%”.

The experimental results for three ablation settings are presented in Tab. 5, which indicate that the absence of any of buffer update strategy, discrepancy-based selective transfer, and label noise handling will lead to performance degradation. Therefore, all components in our CNLDD method are indispensable, as they play crucial roles in alleviating catastrophic forgetting in continual noisy label learning.

8 Conclusion and Future Work

In this paper, we theoretically analyze the problem of learning from streaming noisy data with distribution shift, and we derive an upper bound for the cumulative generalization error. This bound highlights critical factors that lead to catastrophic forgetting and affect the overall continual learning performance, namely buffered data selection bias, distribution shift, and label noise. Our theoretical findings directly induce the proposed method of Continual Noisy Label Learning on Drifting Data Streams (termed "CNLDD"). To address the above challenges, CNLDD contains a two-step buffer update strategy to reduce buffered data selection bias, a selective knowledge transfer technique to mitigate distribution shift, and a density ratio reweighting approach to handle instance-dependent label noise. Thanks to the unified modeling, CNLDD demonstrates superior performance when compared with various state-of-the-art label noise learning and continual learning approaches on standard benchmark and real-world datasets.

For future work, we plan to further develop our theoretical framework to investigate the upper bound of cumulative generalization error in class-incremental continual learning.

References

[1] D. Arpit, S. Jastrzębski, N. Ballas, D. Krueger, E. Bengio, M. S. Kanwal, T. Maharaj, A. Fischer, A. Courville, Y. Bengio *et al.*, "A closer look at memorization in deep networks," in *International Conference on Machine Learning*. PMLR, 2017, pp. 233–242.

[2] P. Awasthi, C. Cortes, and C. Mohri, "Theory and algorithm for batch distribution drift problems," in *International Conference on Artificial Intelligence and Statistics*, 2023, pp. 9826–9851.

[3] J. Bang, H. Koh, S. Park, H. Song, J.-W. Ha, and J. Choi, "Online continual learning on a contaminated data stream with blurry task boundaries," in *IEEE Conference on Computer Vision and Pattern Recognition*, 2022, pp. 9275–9284.

[4] A. Beck, *First-Order Methods in Optimization*. Society for Industrial and Applied Mathematics, 2017.

[5] A. Chaudhry, M. Rohrbach, M. Elhoseiny, T. Ajanthan, P. K. Dokania, P. H. Torr, and M. Ranzato, "On tiny episodic memories in continual learning," *arXiv preprint arXiv:1902.10486*, 2019.

[6] H. Cheng, Z. Zhu, X. Li, Y. Gong, X. Sun, and Y. Liu, "Learning with instance-dependent label noise: A sample sieve approach," in *International Conference on Learning Representations*, 2021.

[7] W. J. Cook, W. H. Cunningham, W. R. Pulleyblank, and A. Schrijver, *Combinatorial Optimization*. Springer, 1998.

[8] F. R. Cordeiro and G. Carneiro, "A survey on deep learning with noisy labels: How to train your model when you cannot trust on the annotations?" in *SIBGRAPI Conference on Graphics, Patterns and Images*, 2020, pp. 9–16.

[9] J. Deng, W. Dong, R. Socher, L.-J. Li, K. Li, and F.-F. Li, "ImageNet: A large-scale hierarchical image database," in *IEEE Conference on Computer Vision and Pattern Recognition*, 2009, pp. 248–255.

[10] M. Eskandar, T. Imtiaz, D. Hill, Z. Wang, and J. Dy, "STAR: Stability-inducing weight perturbation for continual learning," in *International Conference on Learning Representations*, 2025.

[11] M. Farajtabar, N. Azizan, A. Mott, and A. Li, "Orthogonal gradient descent for continual learning," in *International Conference on Artificial Intelligence and Statistics*, 2020, pp. 3762–3773.

[12] T. T. Gido M. van de Ven and A. S. Tolias, "Three types of incremental learning," *Nature Machine Intelligence*, 2022.

[13] C. Gong, Y. Ding, B. Han, G. Niu, J. Yang, J. You, D. Tao, and M. Sugiyama, "Class-wise denoising for robust learning under label noise," *IEEE Transactions on Pattern Analysis and Machine Intelligence*, vol. 45, no. 3, pp. 2835–2848, 2023.

[14] S. L. Hakimi, "Optimum locations of switching centers and the absolute centers and medians of a graph," *Operations Research*, vol. 12, no. 3, pp. 450–459, 1964.

[15] O. B. Halima, B. I. Adebimpe, and N. A. Maxwell, "Adaptive machine learning models: Concepts for real-time financial fraud prevention in dynamic environments," *World Journal of Advanced Engineering Technology and Sciences*, vol. 12, no. 2, pp. 21–34, 2024.

[16] B. Han, Q. Yao, X. Yu, G. Niu, M. Xu, W. Hu, I. Tsang, and M. Sugiyama, "Co-teaching: Robust training of deep neural networks with extremely noisy labels," in *Advances in Neural Information Processing Systems*, vol. 31, 2018, pp. 8527–8537.

[17] K. He, X. Zhang, S. Ren, and J. Sun, "Deep residual learning for image recognition," in *IEEE Conference on Computer Vision and Pattern Recognition*, 2016, pp. 770–778.

[18] D. Hendrycks, N. Mu, E. D. Cubuk, B. Zoph, J. Gilmer, and B. Lakshminarayanan, "AugMix: A simple data processing method to improve robustness and uncertainty," in *International Conference on Learning Representations*, 2020.

[19] R. A. Jacobs, M. I. Jordan, S. J. Nowlan, and G. E. Hinton, "Adaptive mixtures of local experts," *Neural Computation*, vol. 3, no. 1, pp. 79–87, 1991.

[20] N. Karim, U. Khalid, A. Esmaeili, and N. Rahnavard, "CNLL: A semi-supervised approach for continual noisy label learning," in *IEEE Conference on Computer Vision and Pattern Recognition Workshops*, 2022, pp. 3877–3887.

[21] C. D. Kim, J. Jeong, S. Moon, and G. Kim, "Continual learning on noisy data streams via self-purified replay," in *IEEE International Conference on Computer Vision*, 2021, pp. 537–547.

[22] D. Kingma and J. Ba, "Adam: A method for stochastic optimization," in *International Conference on Learning Representations*, 2014.

[23] J. Kirkpatrick, R. Pascanu, N. Rabinowitz, J. Veness, G. Desjardins, A. A. Rusu, K. Milan, J. Quan, T. Ramalho, A. Grabska-Barwinska *et al.*, "Overcoming catastrophic forgetting in neural networks," *Proceedings of the National Academy of Sciences*, vol. 114, no. 13, pp. 3521–3526, 2017.

[24] P. Kumari, C. Joohi, B. Afshin, H. Boqiang, A. Reza, and M. Dorit, "Continual learning in medical image analysis: A comprehensive review of recent advancements and future prospects," *arXiv preprint arXiv:2312.17004*, 2023.

[25] D. Li, Y. Yang, Y.-Z. Song, and T. Hospedales, "Learning to generalize: Meta-learning for domain generalization," in *AAAI Conference on Artificial Intelligence*, 2018.

[26] J. Li, M. Zhang, K. Xu, J. P. Dickerson, and J. Ba, "Noisy labels can induce good representations," *arXiv preprint arXiv:2012.12896*, 2020.

[27] J. Li, R. Socher, and S. C. Hoi, "DivideMix: Learning with noisy labels as semi-supervised learning," in *International Conference on Learning Representations*, 2020.

[28] T. Liu and D. Tao, "Classification with noisy labels by importance reweighting," *IEEE Transactions on Pattern Analysis and Machine Intelligence*, vol. 38, no. 3, pp. 447–461, 2015.

[29] X. Liu, C. Wu, M. Menta, L. Herranz, B. Raducanu, A. D. Bagdanov, S. Jui, and J. v. de Weijer, "Generative feature replay for class-incremental learning," in *IEEE Conference on Computer Vision and Pattern Recognition Workshops*, 2020, pp. 226–227.

[30] W. Luo, S. Chen, T. Liu, B. Han, G. Niu, M. Sugiyama, D. Tao, and C. Gong, "Estimating per-class statistics for label noise learning," *IEEE Transactions on Pattern Analysis and Machine Intelligence*, pp. 1–17, 2024.

[31] Y. Mansour, M. Mohri, and A. Rostamizadeh, "Domain adaptation with multiple sources," in *Advances in Neural Information Processing Systems*, vol. 21, 2008, pp. 1–8.

[32] M. Mohri, A. Rostamizadeh, and A. Talwalkar, *Foundations of Machine Learning*. MIT press, 2018.

[33] E. Mucllari, A. Raghavan, and Z. A. Daniels, "Noise-tolerant coreset-based class incremental continual learning," *arXiv preprint arXiv:2504.16763*, 2025.

[34] P. Pan, S. Swaroop, A. Immer, R. Eschenhagen, R. Turner, and M. E. E. Khan, "Continual deep learning by functional regularisation of memorable past," in *Advances in Neural Information Processing Systems*, vol. 33, 2020, pp. 4453–4464.

[35] O. Sener and S. Savarese, "Active learning for convolutional neural networks: A core-set approach," in *International Conference on Learning Representations*, 2018.

[36] S. Shalev-Shwartz and S. Ben-David, *Understanding Machine Learning: From Theory to Algorithms*. Cambridge University Press, 2014.

[37] H. Shin, J. K. Lee, J. Kim, and J. Kim, "Continual learning with deep generative replay," in *Advances in Neural Information Processing Systems*, vol. 30, 2017.

[38] D. B. Shmoys, "Computing near-optimal solutions to combinatorial optimization problems," *Combinatorial Optimization. DIMACS*

Series in Discrete Mathematics and Theoretical Computer Science., vol. 20, pp. 355–397, 1995.

[39] J. Tang, S. Chen, G. Niu, H. Zhu, J. T. Zhou, C. Gong, and M. Sugiyama, "Direct distillation between different domains," in *European Conference on Computer Vision*, 2025, pp. 154–172.

[40] J. S. Vitter, "Random sampling with a reservoir," *ACM Transactions on Mathematical Software*, vol. 11, no. 1, pp. 37–57, 1985.

[41] R. Volpi, D. Larlus, and G. Rogez, "Continual adaptation of visual representations via domain randomization and meta-learning," in *IEEE Conference on Computer Vision and Pattern Recognition*, 2021, pp. 4443–4453.

[42] J. Wang, X. Zhou, D. Zhai, J. Jiang, X. Ji, and X. Liu, "Epsilon-Softmax: Approximating one-hot vectors for mitigating label noise," in *Advances in Neural Information Processing Systems*, 2024.

[43] L. Wang, X. Zhang, H. Su, and J. Zhu, "A comprehensive survey of continual learning: Theory, method and application," *IEEE Transactions on Pattern Analysis and Machine Intelligence*, vol. 46, no. 8, pp. 5362–5383, 2024.

[44] S. Wang, X. Li, J. Sun, and Z. Xu, "Training networks in null space of feature covariance for continual learning," in *IEEE Conference on Computer Vision and Pattern Recognition*, 2021, pp. 184–193.

[45] X. Xia, B. Han, Y. Zhan, J. Yu, M. Gong, C. Gong, and T. Liu, "Combating noisy labels with sample selection by mining high-discrepancy examples," in *IEEE International Conference on Computer Vision*, 2023, pp. 1833–1843.

[46] X. Xia, P. Lu, C. Gong, B. Han, J. Yu, J. Yu, and T. Liu, "Regularly truncated m-estimators for learning with noisy labels," *IEEE Transactions on Pattern Analysis and Machine Intelligence*, vol. 46, no. 5, pp. 3522–3536, 2024.

[47] H. Yao, C. Choi, B. Cao, Y. Lee, P. W. W. Koh, and C. Finn, "Wild-Time: A benchmark of in-the-wild distribution shift over time," in *Advances in Neural Information Processing Systems*, vol. 35, 2022, pp. 10 309–10 324.

[48] J. Yoo, Y. Liu, F. Wood, and G. Pleiss, "Layerwise proximal replay: A proximal point method for online continual learning," in *International Conference on Machine Learning*, 2024.

[49] F. Zenke, B. Poole, and S. Ganguli, "Continual learning through synaptic intelligence," in *International Conference on Machine Learning*, 2017, pp. 3987–3995.

[50] Z.-Y. Zhang, Y.-Y. Qian, Y.-J. Zhang, Y. Jiang, and Z.-H. Zhou, "Adaptive learning for weakly labeled streams," in *Proceedings of ACM SIGKDD Conference on Knowledge Discovery and Data Mining*, 2022, p. 2556–2564.

[51] Z.-H. Zhou, J.-J. Wang, T. Wei, and M.-L. Zhang, "Weakly-supervised contrastive learning for imprecise class labels," in *International Conference on Machine Learning*, 2025.

[52] Z. Zhu, Y. Song, and Y. Liu, "Clusterability as an alternative to anchor points when learning with noisy labels," in *International Conference on Machine Learning*. PMLR, 2021, pp. 12 912–12 923.

Wenshui Luo received his Master's degree from Nanjing University of Science and Technology in 2025. Currently, he is a Ph.D. student at Shanghai Jiao Tong University, under the supervision of Prof. Chen Gong. His research interests mainly lie in continual learning and weakly-supervised learning.

Shuo Chen is currently an Associate Professor in the School of Intelligence Science and Technology at Nanjing University China. He is also a Visiting Scientist at RIKEN Center for Advanced Intelligence Project (RIKEN-AIP) Japan. Before that, he was a Postdoctoral Researcher and Research Scientist at RIKEN-AIP from 2020 to 2024. He received his doctoral degree from Nanjing University of Science and Technology in 2020, and he was a CSC visiting student at the University of Pittsburgh USA from 2018 to 2019. His research interests mainly include machine learning and pattern recognition, in particular, self-supervised learning and metric learning. He has published more than 50 technical papers at top-tier conferences such as NeurIPS, ICML, ICLR, CVPR, etc., and prominent journals such as IEEE T-PAMI, IEEE T-IP, IEEE T-NNLS, etc. He has served as the (Senior) Area Chair of NeurIPS, ICML, ICLR, CVPR, ECCV, AAAI, and IJCAI over 20 times, and also served as the Action Editor for Neural Network. He won the "Excellent Doctoral Dissertation Award" of Chinese Institute of Electronics (CIE) and the "Excellent Doctoral Dissertation Nomination" of Chinese Association for Artificial Intelligence (CAAI).

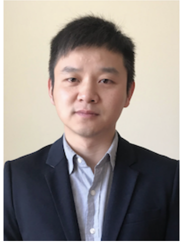

Tao Zhou is currently a Professor at the School of Computer Science and Engineering, Nanjing University of Science and Technology, China. He received a Ph.D. degree from Shanghai Jiao Tong University, in 2016. He was a Postdoctoral Fellow at UNC-CH and a Research Scientist with IIAI. He is an Associate Editor of IEEE TNNLS, IEEE TIP, IEEE TMI, and Pattern Recognition. His research interests include machine learning, computer vision, AI in healthcare, and medical image analysis.

Chen Gong (Senior Member, IEEE) received his dual doctoral degree from Shanghai Jiao Tong University (SJTU) and University of Technology Sydney (UTS), respectively. Currently, he is a full professor in the School of Automation and Intelligent Sensing, Shanghai Jiao Tong University. His research interests mainly include machine learning, data mining, and learning-based vision problems. He has published more than 130 technical papers at prominent journals and conferences such as JMLR, IJCV, IEEE T-PAMI, IEEE T-NNLS, IEEE T-IP, ICML, NeurIPS, ICLR, CVPR, ICCV, ECCV, AAAI, IJCAI, etc. He serves as the associate editor for IEEE T-CSVT, Neural Networks, and NePL, and also the Area Chair or Senior PC member of several top-tier conferences such as ICML, ICLR, AAAI, IJCAI, ECML-PKDD, AISTATS, ICDM, ACM MM, etc. He won the "Excellent Doctorial Dissertation Award" of Chinese Association for Artificial Intelligence, "Young Elite Scientists Sponsorship Program" of China Association for Science and Technology, and "Wu Wen-Jun AI Excellent Youth Scholar Award". He was also selected as the "Global Top Chinese Young Scholars in AI" released by Baidu, and "World's Top 2% Scientists" released by Stanford University.

A Theoretical Perspective on Streaming Noisy Data with Distribution Shift

Wenshui Luo, Shuo Chen, Tao Zhou, *Member, IEEE,* Chen Gong, *Senior Member, IEEE*

Contents

- *This research is supported by National Natural Science Fund of China (Nos: 62336003, 12371510, 62576153, 62506155), Shanghai Municipal Science and Technology Major Project (No: 2025SHZDZX025G12), Provincial Natural Science Fund of Jiangsu (No: BK20251985), and Suzhou Municipal Leading Talents Fund (2025).*

- *W. Luo and C. Gong are with the School of Automation and Intelligent Sensing, Shanghai Jiao Tong University, Shanghai, P. R. China.*
  E-mail: randylo@sjtu.edu.cn; chen.gong@sjtu.edu.cn
- *S. Chen is with the School of Intelligence Science and Technology, Nanjing University, P. R. China, and is also with Center for Advanced Intelligence Project, RIKEN, Japan.*
  E-mail: shuo.chen@nju.edu.cn
- *T. Zhou is with the School of Computer Science and Engineering, Nanjing University of Science and Technology, P. R. China.*
  E-mail: taozhou.ai@gmail.com
- *Corresponding author: C. Gong.*

A Verification of Assumption 2

In this section, we present rationales to support Assumption 2, namely, the loss function and the density ratio function are both upper-bounded.

Boundedness of the loss function. In our paper, the Cross-Entropy (CE) loss is adopted as the loss function, so we first prove that this loss function is indeed upper-bounded. Specifically, the CE loss is given by

$$\ell(f_{\boldsymbol{\theta}}(\mathbf{x}), \mathbf{e}_k) = -\log \widehat{p}(Y = \mathbf{e}_k | X = \mathbf{x}) = -\log f_{\boldsymbol{\theta}}(\mathbf{x})_k. \tag{1}$$

Here, $f_{\boldsymbol{\theta}}(\mathbf{x}) = [\widehat{p}(Y = \mathbf{e}_1 | X = \mathbf{x}), \widehat{p}(Y = \mathbf{e}_2 | X = \mathbf{x}), \cdots, \widehat{p}(Y = \mathbf{e}_C | X = \mathbf{x})]$ is the output probabilities by a neural network, and C is the number of classes. Moreover, for all $i \in \{1, 2, \cdots, C\}$, the probability for the k-th class is $f_{\boldsymbol{\theta}}(\mathbf{x})_k = \frac{\exp(g_{\boldsymbol{\theta}}(\mathbf{x})_k)}{\sum_{k'=1}^{C} \exp(g_{\boldsymbol{\theta}}(\mathbf{x})_{k'})} > 0$, where $g_{\boldsymbol{\theta}}(\mathbf{x})_k$ is the k-th logit. Therefore, there always exists a small positive constant $\epsilon > 0$, such that $\min_k f_{\boldsymbol{\theta}}(\mathbf{x})_k > \epsilon > 0$, and thus it holds that $0 \leq \ell(f_{\boldsymbol{\theta}}(\mathbf{x}), \mathbf{e}_k) < -\log \epsilon$. With this condition, it directly holds that $\sup_{f_{\boldsymbol{\theta}} \in \mathcal{F}_\Theta, \mathbf{x} \in \mathcal{X}, 1 \leq i \leq C} \ell(f_{\boldsymbol{\theta}}(\mathbf{x}), \mathbf{e}_i) < -\log \epsilon =: \overline{L}$. Therefore, the boundedness of the CE loss has been proved. Here, we also provide some examples of classical loss functions which are also upper-bounded:

- The Mean Absolute Error (MAE) loss $\ell(f_{\boldsymbol{\theta}}(\mathbf{x}), \mathbf{e}_k) = \frac{1}{C} \| f_{\boldsymbol{\theta}}(\mathbf{x}) - \mathbf{e}_k \|_1$ is upper-bounded by 1;
- The Mean Squared Error (MSE) loss $\ell(f_{\boldsymbol{\theta}}(\mathbf{x}), \mathbf{e}_k) = \frac{1}{C} \| f_{\boldsymbol{\theta}}(\mathbf{x}) - \mathbf{e}_k \|_2^2$ is also upper-bounded by 1.

It should be mentioned that previous studies, such as [6], [15] (in the setting of label noise learning), and [1] (in the setting of learning from distribution-shifted data), have adopted this assumption as well.

Boundedness of the density ratio function. In our setting (namely continual noisy label learning), the posterior probability w.r.t. the noisy label is given by

$$\widetilde{P}(\widetilde{Y} = \mathbf{e}_k | X = \mathbf{x}) = \sum_{j=1}^{C} P(\widetilde{Y} = \mathbf{e}_k | X = \mathbf{x}, Y = \mathbf{e}_j) \cdot P(Y = \mathbf{e}_j | X = \mathbf{x}) = \sum_{j=1}^{C} T_{jk}(\mathbf{x}) P(Y = \mathbf{e}_j | X = \mathbf{x}), \tag{2}$$

where $T_{jk}(\mathbf{x}) = P(\widetilde{Y} = \mathbf{e}_k | X = \mathbf{x}, Y = \mathbf{e}_j)$ is the (j, k)-th element of the instance-dependent transition matrix $\mathbf{T}(\mathbf{x})$. With this transition matrix, the density ratio function can be formulated as

$$\beta_{\mathbb{P}}(\mathbf{x}, \mathbf{e}_k) = \frac{P(Y = \mathbf{e}_k | X = \mathbf{x})}{\widetilde{P}(\widetilde{Y} = \mathbf{e}_k | X = \mathbf{x})} = \frac{P(Y = \mathbf{e}_k | X = \mathbf{x})}{\sum_{j=1}^{C} T_{jk}(\mathbf{x}) P(Y = \mathbf{e}_j | X = \mathbf{x})}. \tag{3}$$

Next, we prove that $\beta_{\mathbb{P}}(\mathbf{x}, \mathbf{e}_k)$ is upper-bounded by a positive constant. To this end, we first study the instance-independent case, and then we analyze the instance-dependent case.

- **Instance-independent case.** In this case, the transition matrix $\mathbf{T}(\mathbf{x}) = \mathbf{T} = (T_{ij})_{1 \leq i, j \leq C}$ is fixed for each example $(\mathbf{x}, \widetilde{\mathbf{y}})$. In practice, there always exists a positive constant δ, such that $T_{kk} > \delta > 0$, $\forall\, k \in \{1, 2, \cdots, C\}$, otherwise, all the examples with ground-truth label $\mathbf{e}_k$ are mislabeled, which would be unrealistic in real-world scenarios. With this condition, it holds that

  $$\beta_{\mathbb{P}}(\mathbf{x}, \mathbf{e}_k) \leq \frac{P(Y = \mathbf{e}_k | X = \mathbf{x})}{T_{kk} P(Y = \mathbf{e}_k | X = \mathbf{x})} = \frac{1}{T_{kk}} < \frac{1}{\delta}. \tag{4}$$

  Therefore, $\sup_{(\mathbf{x}, \widetilde{\mathbf{y}}) \in \mathrm{supp}(\widetilde{\mathbb{P}})} \beta_{\mathbb{P}}(\mathbf{x}, \widetilde{\mathbf{y}}) < \frac{1}{\delta} =: \overline{\beta}$, and the boundedness of the density ratio function $\beta_{\mathbb{P}}(\mathbf{x}, \mathbf{e}_k)$ in the instance-independent case has been established. Here, we also provide some practical examples to show that $T_{kk} > \delta > 0$, $\forall\, k \in \{1, 2, \cdots, C\}$ can be satisfied:

  (a) Under the symmetric noise case with a noise rate of ϵ, $T_{kk} = 1 - \epsilon$, and $T_{kj} = \frac{\epsilon}{C-1}$, $\forall\, k, j \in \{1, 2, \cdots, C\}, k \neq j$. It directly holds that $T_{kk} \geq 1 - \epsilon = \delta > 0$.

  (b) Under the pairflip noise setting with a noise rate of ϵ, $T_{kk} = 1 - \epsilon$, $\forall\, k \in \{1, 2, \cdots, C\}$, and $T_{kj} = \epsilon$ for a $j \neq k$. It also holds that $T_{kk} \geq 1 - \epsilon = \delta > 0$.

  (c) In binary classification, the noise transition matrix is defined as $T = \begin{bmatrix} 1 - \eta_N & \eta_N \\ \eta_P & 1 - \eta_P \end{bmatrix}$, where η_P and η_N are the flip rates of the positive class and the negative class, respectively. According to [3] (Lemma 1) and [14], the binary classification task (with label noise) is learnable only under the condition $\eta_P + \eta_N < 1$. Consequently, it always holds that $1 - \eta_P > 0$ and $1 - \eta_N > 0$.

- **Instance-dependent case.** In this scenario, two prior works [4], [11] have adopted the "non-degenerate noise condition", which requires that $\sum_{j \neq k} T_{kj}(\mathbf{x}) < 1$. This condition is equivalent to ensuring $T_{kk}(\mathbf{x}) > 0$ for all $k \in \{1, 2, \cdots, C\}$. Moreover, it implies that the overall noise level remains within a reasonable range and the clean label information is not completely lost, which aligns with empirical observations in many real-world applications. Under this condition, the boundedness of $\beta_{\mathbb{P}}(\mathbf{x}, \mathbf{e}_k)$ can be established following a line of analysis similar to that used in the instance-independent case. In practice, a small positive constant μ can be introduced to regularize the learning of a transition matrix, namely, $\mathbf{T}(\mathbf{x}) \leftarrow (1 - \mu)\mathbf{T}(\mathbf{x}) + \mu \mathbf{I}$, where $\mathbf{I} \in \mathbb{R}^{C \times C}$ denotes the identity matrix. This regularization guarantees that $T_{kk} \geq \mu$, and thus the corresponding density ratio is bounded. Notably, this regularization strategy has also been adopted by [10] in their implementation.

In summary, the two conditions in Assumption 2 can be easily satisfied in practice.

B Proofs of Theoretical Results

In this section, we present rigorous and detailed proofs for the theorems presented in this paper. Additionally, we provide supplementary results to further elucidate and support the proposed CNLDD method.

B.1 Proof of Theorem 1

Proof. According to Assumption 1, cumulative generalization error can be formulated and upper bounded as:

$$\begin{aligned}
&\mathbb{E}_{\mathbb{D}_{1:t}}[\ell(f_{\boldsymbol{\theta}}(\mathbf{x}),\mathbf{y})] = (1-\alpha_t)\mathbb{E}_{\mathbb{D}_{1:t-1}}\left[\ell(f_{\boldsymbol{\theta}}(\mathbf{x}),\mathbf{y})\right] + \alpha_t\mathbb{E}_{\mathbb{D}_t}\left[\ell(f_{\boldsymbol{\theta}}(\mathbf{x}),\mathbf{y})\right] \\
&\leq (1-\alpha_t)\mathbb{E}_{\mathbb{P}^{\mathcal{M}}_{1:t-1}}\left[\ell(f_{\boldsymbol{\theta}}(\mathbf{x}),\mathbf{y})\right] + (1-\alpha_t)\left|\mathbb{E}_{\mathbb{P}^{\mathcal{M}}_{1:t-1}}[\ell(f_{\boldsymbol{\theta}}(\mathbf{x}),\mathbf{y})] - \mathbb{E}_{\mathbb{D}_{1:t-1}}[\ell(f_{\boldsymbol{\theta}}(\mathbf{x}),\mathbf{y})]\right| + \alpha_t\mathbb{E}_{\mathbb{D}_t}\left[\ell(f_{\boldsymbol{\theta}}(\mathbf{x}),\mathbf{y})\right] \\
&= (1-\alpha_t)\mathbb{E}_{(\mathbf{x},\widetilde{\mathbf{y}})\sim\widetilde{\mathbb{P}}^{\mathcal{M}}_{1:t-1}}\left[\beta_{\mathbb{P}^{\mathcal{M}}_{1:t-1}}(\mathbf{x},\widetilde{\mathbf{y}})\ell(f_{\boldsymbol{\theta}}(\mathbf{x}),\widetilde{\mathbf{y}})\right] + (1-\alpha_t)Gap(\mathbb{P}^{\mathcal{M}}_{1:t-1},\mathbb{D}_{1:t-1}) + \alpha_t\mathbb{E}_{\widetilde{\mathbb{D}}_t}\left[\beta_{\mathbb{D}_t}(\mathbf{x},\widetilde{\mathbf{y}})\ell(f_{\boldsymbol{\theta}}(\mathbf{x}),\widetilde{\mathbf{y}})\right],
\end{aligned} \tag{5}$$

where $Gap(\mathbb{P}^{\mathcal{M}}_{1:t-1},\mathbb{D}_{1:t-1})$ is defined as:

$$Gap(\mathbb{P}^{\mathcal{M}}_{1:t-1},\mathbb{D}_{1:t-1}) := \left|\mathbb{E}_{\mathbb{P}^{\mathcal{M}}_{1:t-1}}[\ell(f_{\boldsymbol{\theta}}(\mathbf{x}),\mathbf{y})] - \mathbb{E}_{\mathbb{D}_{1:t-1}}[\ell(f_{\boldsymbol{\theta}}(\mathbf{x}),\mathbf{y})]\right|. \tag{6}$$

Therefore, we complete the proof. □

B.2 Proof of Theorem 2

Proof. First, according to the definition of density ratio (*i.e.*, Definition 2), we have $\mathbb{E}_{\widetilde{\mathbb{D}}_t}\left[\beta_{\mathbb{D}_t}(\mathbf{x},\widetilde{\mathbf{y}})\ell(f_{\boldsymbol{\theta}}(\mathbf{x}),\widetilde{\mathbf{y}})\right] = \mathbb{E}_{\mathbb{D}_t}\left[\ell(f_{\boldsymbol{\theta}}(\mathbf{x}),\mathbf{y})\right]$. To facilitate derivation, we define the empirical distributions w.r.t. the K subsets of buffered data as

$$\mathbb{P}_k = \frac{1}{|\mathcal{M}^{(k)}_{1:t-1}|}\sum_{\mathbf{z}=(\mathbf{x},\mathbf{y})\in\mathcal{M}^{(k)}_{1:t-1}}\delta(\mathbf{z}), \quad \forall\, k\in[\![K]\!], \tag{7}$$

where $\delta(\cdot)$ denotes the Dirac delta function. Furthermore, we denote by $m_k = |\mathcal{M}^{(k)}_{1:t-1}|$ the number of examples in the k-th subset of memory buffer, and by $m_{K+1} = n_t = |\widetilde{\mathcal{S}}_t|$ the number of examples in $\widetilde{\mathcal{S}}_t$ at the t-th timestep. The total number of examples is defined as $m = \sum_{i\in[\![K+1]\!]} m_i$. For simplicity and consistency, we use $\mathbb{P}_{K+1}$ to denote the data distribution $\mathbb{D}_t$. The corresponding noisy distributions are denoted by $\{\widetilde{\mathbb{P}}_k\}_{k=1}^K$ and $\widetilde{\mathbb{P}}_{K+1}$, respectively.

Next, we derive the upper bound for Term 3 in Theorem 1, namely $\mathbb{E}_{\widetilde{\mathbb{D}}_t}[\beta_{\mathbb{D}_t}(\mathbf{x},\widetilde{\mathbf{y}})\ell(f_{\boldsymbol{\theta}}(\mathbf{x}),\widetilde{\mathbf{y}})]$. Let $\mathcal{S} = \{(\mathbf{x}_i,\mathbf{y}_i)\}_{i=1}^m$ be a set of m examples drawn from the distribution $\mathbb{P} = \mathbb{P}_1^{m_1}\otimes\mathbb{P}_2^{m_2}\cdots\otimes\mathbb{P}_K^{m_K}\otimes\mathbb{P}_{K+1}^{m_{K+1}}$. Since the injection of label noise is independent for each example in $\mathcal{S}$, the sampling process for $\mathcal{S}$ can equivalently be interpreted as sampling $\widetilde{\mathcal{S}} = \{(\mathbf{x}_i,\widetilde{\mathbf{y}}_i)\}_{i=1}^m$ from the distribution $\widetilde{\mathbb{P}} = \widetilde{\mathbb{P}}_1^{m_1}\otimes\widetilde{\mathbb{P}}_2^{m_2}\cdots\otimes\widetilde{\mathbb{P}}_K^{m_K}\otimes\widetilde{\mathbb{P}}_{K+1}^{m_{K+1}}$.

Inspired by previous work on batch distribution drift [2], the upper bound of $\mathbb{E}_{\widetilde{\mathbb{D}}_t}[\beta_{\mathbb{D}_t}(\mathbf{x},\widetilde{\mathbf{y}})\ell(f_{\boldsymbol{\theta}}(\mathbf{x}),\widetilde{\mathbf{y}})]$ can incorporate empirical losses on both buffered data and newly arrived data. To facilitate derivation of such an upper bound, we introduce the $\mathbf{q}\circ\beta_{\mathbb{P}}$-weighted empirical loss on buffered noisy data and the noisy data $\widetilde{\mathcal{S}}_t$ at timestep t, which is defined as

$$L_{\widetilde{\mathcal{S}}}(\mathbf{q},\beta_{\mathbb{P}},f_{\boldsymbol{\theta}}) := \sum_{i\in[\![m]\!]} q_i\cdot\beta_{\mathbb{P}}(\mathbf{x}_i,\widetilde{\mathbf{y}}_i)\cdot\ell(f_{\boldsymbol{\theta}}(\mathbf{x}_i),\widetilde{\mathbf{y}}_i). \tag{8}$$

Similarly, the $\mathbf{q}$-weighted empirical loss on the corresponding clean data is defined as $L_{\mathcal{S}}(\mathbf{q},f_{\boldsymbol{\theta}}) := \sum_{i\in[\![m]\!]} q_i\cdot\ell(f_{\boldsymbol{\theta}}(\mathbf{x}_i),\mathbf{y}_i)$. The expected risk for each distribution is defined as $\mathcal{L}(\mathbb{P}_k,f_{\boldsymbol{\theta}}) = \mathbb{E}_{\mathbb{P}_k}[\ell(f_{\boldsymbol{\theta}}(\mathbf{x}),\mathbf{y})]$, $\forall\, k\in[\![K+1]\!]$.

Subsequently, to derive the bound on expected risk $\mathcal{L}(\mathbb{P}_k,f_{\boldsymbol{\theta}})$, we further define a function $\Phi(\widetilde{\mathcal{S}})$ as follows [13]:

$$\Phi(\widetilde{\mathcal{S}}) = \sup_{f_{\boldsymbol{\theta}}\in\mathcal{F}_\Theta}\sum_{k=1}^{K+1}\overline{q}_k\mathcal{L}(\mathbb{P}_k,f_{\boldsymbol{\theta}}) - L_{\widetilde{\mathcal{S}}}(\mathbf{q},\beta_{\mathbb{P}},f_{\boldsymbol{\theta}}). \tag{9}$$

By applying McDiarmid's inequality (which only requires independence among random variables), it holds with probability at least $1-\delta$ that

$$\sum_{k=1}^{K+1}\overline{q}_k\mathcal{L}(\mathbb{P}_k,f_{\boldsymbol{\theta}}) - L_{\widetilde{\mathcal{S}}}(\mathbf{q},\beta_{\mathbb{P}},f_{\boldsymbol{\theta}}) \leq \Phi(\widetilde{\mathcal{S}}) \leq \mathbb{E}[\Phi(\widetilde{\mathcal{S}})] + \|\mathbf{q}\|_2\cdot\overline{L}\cdot\sqrt{\frac{\log(1/\delta)}{2}}. \tag{10}$$

Furthermore, since $\mathbb{E}_{\widetilde{\mathcal{S}}}[L_{\widetilde{\mathcal{S}}}(\mathbf{q},\beta_{\mathbb{P}},f_{\boldsymbol{\theta}})] = \sum_{k=1}^{K+1}\overline{q}_k\mathcal{L}(\mathbb{P}_k,f_{\boldsymbol{\theta}})$, by introducing the "ghost sample" [13], it can be shown that

$$\mathbb{E}_{\widetilde{\mathcal{S}}}[\Phi(\widetilde{\mathcal{S}})] \leq 2\cdot\mathfrak{R}_{\mathbf{q}}(\beta_{\mathbb{P}}\circ\ell\circ\mathcal{F}_\Theta) = 2\mathbb{E}_{\widetilde{\mathcal{S}}\sim\widetilde{\mathbb{P}}}\mathbb{E}_{\boldsymbol{\sigma}}\left[\sup_{f_{\boldsymbol{\theta}}\in\mathcal{F}_\Theta}\sigma_i\cdot q_i\cdot\beta_{\mathbb{P}}(\mathbf{x}_i,\widetilde{\mathbf{y}}_i)\cdot\ell(f_{\boldsymbol{\theta}}(\mathbf{x}_i),\widetilde{\mathbf{y}}_i)\right]. \tag{11}$$

Then, we connect the two quantities $\mathbb{E}_{\mathbb{D}_t}[\ell(f_{\boldsymbol{\theta}}(\mathbf{x}),\mathbf{y})]$ and $\sum_{k=1}^{K+1}\overline{q}_k\mathcal{L}(\mathbb{P}_k,f_{\boldsymbol{\theta}})$, which allows us to apply the above inequalities to derive the final upper bound. Based on the notion of distribution discrepancy (namely, Definition 1) and the definition of $\mathcal{L}(\mathbb{P}_k,f_{\boldsymbol{\theta}})$, the following inequality holds with probability at least $1-\delta$:

$$\begin{aligned}
&\mathbb{E}_{\mathbb{D}_t}[\ell(f_{\boldsymbol{\theta}}(\mathbf{x}),\mathbf{y})]-\sum_{k=1}^{K+1}\overline{q}_k\mathcal{L}(\mathbb{P}_k,f_{\boldsymbol{\theta}})\\
&=\sum_{k=1}^{K+1}\overline{q}_k\left\{\mathbb{E}_{\mathbb{D}_t}[\ell(f_{\boldsymbol{\theta}}(\mathbf{x}),\mathbf{y})]-\mathbb{E}_{\mathbb{P}_k}[\ell(f_{\boldsymbol{\theta}}(\mathbf{x}),\mathbf{y})]\right\}\\
&\overset{1}{\leq}\sum_{k=1}^{K+1}\overline{q}_k\sup_{f_{\boldsymbol{\theta}}\in\mathcal{F}_\Theta}\left|\mathbb{E}_{\mathbb{D}_t}[\ell(f_{\boldsymbol{\theta}}(\mathbf{x}),\mathbf{y})]-\mathbb{E}_{\mathbb{P}_k}[\ell(f_{\boldsymbol{\theta}}(\mathbf{x}),\mathbf{y})]\right|\\
&=\sum_{k=1}^{K+1}\overline{q}_k\,disc_{\mathcal{F}_\Theta}(\mathbb{D}_t,\mathbb{P}_k)\\
&\overset{2}{\leq}\sum_{k=1}^{K}\overline{q}_k\,disc_{\mathcal{F}_\Theta}(\mathbb{D}_t,\mathbb{P}_{\mathcal{S}_t})+\sum_{k=1}^{K}\overline{q}_k\,disc_{\mathcal{F}_\Theta}(\mathbb{P}_{\mathcal{S}_t},\mathbb{P}_k)\\
&\overset{3}{\leq}\sum_{k=1}^{K}\overline{q}_k\,disc_{\mathcal{F}_\Theta}(\mathbb{P}_{\mathcal{S}_t},\mathbb{P}_k)+\mathcal{O}\left(\sqrt{\frac{1}{|\widetilde{\mathcal{S}}_t|}}\right),
\end{aligned}\tag{12}$$

where the inequality 2 holds by using triangle inequality and the condition $\mathbb{D}_t=\mathbb{P}_{K+1}$, and the inequality 3 stems from McDiarmid's inequality [13]. Moreover, $\mathbb{P}_{\mathcal{S}_t}$ denotes the empirical distribution of the unobservable clean data $\widetilde{\mathcal{S}}_t$ at timestep t. By combining Eqs. (10), (11), and (12), we have

$$\begin{aligned}
&\mathbb{E}_{\widetilde{\mathbb{D}}_t}[\beta_{\mathbb{D}_t}(\mathbf{x},\widetilde{\mathbf{y}})\ell(f_{\boldsymbol{\theta}}(\mathbf{x}),\widetilde{\mathbf{y}})]\\
&\leq L_{\widetilde{\mathcal{S}}}(\mathbf{q},\beta_{\mathbb{P}},f_{\boldsymbol{\theta}})+2\cdot\mathfrak{R}_{\mathbf{q}}(\beta_{\mathbb{P}}\circ\ell\circ\mathcal{F}_\Theta)\\
&+\sum_{k=1}^{K}\overline{q}_k\,disc_{\mathcal{F}_\Theta}(\mathbb{P}_{\mathcal{S}_t},\mathbb{P}_k)+\|\mathbf{q}\|_2\cdot\overline{L}\cdot\sqrt{\frac{\log(2/\delta)}{2}}+\mathcal{O}\left(\sqrt{\frac{1}{|\widetilde{\mathcal{S}}_t|}}\right)\\
&=\sum_{(\mathbf{x}_i,\widetilde{\mathbf{y}}_i)\in\widetilde{\mathcal{M}}_{1:t-1}\cup\widetilde{\mathcal{S}}_t}q_i\cdot\beta_{\mathbb{P}}(\mathbf{x}_i,\widetilde{\mathbf{y}}_i)\ell(f_{\boldsymbol{\theta}}(\mathbf{x}_i),\widetilde{\mathbf{y}}_i)+\sum_{k=1}^{K}\overline{q}_k\cdot disc_{\mathcal{F}_\Theta}(\mathbb{P}_k,\mathbb{P}_{\mathcal{S}_t})+\mathcal{O}\left(\sqrt{\frac{1}{|\widetilde{\mathcal{S}}_t|}}\right)\\
&+2\mathfrak{R}_{\mathbf{q}}(\beta_{\mathbb{P}}\circ\ell\circ\mathcal{F}_\Theta)+\|\mathbf{q}\|_2\overline{L}\sqrt{\frac{\log(2/\delta)}{2}}.
\end{aligned}\tag{13}$$

Therefore, we complete the proof.

□

B.3 Convergence of $\widehat{disc}_{\mathcal{F}_\Theta^{\text{lin}}}(\widetilde{\mathbb{P}}_n,\widetilde{\mathbb{Q}}_m)$ to $disc_{\mathcal{F}_\Theta^{\text{lin}}}(\mathbb{P},\mathbb{Q})$

The convergence of $\widehat{disc}_{\mathcal{F}_\Theta^{\text{lin}}}(\widetilde{\mathbb{P}}_n,\widetilde{\mathbb{Q}}_m)$ to $disc_{\mathcal{F}_\Theta^{\text{lin}}}(\mathbb{P},\mathbb{Q})$ is demonstrated in the following theorem:

Theorem 5. *Based on Assumption 2, we further assume that the loss function $\ell(\cdot,\cdot)$ is λ^ℓ-Lipschitz continuous with respect to its first argument. Let $\widetilde{\mathbb{P}}_n$ and $\widetilde{\mathbb{Q}}_m$ denote the distributions over datasets consisting of n and m examples drawn i.i.d. from $\mathbb{P}$ and $\mathbb{Q}$, respectively. Suppose that the norms of input example and parameter are bounded above by $\overline{X}$ and $\overline{\Theta}$, respectively, that is, $\overline{X}=\sup_{\mathbf{x}\in\mathcal{X}}\|\mathbf{x}\|_2$ and $\overline{\Theta}=\sup_{\boldsymbol{\theta}\in\Theta}\|\boldsymbol{\theta}\|_2$. Then, the following bound holds with probability at least $1-\delta$:*

$$disc_{\mathcal{F}_\Theta^{\text{lin}}}(\mathbb{P},\mathbb{Q})\leq\widehat{disc}_{\mathcal{F}_\Theta^{\text{lin}}}(\widetilde{\mathbb{P}}_n,\widetilde{\mathbb{Q}}_m)+\mathcal{O}\left(\sqrt{\frac{1}{m}+\frac{1}{n}}\right),\tag{14}$$

where the empirical estimation term $\widehat{disc}_{\mathcal{F}_\Theta^{\text{lin}}}(\widetilde{\mathbb{P}}_n,\widetilde{\mathbb{Q}}_m)$ is defined as

$$\widehat{disc}_{\mathcal{F}_\Theta^{\text{lin}}}(\widetilde{\mathbb{P}}_n,\widetilde{\mathbb{Q}}_m)=\sup_{f_{\boldsymbol{\theta}}\in\mathcal{F}_\Theta^{\text{lin}}}\left|\mathbb{E}_{\widetilde{\mathbb{P}}_n}\left[\beta_{\mathbb{P}}(\mathbf{x},\widetilde{\mathbf{y}})\ell(f_{\boldsymbol{\theta}}(\mathbf{x}),\widetilde{\mathbf{y}})\right]-\mathbb{E}_{\widetilde{\mathbb{Q}}_m}\left[\beta_{\mathbb{Q}}(\mathbf{x},\widetilde{\mathbf{y}})\ell(f_{\boldsymbol{\theta}}(\mathbf{x}),\widetilde{\mathbf{y}})\right]\right|.\tag{15}$$

Proof. By applying concentration inequalities, the following bounds hold uniformly over $f_{\boldsymbol{\theta}}\in\mathcal{F}_\Theta^{\text{lin}}$, with probability at least $1-\delta$:

$$\begin{aligned}
&\sup_{f_{\boldsymbol{\theta}}\in\mathcal{F}_\Theta}\left|\frac{1}{n}\sum_{(\mathbf{x},\widetilde{\mathbf{y}})\in\widetilde{\mathbb{P}}_n}\beta_{\mathbb{P}}(\mathbf{x},\widetilde{\mathbf{y}})\ell(f_{\boldsymbol{\theta}}(\mathbf{x}),\widetilde{\mathbf{y}})-\mathbb{E}_{\mathbb{P}}[\ell(f_{\boldsymbol{\theta}}(\mathbf{x}),\mathbf{y})]\right|\leq 2\mathfrak{R}_n(\beta_{\mathbb{P}}\circ\ell\circ\mathcal{F}_\Theta^{\mathrm{lin}})+\overline{L}\sqrt{\frac{\log(2/\delta)}{2n}},\\
&\sup_{f_{\boldsymbol{\theta}}\in\mathcal{F}_\Theta}\left|\frac{1}{m}\sum_{(\mathbf{x},\widetilde{\mathbf{y}})\in\widetilde{\mathbb{Q}}_m}\beta_{\mathbb{Q}}(\mathbf{x},\widetilde{\mathbf{y}})\ell(f_{\boldsymbol{\theta}}(\mathbf{x}),\widetilde{\mathbf{y}})-\mathbb{E}_{\mathbb{Q}}[\ell(f_{\boldsymbol{\theta}}(\mathbf{x}),\mathbf{y})]\right|\leq 2\mathfrak{R}_m(\beta_{\mathbb{Q}}\circ\ell\circ\mathcal{F}_\Theta^{\mathrm{lin}})+\overline{L}\sqrt{\frac{\log(2/\delta)}{2m}}.
\end{aligned}\tag{16}$$

Here, $\mathfrak{R}_n(\beta_{\mathbb{P}}\circ\ell\circ\mathcal{F}_\Theta^{\mathrm{lin}})$ denotes the Rademacher complexity with n examples, and $\mathfrak{R}_m(\beta_{\mathbb{Q}}\circ\ell\circ\mathcal{F}_\Theta^{\mathrm{lin}})$ is defined in the same manner. Since the density ratio function is bounded above by some $\overline{\beta}>0$ (see Assumption 2), it follows that $\mathfrak{R}_n(\beta_{\mathbb{P}}\circ\ell\circ\mathcal{F}_\Theta^{\mathrm{lin}})\leq\overline{\beta}\cdot\mathfrak{R}_n(\ell\circ\mathcal{F}_\Theta^{\mathrm{lin}})$. Let $f_{\boldsymbol{\theta},k}(\cdot)$ denote the k-th output of $f_{\boldsymbol{\theta}}$. By applying the vector contraction inequality [12], we have

$$\mathfrak{R}_n(\ell\circ\mathcal{F}_\Theta^{\mathrm{lin}})\leq\sqrt{2}\lambda^\ell\cdot\mathbb{E}\left[\sup_{f_{\boldsymbol{\theta}}\in\mathcal{F}_\Theta}\frac{1}{n}\sum_{i=1}^{n}\sum_{k=1}^{C}\sigma_{ik}f_{\boldsymbol{\theta},k}(\mathbf{x}_i)\right],\tag{17}$$

where each σ_{ik} denotes an independent Rademacher random variable, and C is the number of classes.

For a linear hypothesis $f_{\boldsymbol{\theta}}\in\mathcal{F}_\Theta^{\mathrm{lin}}$ and a certain input $\mathbf{x}$, the k-th output of the hypothesis $f_{\boldsymbol{\theta}}$ is defined as $f_{\boldsymbol{\theta},k}(\mathbf{x})=\boldsymbol{\theta}_k^\top\mathbf{x}$, where $\boldsymbol{\theta}_k$ is the k-th column of the parameter $\boldsymbol{\theta}=[\boldsymbol{\theta}_1,\boldsymbol{\theta}_2,\cdots,\boldsymbol{\theta}_C]$. Then, by following Eq. (17), we have

$$\begin{aligned}
\mathfrak{R}_n(\ell\circ\mathcal{F}_\Theta^{\mathrm{lin}})&\leq\sqrt{2}\lambda^\ell\cdot\mathbb{E}\left[\sup_{f_{\boldsymbol{\theta}}\in\mathcal{F}_\Theta}\frac{1}{n}\sum_{i=1}^{n}\sum_{k=1}^{C}\sigma_{ik}\boldsymbol{\theta}_k^\top\mathbf{x}_i\right]\\
&\leq\sqrt{2}\lambda^\ell\cdot\mathbb{E}\left[\sup_{f_{\boldsymbol{\theta}}\in\mathcal{F}_\Theta}\sum_{k=1}^{C}\langle\boldsymbol{\theta}_k,\sum_{i=1}^{n}\sigma_{ik}\mathbf{x}_i\rangle\right]\\
&\leq\sqrt{2}\lambda^\ell\cdot\sum_{k=1}^{C}\mathbb{E}\left[\sup_{f_{\boldsymbol{\theta}}\in\mathcal{F}_\Theta}\langle\boldsymbol{\theta}_k,\frac{1}{n}\sum_{i=1}^{n}\sigma_{ik}\mathbf{x}_i\rangle\right]\\
&\leq\sqrt{2}\lambda^\ell\cdot\sum_{k=1}^{C}\mathbb{E}\left[\sup_{f_{\boldsymbol{\theta}}\in\mathcal{F}_\Theta}\|\boldsymbol{\theta}_k\|_2\left\|\frac{1}{n}\sum_{i=1}^{n}\sigma_{ik}\mathbf{x}_i\right\|_2\right]\\
&\leq\sqrt{2}\lambda^\ell\cdot\sum_{k=1}^{C}\sup_{f_{\boldsymbol{\theta}}\in\mathcal{F}_\Theta}\|[\boldsymbol{\theta}_1,\boldsymbol{\theta}_2,\cdots,\boldsymbol{\theta}_C]\|_2\,\mathbb{E}\left[\left\|\frac{1}{n}\sum_{i=1}^{n}\sigma_{ik}\mathbf{x}_i\right\|_2\right]\\
&\leq\sqrt{2}\lambda^\ell\cdot\sum_{k=1}^{C}\sup_{\boldsymbol{\theta}\in\Theta}\|\boldsymbol{\theta}\|_2\left(\mathbb{E}\left[\langle\frac{1}{n}\sum_{i=1}^{n}\sigma_{ik}\mathbf{x}_i,\frac{1}{n}\sum_{i=1}^{n}\sigma_{ik}\mathbf{x}_i\rangle\right]\right)^{1/2}\\
&\leq\sqrt{2}\lambda^\ell\overline{\Theta}\cdot\sum_{k=1}^{C}\left(\mathbb{E}\left[\frac{1}{n^2}\sum_{i=1}^{n}\sigma_{ik}^2\|\mathbf{x}_i\|_2^2\right]\right)^{1/2}\\
&\leq\sqrt{2}\lambda^\ell\overline{\Theta}C\frac{\overline{X}}{\sqrt{n}}.
\end{aligned}\tag{18}$$

By leveraging Eq. (16) and Eq. (18), with probability at least $1-\delta$, it follows that

$$\begin{aligned}
disc_{\mathcal{F}_\Theta^{\mathrm{lin}}}(\mathbb{P},\mathbb{Q})=\sup_{f_{\boldsymbol{\theta}}\in\mathcal{F}_\Theta}\Big|&\mathbb{E}_{\mathbb{P}}[\ell(f_{\boldsymbol{\theta}}(\mathbf{x}),\mathbf{y})]-\frac{1}{n}\sum_{(\mathbf{x},\widetilde{\mathbf{y}})\in\widetilde{\mathbb{P}}_n}\beta_{\mathbb{P}}(\mathbf{x},\widetilde{\mathbf{y}})\ell(f_{\boldsymbol{\theta}}(\mathbf{x}),\widetilde{\mathbf{y}})+\frac{1}{n}\sum_{(\mathbf{x},\widetilde{\mathbf{y}})\in\widetilde{\mathbb{P}}_n}\beta_{\mathbb{P}}(\mathbf{x},\widetilde{\mathbf{y}})\ell(f_{\boldsymbol{\theta}}(\mathbf{x}),\widetilde{\mathbf{y}})\\
&-\mathbb{E}_{\mathbb{Q}}[\ell(f_{\boldsymbol{\theta}}(\mathbf{x}),\mathbf{y})]+\frac{1}{m}\sum_{(\mathbf{x},\widetilde{\mathbf{y}})\in\widetilde{\mathbb{Q}}_m}\beta_{\mathbb{Q}}(\mathbf{x},\widetilde{\mathbf{y}})\ell(f_{\boldsymbol{\theta}}(\mathbf{x}),\widetilde{\mathbf{y}})-\frac{1}{m}\sum_{(\mathbf{x},\widetilde{\mathbf{y}})\in\widetilde{\mathbb{Q}}_m}\beta_{\mathbb{Q}}(\mathbf{x},\widetilde{\mathbf{y}})\ell(f_{\boldsymbol{\theta}}(\mathbf{x}),\widetilde{\mathbf{y}})\Big|\\
\leq\widehat{disc}_{\mathcal{F}_\Theta^{\mathrm{lin}}}(\widetilde{\mathbb{P}}_n,\widetilde{\mathbb{Q}}_m)&+\sup_{f_{\boldsymbol{\theta}}\in\mathcal{F}_\Theta}\left|\frac{1}{n}\sum_{(\mathbf{x},\widetilde{\mathbf{y}})\in\widetilde{\mathbb{P}}_n}\beta_{\mathbb{P}}(\mathbf{x},\widetilde{\mathbf{y}})\ell(f_{\boldsymbol{\theta}}(\mathbf{x}),\widetilde{\mathbf{y}})-\mathbb{E}_{\mathbb{P}}[\ell(f_{\boldsymbol{\theta}}(\mathbf{x}),\mathbf{y})]\right|\\
&+\sup_{f_{\boldsymbol{\theta}}\in\mathcal{F}_\Theta}\left|\frac{1}{m}\sum_{(\mathbf{x},\widetilde{\mathbf{y}})\in\widetilde{\mathbb{Q}}_m}\beta_{\mathbb{Q}}(\mathbf{x},\widetilde{\mathbf{y}})\ell(f_{\boldsymbol{\theta}}(\mathbf{x}),\widetilde{\mathbf{y}})-\mathbb{E}_{\mathbb{Q}}[\ell(f_{\boldsymbol{\theta}}(\mathbf{x}),\mathbf{y})]\right|\\
\leq\widehat{disc}_{\mathcal{F}_\Theta^{\mathrm{lin}}}(\widetilde{\mathbb{P}}_n,\widetilde{\mathbb{Q}}_m)&+\left(2\sqrt{2}\cdot\overline{\beta}\lambda^\ell\overline{\Theta}C\overline{X}+\overline{L}\sqrt{\frac{1}{2}\log(\frac{4}{\delta})}\right)\cdot\left(\frac{1}{\sqrt{n}}+\frac{1}{\sqrt{m}}\right).
\end{aligned}\tag{19}$$

Since $\frac{1}{\sqrt{n}}+\frac{1}{\sqrt{m}}\leq\sqrt{2\cdot(\frac{1}{n}+\frac{1}{m})}$, Eq. (14) directly holds.

Therefore, we complete the proof.

$\square$

Theorem 5 shows that the empirical value $\widehat{disc}_{\mathcal{F}_\Theta^{\text{lin}}}(\widetilde{\mathbb{P}}_n, \widetilde{\mathbb{Q}}_m)$ has an approximation error of $\mathcal{O}\left(\sqrt{\frac{1}{n}+\frac{1}{m}}\right)$ w.r.t. the expected value $disc_{\mathcal{F}_\Theta^{\text{lin}}}(\mathbb{P}, \mathbb{Q})$.

B.4 Proof of Theorem 3

Proof. By combining Theorem 1 and Theorem 2, with probability at least $1-\delta$, the following upper bound on the cumulative generalization error holds:

$$\begin{aligned}
&\mathbb{E}_{\mathbb{D}_{1:t}}[\ell(f_{\boldsymbol{\theta}}(\mathbf{x}), \mathbf{y})] \\
&\leq (1-\alpha_t)\frac{1}{|\widetilde{\mathcal{M}}_{1:t-1}|}\sum_{i=1}^{|\widetilde{\mathcal{M}}_{1:t-1}|}\beta_{\mathbb{P}^{\mathcal{M}}_{1:t-1}}(\mathbf{x}_i, \widetilde{\mathbf{y}}_i)\ell(f_{\boldsymbol{\theta}}(\mathbf{x}_i), \widetilde{\mathbf{y}}_i) + (1-\alpha_t)Gap(\mathbb{P}^{\mathcal{M}}_{1:t-1}, \mathbb{D}_{1:t-1}) \\
&+ \alpha_t \sum_{(\mathbf{x}_i, \widetilde{\mathbf{y}}_i)\in\widetilde{\mathcal{M}}_{1:t-1}\cup\widetilde{\mathcal{S}}_t} q_i \cdot \beta_{\mathbb{P}}(\mathbf{x}_i, \widetilde{\mathbf{y}}_i)\ell(f_{\boldsymbol{\theta}}(\mathbf{x}_i), \widetilde{\mathbf{y}}_i) + \alpha_t\sum_{k=1}^{K}\overline{q}_k \cdot disc_{\mathcal{F}_\Theta}(\mathbb{P}_k, \mathbb{P}_{\mathcal{S}_t}) \\
&+ \mathcal{O}\left(\sqrt{\frac{1}{|\widetilde{\mathcal{S}}_t|}}\right) + 2\alpha_t\mathfrak{R}_{\mathbf{q}}(\beta_{\mathbb{P}}\circ\ell\circ\mathcal{F}_\Theta) + \alpha_t\|\mathbf{q}\|_2\overline{L}\sqrt{\frac{\log(2/\delta)}{2}} \qquad (20) \\
&= \sum_{(\mathbf{x}_i, \widetilde{\mathbf{y}}_i)\in\widetilde{\mathcal{M}}_{1:t-1}}\left(\tfrac{1-\alpha_t}{|\widetilde{\mathcal{M}}_{1:t-1}|} + \alpha_t q_i\right)\beta_{\mathbb{P}^{\mathcal{M}}_{1:t-1}}(\mathbf{x}_i, \widetilde{\mathbf{y}}_i)\ell(f_{\boldsymbol{\theta}}(\mathbf{x}_i), \widetilde{\mathbf{y}}_i) + \alpha_t \cdot \sum_{(\mathbf{x}_j, \widetilde{\mathbf{y}}_j)\in\widetilde{\mathcal{S}}_t} q_j\beta_{\mathbb{D}_t}(\mathbf{x}_j, \widetilde{\mathbf{y}}_j)\ell(f_{\boldsymbol{\theta}}(\mathbf{x}_j), \widetilde{\mathbf{y}}_j) \\
&+ \alpha_t\sum_{k=1}^{K}\overline{q}_k \cdot disc_{\mathcal{F}_\Theta}(\mathbb{P}_k, \mathbb{P}_{\mathcal{S}_t}) + \mathcal{O}\left(\sqrt{\frac{1}{n_t}}\right) + 2\alpha_t\mathfrak{R}_{\mathbf{q}}(\beta_{\mathbb{P}}\circ\ell\circ\mathcal{F}_\Theta) + \alpha_t\|\mathbf{q}\|_2\overline{L}\sqrt{\frac{\log(2/\delta)}{2}} \\
&+ (1-\alpha_t)Gap(\mathbb{P}^{\mathcal{M}}_{1:t-1}, \mathbb{D}_{1:t-1}),
\end{aligned}$$

where $(1-\alpha_t)Gap(\mathbb{P}^{\mathcal{M}}_{1:t-1}, \mathbb{D}_{1:t-1})$ is the selection bias of buffered data. Here, we still need to bound the expected distribution discrepancy term $disc_{\mathcal{F}_\Theta}(\mathbb{P}_k, \mathbb{P}_{\mathcal{S}_t})$ by empirical values. Moreover, the Rademacher complexity term (*i.e.*, $2\alpha_t\mathfrak{R}_{\mathbf{q}}(\beta_{\mathbb{P}}\circ\ell\circ\mathcal{F}_\Theta)$) and the approximation error term $\alpha_t\|\mathbf{q}\|_2\overline{L}\sqrt{\frac{\log(2/\delta)}{2}}$ must be considered. For the discrepancy term, by applying Theorem 5, we obtain:

$$\begin{aligned}
\alpha_t\sum_{k=1}^{K}\overline{q}_k \cdot disc_{\mathcal{F}_\Theta}(\mathbb{P}_k, \mathbb{P}_{\mathcal{S}_t}) &\leq \alpha_t\sum_{k=1}^{K}\overline{q}_k\widehat{disc}_{\mathcal{F}_\Theta}(\widetilde{\mathbb{P}}_k, \widetilde{\mathbb{P}}_{\mathcal{S}_t}) + \alpha_t\sum_{k=1}^{K}\overline{q}_k\mathcal{O}\left(\sqrt{\frac{1}{m_k}} + \sqrt{\frac{1}{n_t}}\right) \\
&\leq \alpha_t\sum_{k=1}^{K}\overline{q}_k\widehat{disc}_{\mathcal{F}_\Theta}(\widetilde{\mathbb{P}}_k, \widetilde{\mathbb{P}}_{\mathcal{S}_t}) + \mathcal{O}\left(\sqrt{\frac{1}{n_t}} + \sum_{k=1}^{K}\overline{q}_k\sqrt{\frac{1}{m_k}}\right) \qquad (21) \\
&= \alpha_t\sum_{k=1}^{K}\overline{q}_k\widehat{disc}_{\mathcal{F}_\Theta}(\widetilde{\mathbb{P}}_k, \widetilde{\mathbb{P}}_{\mathcal{S}_t}) + \mathcal{O}(1).
\end{aligned}$$

Eq. (21) shows that with a large number of examples in each subset $\mathcal{M}^{(k)}_{1:t-1}$ of memory buffer and in the newly arrived data $\widetilde{\mathcal{S}}_t$, the constant approximation error $\mathcal{O}\left(\sqrt{\frac{1}{n_t}} + \sum_{k=1}^{K}\overline{q}_k\sqrt{\frac{1}{m_k}}\right)$ becomes small.

Subsequently, we consider the $\mathbf{q}\circ\beta_{\mathbb{P}}$-weighted Rademacher complexity term $2\alpha_t\mathfrak{R}_{\mathbf{q}}(\beta_{\mathbb{P}}\circ\ell\circ\mathcal{F}_\Theta)$. Since $0 \leq q_i \leq 1$, $\forall i \in [\![m]\!]$, we have $\mathfrak{R}_{\mathbf{q}}(\beta_{\mathbb{P}}\circ\ell\circ\mathcal{F}_\Theta) < \mathfrak{R}_m(\beta_{\mathbb{P}}\circ\ell\circ\mathcal{F}_\Theta)$, where $\mathfrak{R}_m(\beta_{\mathbb{P}}\circ\ell\circ\mathcal{F}_\Theta)$ is the conventional Rademacher complexity with m examples. As shown in the proof of Theorem 5, if a linear hypothesis space is adopted, then $\mathfrak{R}_m(\beta_{\mathbb{P}}\circ\ell\circ\mathcal{F}_\Theta)$ has the order of $\mathcal{O}\left(\frac{1}{m}\right) = \mathcal{O}\left(\frac{1}{\sum_{k=1}^{K} m_k + n_t}\right) = \mathcal{O}(1)$. It is worth noting that such a bound also holds for complex Multi-Layer Perceptron (MLP) network [5], [6] under the assumptions of boundedness of both the parameter space and the feature space. Therefore, in general, we have $2\alpha_t\mathfrak{R}_{\mathbf{q}}(\beta_{\mathbb{P}}\circ\ell\circ\mathcal{F}_\Theta) \leq \mathcal{O}(1)$. Additionally, since $\|\mathbf{q}\|_2 \leq 1$, the term $\alpha_t\|\mathbf{q}\|_2\overline{L}\sqrt{\frac{\log(2/\delta)}{2}}$ can be treated as a constant. It is worth noting that if $q_i = {}^1\!/_m$, $\forall\, i \in [\![m]\!]$, we have $\alpha_t\|\mathbf{q}\|_2\overline{L}\sqrt{\frac{\log(2/\delta)}{2}} = \mathcal{O}({}^1\!/\!\sqrt{m})$. By considering all the factors, with probability at least $1-\delta$, the final cumulative generalization error bound for any $f_{\boldsymbol{\theta}} \in \mathcal{F}_\Theta$

is:

$$
\begin{aligned}
&\mathbb{E}_{\mathbb{D}_{1:t}}[\ell(f_{\boldsymbol{\theta}}(\mathbf{x}),\mathbf{y})] \\
&\leq \underbrace{\sum_{(\mathbf{x}_i,\widetilde{\mathbf{y}}_i)\in\widetilde{\mathcal{M}}_{1:t-1}} \left(\tfrac{1-\alpha_t}{|\widetilde{\mathcal{M}}_{1:t-1}|}+\alpha_t q_i\right)\beta_{\mathbb{P}^{\mathcal{M}}_{1:t-1}}(\mathbf{x}_i,\widetilde{\mathbf{y}}_i)\ell(f_{\boldsymbol{\theta}}(\mathbf{x}_i),\widetilde{\mathbf{y}}_i)}_{\text{Weighted loss on buffered data}} + \underbrace{\alpha_t \cdot \sum_{(\mathbf{x}_j,\widetilde{\mathbf{y}}_j)\in\widetilde{\mathcal{S}}_t} q_j\beta_{\mathbb{D}_t}(\mathbf{x}_j,\widetilde{\mathbf{y}}_j)\ell(f_{\boldsymbol{\theta}}(\mathbf{x}_j),\widetilde{\mathbf{y}}_j)}_{\text{Weighted loss on new data}} \\
&+ \underbrace{O(1)}_{\text{Approximation error}} + \underbrace{\alpha_t\sum_{k=1}^{K}\overline{q}_k\widehat{disc}_{\mathcal{F}_\Theta}(\widetilde{\mathbb{P}}_k,\widetilde{\mathbb{P}}_{\mathcal{S}_t})}_{\text{Distribution shift}} + \underbrace{(1-\alpha_t)Gap(\mathbb{P}^{\mathcal{M}}_{1:t-1},\mathbb{D}_{1:t-1})}_{\text{Buffered data selection bias}}.
\end{aligned}
\tag{22}
$$

Therefore, we complete the proof.

□

B.5 Proof of Lemma 1

Proof. For a certain example $(\mathbf{x},\widetilde{\mathbf{y}})$ in the cumulative sample set $\widetilde{\mathcal{S}}_{1:t-1}$(up to timestep $t-1$), it must be sampled either from $\widetilde{\mathcal{S}}_{1:t-2}$ or from $\widetilde{\mathcal{S}}_{t-1}$. Therefore, according to our assumptions (namely, the memory buffer $\widetilde{\mathcal{M}}_{1:t-2}$ with size k_1 is a γ-cover of the entire dataset $\widetilde{\mathcal{S}}_{1:t-2}$; the temporary buffer $\widetilde{\mathcal{M}}_{t-1}$ with size k_2 is a γ'-cover of the data $\widetilde{\mathcal{S}}_{t-1}$), there exists $(\mathbf{x}',\widetilde{\mathbf{y}}')\in\widetilde{\mathcal{M}}_{1:t-2}$ such that $\|\mathbf{x}-\mathbf{x}'\|_2\leq\gamma$ or there exists $(\mathbf{x}',\widetilde{\mathbf{y}}')\in\widetilde{\mathcal{M}}_{t-1}$ such that $\|\mathbf{x}-\mathbf{x}'\|_2\leq\gamma'$. As a result, it necessarily holds that $\|\mathbf{x}-\mathbf{x}'\|_2\leq\max\{\gamma,\gamma'\}$. Furthermore, for the example $(\mathbf{x}',\widetilde{\mathbf{y}}')$ obtained above, since $\widetilde{\mathcal{M}}_{1:t-1}$ with size k_3 is a γ''-cover of $\widetilde{\mathcal{M}}_{1:t-2}\cup\widetilde{\mathcal{M}}_{t-1}$, there exists at least one $(\mathbf{x}'',\widetilde{\mathbf{y}}'')\in\widetilde{\mathcal{M}}_{1:t-1}$ such that $\|\mathbf{x}'-\mathbf{x}''\|_2\leq\gamma''$. According to the triangle inequality, we have $\|\mathbf{x}-\mathbf{x}''\|_2\leq\|\mathbf{x}-\mathbf{x}'\|_2+\|\mathbf{x}'-\mathbf{x}''\|_2\leq\max\{\gamma,\gamma'\}+\gamma''$. Therefore, the memory buffer $\widetilde{\mathcal{M}}_{1:t-1}$ is a $\max\{\gamma,\gamma'\}+\gamma''$-cover of the overall noisy data up to timestep $t-1$ (namely, $\widetilde{\mathcal{S}}_{1:t-1}$). Moreover, since the derivation above depends only on the feature $\mathbf{x}$, the memory buffer with ground-truth labels (namely, $\mathcal{M}_{1:t-1}$) is also a $\max\{\gamma,\gamma'\}+\gamma''$-cover of the overall clean data up to timestep $t-1$ (namely, $\mathcal{S}_{1:t-1}$). This property will be later used to derive an upper bound on the loss value of each example in $\mathcal{S}_{1:t-1}$.

Now, according to the assumption, the trained model achieves sufficiently small loss value on buffered data, that is:

$$
\mathbb{E}_{\mathbb{P}^{\mathcal{M}}_{1:t-1}}[\ell(f_{\boldsymbol{\theta}}(\mathbf{x}),\mathbf{y})]=\frac{1}{|\mathcal{M}_{1:t-1}|}\sum_{(\mathbf{x},\mathbf{y})\in\mathcal{M}_{1:t-1}}\ell(f_{\boldsymbol{\theta}}(\mathbf{x}),\mathbf{y})<\epsilon. \tag{23}
$$

Therefore, the distribution gap term can be upper bounded by

$$
\begin{aligned}
Gap(\mathbb{P}^{\mathcal{M}}_{1:t-1},\mathbb{D}_{1:t-1}) &< \left|\mathbb{E}_{\mathbb{D}_{1:t-1}}[\ell(f_{\boldsymbol{\theta}}(\mathbf{x}),\mathbf{y})]\right|+\epsilon \\
&< \left|\mathbb{E}_{\mathbb{D}_{1:t-1}}[\ell(f_{\boldsymbol{\theta}}(\mathbf{x}),\mathbf{y})]-\mathbb{E}_{\mathbb{P}_{\mathcal{S}_{1:t-1}}}[\ell(f_{\boldsymbol{\theta}}(\mathbf{x}),\mathbf{y})]+\mathbb{E}_{\mathbb{P}_{\mathcal{S}_{1:t-1}}}[\ell(f_{\boldsymbol{\theta}}(\mathbf{x}),\mathbf{y})]\right|+\epsilon,
\end{aligned}
\tag{24}
$$

where $\mathbb{P}_{\mathcal{S}_{1:t-1}}$ is the empirical distribution defined on the cumulative dataset $\mathcal{S}_{1:t-1}$. By Hoeffding's inequality [13], for any $\delta\in(0,1)$, with probability at least $1-\delta$, we have

$$
\left|\mathbb{E}_{\mathbb{D}_{1:t-1}}[\ell(f_{\boldsymbol{\theta}}(\mathbf{x}),\mathbf{y})]-\mathbb{E}_{\mathbb{P}_{\mathcal{S}_{1:t-1}}}[\ell(f_{\boldsymbol{\theta}}(\mathbf{x}),\mathbf{y})]\right|<\overline{L}\sqrt{\frac{\log(1/\delta)}{2|\mathcal{S}_{1:t-1}|}}. \tag{25}
$$

Subsequently, we use the covering property derived above to bound the empirical risk $\left|\mathbb{E}_{\mathbb{P}_{\mathcal{S}_{1:t-1}}}[\ell(f_{\boldsymbol{\theta}}(\mathbf{x}),\mathbf{y})]\right|$ in Eq. (24). Specifically, for any $(\mathbf{x}_i,\mathbf{y}_i)\in\mathcal{S}_{1:t-1}$, there exists an example $(\mathbf{x}_j,\mathbf{y}_j)\in\mathcal{M}_{1:t-1}$ such that $\mathbf{x}_j$ lies within a ball of radius $\max\{\gamma,\gamma'\}+\gamma''$ centered at $\mathbf{x}_i$. Therefore, we can obtain

$$
\begin{aligned}
&\mathbb{E}_{\mathbf{y}_i\sim P(Y|X=\mathbf{x}_i)}[\ell(f_{\boldsymbol{\theta}}(\mathbf{x}_i),\mathbf{y}_i)]=\sum_{k\in[C]}P(Y=\mathbf{e}_k|X=\mathbf{x}_i)\ell(f_{\boldsymbol{\theta}}(\mathbf{x}_i),\mathbf{e}_k) \\
&\leq\sum_{k\in[C]}P(Y=\mathbf{e}_k|X=\mathbf{x}_j)\ell(f_{\boldsymbol{\theta}}(\mathbf{x}_i),\mathbf{e}_k)+\sum_{k\in[C]}\left|P(Y=\mathbf{e}_k|X=\mathbf{x}_i)-P(Y=\mathbf{e}_k|X=\mathbf{x}_j)\right|\ell(f_{\boldsymbol{\theta}}(\mathbf{x}_i),\mathbf{e}_k).
\end{aligned}
\tag{26}
$$

For any timestep t and label $\mathbf{y}$, the class posterior probability distribution $P_t(Y_t=\mathbf{y}\mid X_t=\mathbf{x})$ is λ^P-Lipschitz continuous w.r.t. $\mathbf{x}$, and for any $\mathbf{y}$, the loss function is bounded by $\overline{L}$. Therefore, we have

$$
\begin{aligned}
&\sum_{k\in[C]}\left|P(Y=\mathbf{e}_k\mid X=\mathbf{x}_i)-P(Y=\mathbf{e}_k\mid X=\mathbf{x}_j)\right|\ell(f_{\boldsymbol{\theta}}(\mathbf{x}_i),\mathbf{e}_k) \\
&\leq\lambda^P C\overline{L}\|\mathbf{x}_i-\mathbf{x}_j\|_2\leq(\max\{\gamma,\gamma'\}+\gamma'')\cdot\lambda^P C\overline{L}.
\end{aligned}
\tag{27}
$$

Moreover, the term $\mathbb{E}_{\mathbf{y}\sim P(Y|X=\mathbf{x}_j)}\left[\ell(f_{\boldsymbol{\theta}}(\mathbf{x}_i),\mathbf{y})\right]$ in Eq. (26) can be decomposed as:

$$
\mathbb{E}_{\mathbf{y}\sim P(Y|X=\mathbf{x}_j)}\left[\ell(f_{\boldsymbol{\theta}}(\mathbf{x}_i),\mathbf{y})\right]=\mathbb{E}_{\mathbf{y}\sim P(Y|X=\mathbf{x}_j)}\left[\ell(f_{\boldsymbol{\theta}}(\mathbf{x}_i),\mathbf{y})-\ell(f_{\boldsymbol{\theta}}(\mathbf{x}_j),\mathbf{y})\right]+\mathbb{E}_{\mathbf{y}\sim P(Y|X=\mathbf{x}_j)}\ell(f_{\boldsymbol{\theta}}(\mathbf{x}_j),\mathbf{y}). \tag{28}
$$

Since the loss function $\ell(f_{\boldsymbol{\theta}}(\mathbf{x}), \mathbf{y})$ is λ^{ℓ}-Lipschitz continuous w.r.t. $\mathbf{x}$ for any $\mathbf{y}$, it holds that

$$\begin{aligned} \mathbb{E}_{\mathbf{y} \sim P(Y|X=\mathbf{x}_j)} \left[\ell(f_{\boldsymbol{\theta}}(\mathbf{x}_i), \mathbf{y})\right] \leq \mathbb{E}_{\mathbf{y} \sim P(Y|X=\mathbf{x}_j)} \left[\lambda^{\ell} \|\mathbf{x}_i - \mathbf{x}_j\|_2\right] &= \lambda^{\ell} \|\mathbf{x}_i - \mathbf{x}_j\|_2 \\ &\leq \lambda^{\ell} \cdot (\max\{\gamma, \gamma'\} + \gamma'') \,. \end{aligned} \tag{29}$$

By combining Eqs. (26)∼(29), we have

$$\left|\mathbb{E}_{\mathbb{P}_{\mathcal{S}_{1:t-1}}}\left[\ell(f_{\boldsymbol{\theta}}(\mathbf{x}), \mathbf{y})\right]\right| = \left|\mathbb{E}_{\mathbf{x}_i \sim P(X=\mathbf{x}_i)} \mathbb{E}_{\mathbf{y}_i \sim P(Y|X=\mathbf{x}_i)} \left[\ell(f_{\boldsymbol{\theta}}(\mathbf{x}_i), \mathbf{y}_i)\right]\right| \leq \epsilon + (\max\{\gamma, \gamma'\} + \gamma'') \left(\lambda^{\ell} + \lambda^{P} \overline{L} C\right). \tag{30}$$

Furthermore, by combining Eqs. (24), (25), and (30), with probability at least $1 - \delta$, the following inequality holds:

$$Gap(\mathbb{P}^{\mathcal{M}}_{1:t-1}, \mathbb{D}_{1:t-1}) < 2\epsilon + (\max\{\gamma, \gamma'\} + \gamma'') \left(\lambda^{\ell} + \lambda^{P} \overline{L} C\right) + 2\overline{L} \sqrt{\frac{\log(2/\delta)}{2 \sum_{i=1}^{t-1} n_i}}. \tag{31}$$

Therefore, we complete the proof. □

B.6 Proof of Theorem 4

Proof. The proof of this theorem adopts an inductive technique. First, consider the case where $t - 1 = 1$: the model receives data $\widetilde{\mathcal{S}}_1$, and the initial memory buffer is $\widetilde{\mathcal{M}}_0 = \emptyset$. The updated memory buffer is denoted by $\widetilde{\mathcal{M}}_1$, which forms a $\frac{\gamma}{2}$-cover of $\widetilde{\mathcal{M}}_0 \cup \widetilde{\mathcal{S}}_1 = \widetilde{\mathcal{S}}_1$. Subsequently, according to Lemma 1, for $t - 1 = 2$, the buffer $\widetilde{\mathcal{M}}_{1:2}$ constitutes a $\max\{\frac{\gamma}{2}, \frac{\gamma}{3}\} + \frac{\gamma}{3}$-cover of $\widetilde{\mathcal{S}}_1 \cup \widetilde{\mathcal{S}}_2$. By induction, for any time $t - 1 > 2$, $\widetilde{\mathcal{M}}_{1:t-2}$ is a $\sum_{2 \leq i \leq t-1} \frac{\gamma}{i}$-cover of $\widetilde{\mathcal{S}}_{1:t-2}$. According to Lemma 1, $\widetilde{\mathcal{M}}_{1:t-1}$ is a $\max\left\{\sum_{2 \leq i \leq t-1} \frac{\gamma}{i}, \frac{\gamma}{t}\right\} + \frac{\gamma}{t}$-cover of $\widetilde{\mathcal{S}}_{1:t-1}$. Since $\max\left\{\sum_{2 \leq i \leq t-1} \frac{\gamma}{i}, \frac{\gamma}{t}\right\} + \frac{\gamma}{t} = \sum_{2 \leq i \leq t} \frac{\gamma}{i} < \sum_{i=1}^{\infty} \frac{\gamma}{i} = \log(t+1) \cdot \gamma$, it follows that $\widetilde{\mathcal{M}}_{1:t-1}$ is a $\log(t+1) \cdot \gamma$-cover of $\widetilde{\mathcal{S}}_{1:t-1}$. By adopting the same technique used in the proof of Lemma 1, we can readily draw the conclusion: with probability at least $1 - \delta$, it holds that

$$\begin{aligned} Gap(\mathbb{P}^{\mathcal{M}}_{1:t-1}, \mathbb{D}_{1:t-1}) &< \gamma \log(t+1)(\lambda^{\ell} + \lambda^{P} \overline{L} C) + 2\epsilon + 2\overline{L} \sqrt{\frac{\log(2/\delta)}{2|\mathcal{S}_{1:t-1}|}} \\ &= \widetilde{\mathcal{O}}(\gamma) + \mathcal{O}\left(\sqrt{\frac{1}{|\mathcal{S}_{1:t-1}|}} + \epsilon\right) \\ &= \widetilde{\mathcal{O}}(\gamma) + \mathcal{O}\left(\sqrt{\frac{1}{\sum_{i=1}^{t-1} n_i}} + \epsilon\right), \end{aligned} \tag{32}$$

where $\widetilde{\mathcal{O}}(\cdot)$ denotes the big-$\mathcal{O}$ that hides all logarithmic factors. Therefore, we complete the proof. □

B.7 Upper Bound of Cumulative Generalization Error with Prior Inclusion for $\mathbf{q}$

As mentioned in Section 5.4, we can introduce $\mathbf{p}_0$ as a prior for regularizing $\mathbf{q}$. In this case, the upper bound on the cumulative generalization error presented in Theorem 3 should be slightly extended, as given in Theorem 6 below. Disregarding the approximation error, the objective $\mathcal{L}_t(\boldsymbol{\theta}, \mathbf{q})$ in Eq. (17) serves as an exact upper bound for the cumulative generalization error. Consequently, minimizing $\mathcal{L}_t(\boldsymbol{\theta}, \mathbf{q})$ can lead to a reduction in generalization error, and thus the proposed CNLDD method can effectively mitigate catastrophic forgetting induced by distribution shift and label noise.

Theorem 6. *Under Assumption 2, when the dataset* $\{\widetilde{\mathcal{M}}^{(k)}_{1:t-1}\}_{k=1}^{K} \cup \widetilde{\mathcal{S}}_t$ *is sampled from the distribution* $\widetilde{\mathbb{P}} = \widetilde{\mathbb{P}}_1^{m_1} \otimes \widetilde{\mathbb{P}}_2^{m_2} \otimes \cdots \otimes \widetilde{\mathbb{P}}_K^{m_K} \otimes \widetilde{\mathbb{D}}_t^{n_t}$*, for any* $f_{\boldsymbol{\theta}} \in \mathcal{F}_{\Theta}$*,* $0 \leq \Delta < 1$*, and* $\mathbf{q} \in \{\mathbf{q} : 0 \leq \|\mathbf{q} - \mathbf{p}^0\|_1 < 1 - \Delta\}$*, with probability at least* $1 - \delta$*, it holds that:*

$$\begin{aligned} &\mathbb{E}_{\mathbb{D}_{1:t}}\left[\ell(f_{\boldsymbol{\theta}}(\mathbf{x}), \mathbf{y})\right] \\ &\leq \underbrace{\sum_{(\mathbf{x}_i, \widetilde{\mathbf{y}}_i) \in \widetilde{\mathcal{M}}_{1:t-1}} \left(\tfrac{1-\alpha_t}{|\widetilde{\mathcal{M}}_{1:t-1}|} + \alpha_t q_i\right) \beta_{\mathbb{P}^{\mathcal{M}}_{1:t-1}}(\mathbf{x}_i, \widetilde{\mathbf{y}}_i) \ell(f_{\boldsymbol{\theta}}(\mathbf{x}_i), \widetilde{\mathbf{y}}_i)}_{\textit{Weighted loss on buffered data}} + \underbrace{\alpha_t \cdot \sum_{(\mathbf{x}_j, \widetilde{\mathbf{y}}_j) \in \widetilde{\mathcal{S}}_t} q_j \beta_{\mathbb{D}_t}(\mathbf{x}_j, \widetilde{\mathbf{y}}_j) \ell(f_{\boldsymbol{\theta}}(\mathbf{x}_j), \widetilde{\mathbf{y}}_j)}_{\textit{Weighted loss on new data}} \\ &+ \underbrace{O(1)}_{\textit{Approximation error}} + \underbrace{C_1(\alpha_t, \delta, \Delta) \cdot \|\mathbf{q} - \mathbf{p}^0\|_1}_{\ell_1 \textit{ regularization term with prior } \mathbf{p}^0} + \underbrace{C_2(\alpha_t, \delta, \Delta) \cdot \|\mathbf{q}\|_2}_{\ell_2 \textit{ regularization term}} \\ &+ \underbrace{\alpha_t \sum_{k=1}^{K} \overline{q}_k \widehat{disc}_{\mathcal{F}_{\Theta}}(\widetilde{\mathbb{P}}_k, \widetilde{\mathbb{P}}_{\mathcal{S}_t})}_{\textit{Distribution shift}} + \underbrace{(1 - \alpha_t) Gap(\mathbb{P}^{\mathcal{M}}_{1:t-1}, \mathbb{D}_{1:t-1})}_{\textit{Buffered data selection bias}}, \end{aligned} \tag{33}$$

where $C_1(\alpha_t, \delta, \Delta)$ *and* $C_2(\alpha_t, \delta, \Delta)$ *are two constants depending only on* α_t*,* δ*, and* Δ*.*

Proof. Based on Theorem 2, for any sequence $(\epsilon_s)_{s=1}^{\infty}$ and $(\mathbf{q}^s)_{s=1}^{\infty}$, the following probabilistic inequality holds:

$$\begin{aligned}P\Bigg(&\mathbb{E}_{\widetilde{\mathbb{D}}_t}\left[\beta_{\mathbb{D}_t}(\mathbf{x},\widetilde{\mathbf{y}})\,\ell(f_{\boldsymbol{\theta}}(\mathbf{x}),\widetilde{\mathbf{y}})\right] > \sum_{(\mathbf{x}_i,\widetilde{\mathbf{y}}_i)\in\widetilde{\mathcal{M}}_{1:t-1}\cup\widetilde{\mathcal{S}}_t} q_i^s\cdot\beta_{\mathbb{P}}(\mathbf{x}_i,\widetilde{\mathbf{y}}_i)\,\ell(f_{\boldsymbol{\theta}}(\mathbf{x}_i),\widetilde{\mathbf{y}}_i)\\ &+\sum_{k=1}^{K}\overline{q}_k^s\,disc(\mathbb{P}_k,\mathbb{P}_{\mathcal{S}_t})+\mathcal{O}\left(\frac{1}{\sqrt{|\widetilde{\mathcal{S}}_t|}}\right)+2\mathfrak{R}_{\mathbf{q}^s}(\beta_{\mathbb{P}}\circ\ell\circ\mathcal{F}_{\Theta})+\|\mathbf{q}^s\|_2\overline{L}\frac{\epsilon_s}{\sqrt{2}}\Bigg) < 2\exp(-\epsilon_s^2),\end{aligned}\tag{34}$$

where q_i^s is the i-th element of $\mathbf{q}^s$, and $\overline{q}_k^s$ is the sum of the weights assigned to the k-th cluster of the buffered data. Therefore, by applying the union bound inequality and taking $\epsilon_s=\epsilon+\sqrt{2\log(s+1)}$, we have:

$$\begin{aligned}P\Bigg(&\exists\, k\geq 0:\mathbb{E}_{\widetilde{\mathbb{D}}_t}\left[\beta_{\mathbb{D}_t}(\mathbf{x},\widetilde{\mathbf{y}})\ell(f_{\boldsymbol{\theta}}(\mathbf{x}),\widetilde{\mathbf{y}})\right] > \sum_{(\mathbf{x}_i,\widetilde{\mathbf{y}}_i)\in\widetilde{\mathcal{M}}_{1:t-1}\cup\widetilde{\mathcal{S}}_t} q_i^s\cdot\beta_{\mathbb{P}}(\mathbf{x}_i,\widetilde{\mathbf{y}}_i)\ell(f_{\boldsymbol{\theta}}(\mathbf{x}_i),\widetilde{\mathbf{y}}_i)\\ &+\sum_{k=1}^{K}\overline{q}_k^s\,disc(\mathbb{P}_k,\mathbb{P}_{\mathcal{S}_t})+\mathcal{O}\left(\frac{1}{\sqrt{|\widetilde{\mathcal{S}}_t|}}\right)+2\mathfrak{R}_{\mathbf{q}^s}(\beta_{\mathbb{P}}\circ\ell\circ\mathcal{F}_{\Theta})+\|\mathbf{q}^s\|_2\overline{L}\frac{\epsilon_s}{\sqrt{2}}\Bigg)\\ &< 2\sum_{k=0}^{\infty}\exp(-\epsilon_s^2)=2\exp(-\epsilon^2)\sum_{k=0}^{\infty}\frac{1}{(k+1)^2}<\frac{\pi^2}{3}\exp(-\epsilon^2)<4\exp(-\epsilon^2).\end{aligned}\tag{35}$$

Next, we choose $\mathbf{q}^s$ such that $\|\mathbf{q}^s-\mathbf{p}^0\|_1=1-\frac{1}{2^s}$. According to this definition, for any $\mathbf{q}\in\{\mathbf{q}:0\leq\|\mathbf{q}-\mathbf{p}^0\|_1<1-\Delta\}$, there exists $s>0$ such that $\|\mathbf{q}^s-\mathbf{p}^0\|_1\leq\|\mathbf{q}-\mathbf{p}^0\|_1\leq\|\mathbf{q}^{s+1}-\mathbf{p}^0\|_1$, and thus we have

$$\begin{aligned}\epsilon_s&=\epsilon+\sqrt{2\log(s+1)}\\ &=\epsilon+\sqrt{2\log\log_2\left(\frac{1}{1-\|\mathbf{q}^{s+1}-\mathbf{p}^0\|_1}\right)}\\ &=\epsilon+\sqrt{2\log\log_2\left(\frac{2}{1-\|\mathbf{q}^{s}-\mathbf{p}^0\|_1}\right)}\\ &\leq\epsilon+\sqrt{2\log\log_2\left(\frac{2}{1-\|\mathbf{q}-\mathbf{p}^0\|_1}\right)}\\ &\leq\epsilon+\sqrt{2\log\log_2\left(\frac{1}{\Delta}\right)}.\end{aligned}\tag{36}$$

Subsequently, we derive the corresponding bound for each term involving $\mathbf{q}^s$ in Eq. (35). First, for the weighted loss term $\sum_{(\mathbf{x}_i,\widetilde{\mathbf{y}}_i)\in\widetilde{\mathcal{M}}_{1:t-1}\cup\widetilde{\mathcal{S}}_t} q_i^s\cdot\beta_{\mathbb{P}}(\mathbf{x}_i,\widetilde{\mathbf{y}}_i)\ell(f_{\boldsymbol{\theta}}(\mathbf{x}_i),\widetilde{\mathbf{y}}_i)$, we have

$$\begin{aligned}&\sum_{(\mathbf{x}_i,\widetilde{\mathbf{y}}_i)\in\widetilde{\mathcal{M}}_{1:t-1}\cup\widetilde{\mathcal{S}}_t} q_i^s\cdot\beta_{\mathbb{P}}(\mathbf{x}_i,\widetilde{\mathbf{y}}_i)\ell(f_{\boldsymbol{\theta}}(\mathbf{x}_i),\widetilde{\mathbf{y}}_i)\\ &\leq\overline{\beta}\cdot\overline{L}\|\mathbf{q}^s-\mathbf{q}\|_1+\sum_{(\mathbf{x}_i,\widetilde{\mathbf{y}}_i)\in\widetilde{\mathcal{M}}_{1:t-1}\cup\widetilde{\mathcal{S}}_t} q_i\cdot\beta_{\mathbb{P}}(\mathbf{x}_i,\widetilde{\mathbf{y}}_i)\ell(f_{\boldsymbol{\theta}}(\mathbf{x}_i),\widetilde{\mathbf{y}}_i)\\ &\leq\overline{\beta}\cdot\overline{L}\|\mathbf{q}^s-\mathbf{p}_0\|_1+\overline{\beta}\cdot\overline{L}\|\mathbf{p}_0-\mathbf{q}\|_1+\sum_{(\mathbf{x}_i,\widetilde{\mathbf{y}}_i)\in\widetilde{\mathcal{M}}_{1:t-1}\cup\widetilde{\mathcal{S}}_t} q_i\cdot\beta_{\mathbb{P}}(\mathbf{x}_i,\widetilde{\mathbf{y}}_i)\ell(f_{\boldsymbol{\theta}}(\mathbf{x}_i),\widetilde{\mathbf{y}}_i)\\ &\leq 2\overline{\beta}\cdot\overline{L}\|\mathbf{q}-\mathbf{p}_0\|_1+\sum_{(\mathbf{x}_i,\widetilde{\mathbf{y}}_i)\in\widetilde{\mathcal{M}}_{1:t-1}\cup\widetilde{\mathcal{S}}_t} q_i\cdot\beta_{\mathbb{P}}(\mathbf{x}_i,\widetilde{\mathbf{y}}_i)\ell(f_{\boldsymbol{\theta}}(\mathbf{x}_i),\widetilde{\mathbf{y}}_i).\end{aligned}\tag{37}$$

Second, for the distribution discrepancy term (*i.e.*, $\sum_{k=1}^{K} \overline{q}_k^s \, disc(\mathbb{P}_k, \mathbb{P}_{\mathcal{S}_t})$ in Eq. (35)), we have

$$\begin{aligned}
&\sum_{k=1}^{K} \overline{q}_k^s \, disc(\mathbb{P}_k, \mathbb{P}_{\mathcal{S}_t}) \le \sum_{k=1}^{K} \overline{q}_k \, disc(\mathbb{P}_k, \mathbb{P}_{\mathcal{S}_t}) + \sum_{k=1}^{K} (\overline{q}_k - \overline{q}_k^s) \, disc(\mathbb{P}_k, \mathbb{P}_{\mathcal{S}_t}) \\
&\le \sum_{k=1}^{K} \overline{q}_k \, disc(\mathbb{P}_k, \mathbb{P}_{\mathcal{S}_t}) + \sum_{k=1}^{K} (\overline{q}_k^s - \overline{q}_k) \sup_{f_{\boldsymbol{\theta}} \in \mathcal{F}_\Theta} \left| \mathbb{E}_{\mathbb{P}_k}[\ell(f_{\boldsymbol{\theta}}(\mathbf{x}, \mathbf{y}))] - \mathbb{E}_{\mathbb{P}_{\mathcal{S}_t}}[\ell(f_{\boldsymbol{\theta}}(\mathbf{x}, \mathbf{y}))] \right| \\
&\le \sum_{k=1}^{K} \overline{q}_k \, disc(\mathbb{P}_k, \mathbb{P}_{\mathcal{S}_t}) + \sum_{k=1}^{K} (\overline{q}_k^s - \overline{q}_k) \left(\mathbb{E}_{\mathbb{P}_k} \left[\left| \sup_{f_{\boldsymbol{\theta}} \in \mathcal{F}_\Theta} \ell(f_{\boldsymbol{\theta}}(\mathbf{x}), \mathbf{y}) \right| \right] + \mathbb{E}_{\mathbb{P}_{\mathcal{S}_t}} \left[\left| \sup_{f_{\boldsymbol{\theta}} \in \mathcal{F}_\Theta} \ell(f_{\boldsymbol{\theta}}(\mathbf{x}), \mathbf{y}) \right| \right] \right) \\
&\le \sum_{k=1}^{K} \overline{q}_k \, disc(\mathbb{P}_k, \mathbb{P}_{\mathcal{S}_t}) + 2\overline{L} \|\mathbf{q}^s - \mathbf{q}\|_1 \\
&\le \sum_{k=1}^{K} \overline{q}_k \, disc(\mathbb{P}_k, \mathbb{P}_{\mathcal{S}_t}) + 4\overline{L} \|\mathbf{q} - \mathbf{p}_0\|_1 .
\end{aligned} \tag{38}$$

Moreover, the Rademacher complexity term in Eq. (35) can also be bounded as follows:

$$\begin{aligned}
\mathfrak{R}_{\mathbf{q}^s}(\beta_{\mathbb{P}} \circ \ell \circ \mathcal{F}_\Theta) &= \mathbb{E}_{\widetilde{\mathcal{S}} \sim \widetilde{\mathbb{P}}} \mathbb{E}_{\boldsymbol{\sigma}} \left[\sup_{f_{\boldsymbol{\theta}} \in \mathcal{F}_\Theta} \sum_i \sigma_i q_i \beta_{\mathbb{P}}(\mathbf{x}_i, \widetilde{\mathbf{y}}_i) \ell(f_{\boldsymbol{\theta}}(\mathbf{x}_i), \widetilde{\mathbf{y}}_i) \right] \\
&\quad + \mathbb{E}_{\widetilde{\mathcal{S}} \sim \widetilde{\mathbb{P}}} \mathbb{E}_{\boldsymbol{\sigma}} \left[\sup_{f_{\boldsymbol{\theta}} \in \mathcal{F}_\Theta} \sum_i \sigma_i (q_i^s - q_i) \beta_{\mathbb{P}}(\mathbf{x}_i, \widetilde{\mathbf{y}}_i) \ell(f_{\boldsymbol{\theta}}(\mathbf{x}_i), \widetilde{\mathbf{y}}_i) \right] \\
&= \mathfrak{R}_{\mathbf{q}}(\beta_{\mathbb{P}} \circ \ell \circ \mathcal{F}_\Theta) + \mathbb{E}_{\widetilde{\mathcal{S}}, \boldsymbol{\sigma}} \left[\sup_{f_{\boldsymbol{\theta}} \in \mathcal{F}_\Theta} \left| \sum_i \sigma_i (q_i^s - q_i) \beta_{\mathbb{P}}(\mathbf{x}_i, \widetilde{\mathbf{y}}_i) \ell(f_{\boldsymbol{\theta}}(\mathbf{x}_i), \widetilde{\mathbf{y}}_i) \right| \right] \\
&\le \mathfrak{R}_{\mathbf{q}}(\beta_{\mathbb{P}} \circ \ell \circ \mathcal{F}_\Theta) + \mathbb{E}_{\widetilde{\mathcal{S}}, \boldsymbol{\sigma}} \left[\sum_i |q_i^s - q_i| \cdot \sup_{f_{\boldsymbol{\theta}} \in \mathcal{F}_\Theta} |\sigma_i \beta_{\mathbb{P}}(\mathbf{x}_i, \widetilde{\mathbf{y}}_i) \ell(f_{\boldsymbol{\theta}}(\mathbf{x}_i), \widetilde{\mathbf{y}}_i)| \right] \\
&\le \mathfrak{R}_{\mathbf{q}}(\beta_{\mathbb{P}} \circ \ell \circ \mathcal{F}_\Theta) + \overline{\beta}\, \overline{L} \cdot \mathbb{E}_{\widetilde{\mathcal{S}}, \boldsymbol{\sigma}} \left[\sum_i |q_i^s - q_i| \right] \\
&\le \mathfrak{R}_{\mathbf{q}}(\beta_{\mathbb{P}} \circ \ell \circ \mathcal{F}_\Theta) + \overline{\beta} \cdot \overline{L} \|\mathbf{q}^s - \mathbf{q}\|_1 \\
&\le \mathfrak{R}_{\mathbf{q}}(\beta_{\mathbb{P}} \circ \ell \circ \mathcal{F}_\Theta) + 2\overline{\beta} \cdot \overline{L} \|\mathbf{q} - \mathbf{p}_0\|_1 .
\end{aligned} \tag{39}$$

Additionally, it remains to bound the term $\|\mathbf{q}^s\|_2$ in Eq. (35). By applying the triangle inequality, this term can be upper bounded as follows:

$$\|\mathbf{q}^s\|_2 \le \|\mathbf{q}^s - \mathbf{q}\|_2 + \|\mathbf{q}\|_2 \le 2\|\mathbf{q} - \mathbf{p}_0\|_2 + \|\mathbf{q}\|_2 \le 2\|\mathbf{q} - \mathbf{p}_0\|_1 + \|\mathbf{q}\|_2 . \tag{40}$$

By substituting Eqs. (36), (37), (38), (39), and (40) into Eq. (35), we obtain that, with probability at least $1 - \delta$, the following inequality holds:

$$\begin{aligned}
&\mathbb{E}_{\widetilde{\mathbb{D}}_t} \left[\beta_{\mathbb{D}_t}(\mathbf{x}, \widetilde{\mathbf{y}}) \ell(f_{\boldsymbol{\theta}}(\mathbf{x}), \widetilde{\mathbf{y}}) \right] \\
&\le \sum_{(\mathbf{x}_i, \widetilde{\mathbf{y}}_i) \in \widetilde{\mathcal{M}}_{1:t-1} \cup \widetilde{\mathcal{S}}_t} q_i \cdot \beta_{\mathbb{P}}(\mathbf{x}_i, \widetilde{\mathbf{y}}_i) \ell(f_{\boldsymbol{\theta}}(\mathbf{x}_i), \widetilde{\mathbf{y}}_i) + \sum_{k=1}^{K} \overline{q}_k \, disc(\mathbb{P}_k, \mathbb{P}_{\mathcal{S}_t}) + \mathcal{O}\left(\frac{1}{\sqrt{|\widetilde{\mathcal{S}}_t|}} \right) + 2\mathfrak{R}_{\mathbf{q}}(\beta_{\mathbb{P}} \circ \ell \circ \mathcal{F}_\Theta) \\
&\quad + \left(4\overline{\beta L} + 4\overline{L} + 2\overline{L} \sqrt{\frac{\log(4/\delta)}{2}} + 2\sqrt{2 \log \log_2(1/\Delta)} \right) \|\mathbf{q} - \mathbf{p}_0\|_1 \\
&\quad + \left(\overline{L} \sqrt{\frac{\log(4/\delta)}{2}} + \sqrt{2 \log \log_2(1/\Delta)} \right) \|\mathbf{q}\|_2 .
\end{aligned} \tag{41}$$

Analogous to the derivation in the proof of Theorem 3, the term $\sum_{k=1}^{K} \overline{q}_k \, disc(\mathbb{P}_k, \mathbb{P}_{\mathcal{S}_t})$ in Eq. (41) is bounded from above by $\sum_{k=1}^{K} \overline{q}_k \, \widehat{disc}(\widetilde{\mathbb{P}}_k, \widetilde{\mathbb{P}}_{\mathcal{S}_t}) + \mathcal{O}(1)$, and the Rademacher complexity term $\mathfrak{R}_{\mathbf{q}}(\beta_{\mathbb{P}} \circ \ell \circ \mathcal{F}_\Theta)$ is bounded by $\mathcal{O}(1)$. Finally, as in the proof in Section B.4, we have

$$
\begin{aligned}
&\mathbb{E}_{\mathbb{D}_{1:t}}[\ell(f_{\boldsymbol{\theta}}(\mathbf{x}),\mathbf{y})] \\
&\leq \sum_{(\mathbf{x}_i,\widetilde{\mathbf{y}}_i)\in\widetilde{\mathcal{M}}_{1:t-1}} \left(\tfrac{1-\alpha_t}{|\widetilde{\mathcal{M}}_{1:t-1}|}+\alpha_t q_i\right)\beta_{\mathbb{P}^{\mathcal{M}}_{1:t-1}}(\mathbf{x}_i,\widetilde{\mathbf{y}}_i)\ell(f_{\boldsymbol{\theta}}(\mathbf{x}_i),\widetilde{\mathbf{y}}_i)+\alpha_t\cdot\sum_{(\mathbf{x}_j,\widetilde{\mathbf{y}}_j)\in\widetilde{\mathcal{S}}_t} q_j\beta_{\mathbb{D}_t}(\mathbf{x}_j,\widetilde{\mathbf{y}}_j)\ell(f_{\boldsymbol{\theta}}(\mathbf{x}_j),\widetilde{\mathbf{y}}_j) \\
&+O(1)+C_1(\alpha_t,\delta,\Delta)\cdot\|\mathbf{q}-\mathbf{p}^0\|_1+C_2(\alpha_t,\delta,\Delta)\cdot\|\mathbf{q}\|_2 \\
&+\alpha_t\sum_{k=1}^{K}\overline{q}_k\widehat{disc}_{\mathcal{F}_\Theta}(\widetilde{\mathbb{P}}_k,\widetilde{\mathbb{P}}_{\mathcal{S}_t})+(1-\alpha_t)Gap(\mathbb{P}^{\mathcal{M}}_{1:t-1},\mathbb{D}_{1:t-1}),
\end{aligned}
\tag{42}
$$

where $C_1(\alpha_t,\delta,\Delta)$ and $C_2(\alpha_t,\delta,\Delta)$ are two constants, given by

$$
\begin{cases}
C_1(\alpha_t,\delta,\Delta)=\alpha_t\cdot\left(4\overline{\beta L}+4\overline{L}+2\overline{L}\sqrt{\frac{\log(4/\delta)}{2}}+2\sqrt{2\log\log_2(1/\Delta)}\right) \\
C_2(\alpha_t,\delta,\Delta)=\alpha_t\cdot\left(\overline{L}\sqrt{\frac{\log(4/\delta)}{2}}+\sqrt{2\log\log_2(1/\Delta)}\right)
\end{cases}.
\tag{43}
$$

Therefore, we complete the proof.

□

C Implementation Details

In this section, we present detailed supplementary information regarding the implementation of our CNLDD method.

C.1 Procedure for solving the problem in Eq. (16)

First, recall that the optimization problem in Eq. (16) is

$$
\min_{f_{\boldsymbol{\theta}}\in\mathcal{F}^{\mathrm{lin}}_{\Theta}}\left\{\frac{1}{n}\sum_{i=1}^{n}\beta_{1i}\ell(f_{\boldsymbol{\theta}}(\mathbf{x}_i),\widetilde{\mathbf{y}}_i)-\frac{1}{m}\sum_{j=1}^{m}\beta_{2j}\ell(f_{\boldsymbol{\theta}}(\mathbf{x}_j),\widetilde{\mathbf{y}}_j)\right\},
\tag{44}
$$

where $\boldsymbol{\theta}=[\boldsymbol{\theta}_1,\boldsymbol{\theta}_2,\cdots,\boldsymbol{\theta}_C]\in\Theta$ is the parameter matrix of size $d\times C$. Here, d and C are the dimension of the feature and the number of classes, respectively. The hypothesis $f_{\boldsymbol{\theta}}(\mathbf{x})$ is defined as $f_{\boldsymbol{\theta}}(\mathbf{x}){:=}\boldsymbol{\theta}^\top\mathbf{x}\in\mathbb{R}^C$, and the k-th output of $f_{\boldsymbol{\theta}}(\mathbf{x})$ is denoted as $f_{\boldsymbol{\theta}}(\mathbf{x})_k=\boldsymbol{\theta}_k^\top\mathbf{x}$. Since the cross-entropy loss is typically adopted in classification scenarios, we also use it as the loss function. To facilitate derivation, we denote $\sigma(\boldsymbol{\theta}^\top\mathbf{x})=[\sigma_1(\boldsymbol{\theta}^\top\mathbf{x}),\sigma_2(\boldsymbol{\theta}^\top\mathbf{x}),\cdots,\sigma_C(\boldsymbol{\theta}^\top\mathbf{x})]\in\Delta^C$ as the softmax function, of which the c-th element is given by

$$
\sigma_c(\boldsymbol{\theta}^\top\mathbf{x})=\frac{\exp(\boldsymbol{\theta}_c^\top\mathbf{x})}{\sum_{c'=1}^{C}\exp(\boldsymbol{\theta}_{c'}^\top\mathbf{x})}.
\tag{45}
$$

Then, the Cross-Entropy loss is defined as $\ell(f_{\boldsymbol{\theta}}(\mathbf{x}),\mathbf{e}_c){:=}-\log\sigma_c(\boldsymbol{\theta}^\top\mathbf{x})$. Based on the definitions above, the problem in Eq. (44) can be reformulated as

$$
\min_{\boldsymbol{\theta}\in\Theta} J(\boldsymbol{\theta}){:=}-\frac{1}{n}\sum_{i=1}^{n}\beta_{1i}\log\frac{\exp(\widetilde{\mathbf{y}}_i^\top\boldsymbol{\theta}^\top\mathbf{x}_i)}{\sum_{c'=1}^{C}\exp(\boldsymbol{\theta}_{c'}^\top\mathbf{x}_i)}+\frac{1}{m}\sum_{j=1}^{m}\beta_{2j}\log\frac{\exp(\widetilde{\mathbf{y}}_j^\top\boldsymbol{\theta}^\top\mathbf{x}_j)}{\sum_{c'=1}^{C}\exp(\boldsymbol{\theta}_{c'}^\top\mathbf{x}_j)}.
\tag{46}
$$

Since the Cross-Entropy loss is convex, the task is to solve a DC-Programming (difference of convex functions) problem in Eq. (46). Here, we solve this problem with the Concave-Convex Procedure (CCCP) proposed by Yuille et al. [16] to update $\boldsymbol{\theta}$, and it is widely adopted in the machine learning community [7]. Specifically, CCCP decomposes the nonconvex objective function $J(\boldsymbol{\theta})$ as the difference of two convex functions $J_1(\boldsymbol{\theta})=-\frac{1}{n}\sum_{i=1}^{n}\beta_{1i}\log\frac{\exp(\widetilde{\mathbf{y}}_i^\top\boldsymbol{\theta}^\top\mathbf{x}_i)}{\sum_{c'=1}^{C}\exp(\boldsymbol{\theta}_{c'}^\top\mathbf{x}_i)}$ and $J_2(\boldsymbol{\theta})=-\frac{1}{m}\sum_{j=1}^{m}\beta_{2j}\log\frac{\exp(\widetilde{\mathbf{y}}_j^\top\boldsymbol{\theta}^\top\mathbf{x}_j)}{\sum_{c'=1}^{C}\exp(\boldsymbol{\theta}_{c'}^\top\mathbf{x}_j)}$, namely $J(\boldsymbol{\theta})=J_1(\boldsymbol{\theta})-J_2(\boldsymbol{\theta})$, and then CCCP solves the original nonconvex optimization problem as a sequence of convex programming. In detail, we initialize $\boldsymbol{\theta}^{(0)}=\mathbf{O}$, and at the k-th iteration, $J_2(\boldsymbol{\theta})$ is replaced by its linearized approximation, namely,

$$
\begin{aligned}
\widetilde{J}_2(\boldsymbol{\theta}){:=}&J_2(\boldsymbol{\theta}^{(k)})+\langle\nabla J_2(\boldsymbol{\theta})\big|_{\boldsymbol{\theta}^{(k)}},\boldsymbol{\theta}-\boldsymbol{\theta}^{(k)}\rangle \\
=&J_2(\boldsymbol{\theta}^{(k)})+\langle\frac{1}{m}\sum_{j=1}^{m}\beta_{2j}\cdot\mathbf{x}_j(\sigma(\boldsymbol{\theta}^{(k)\top}\mathbf{x}_j)-\widetilde{\mathbf{y}}_j)^\top,\boldsymbol{\theta}-\boldsymbol{\theta}^{(k)}\rangle.
\end{aligned}
\tag{47}
$$

Subsequently, $\boldsymbol{\theta}^{(k+1)}$ is obtained by solving the convex subproblem, namely

$$
\boldsymbol{\theta}^{(k+1)}\in\arg\min_{\boldsymbol{\theta}\in\Theta}\widetilde{J}(\boldsymbol{\theta}){:=}J_1(\boldsymbol{\theta})-\widetilde{J}_2(\boldsymbol{\theta}).
\tag{48}
$$

We propose to employ Gradient Descent (GD) to solve this subproblem, where the gradient of $\widetilde{J}(\boldsymbol{\theta})$ w.r.t. $\boldsymbol{\theta}$ is given by

$$\nabla \widetilde{J}(\boldsymbol{\theta}) = \frac{1}{n}\sum_{i=1}^{n}\beta_{1i}\cdot \mathbf{x}_i(\sigma(\boldsymbol{\theta}^\top \mathbf{x}_i) - \widetilde{\mathbf{y}}_i)^\top - \frac{1}{m}\sum_{j=1}^{m}\beta_{2j}\cdot \mathbf{x}_j(\sigma(\boldsymbol{\theta}^{(k)\top}\mathbf{x}_j) - \widetilde{\mathbf{y}}_j)^\top. \tag{49}$$

Theoretical analyses suggest that CCCP process converges to a local minimum [9]. Therefore, it is guaranteed that the discrepancy term, namely the Term 5 in $\mathcal{L}_t(\boldsymbol{\theta}, \mathbf{q})$ (Eq. (17)), can be precisely calculated.

D Computational Complexity Analysis

In this section, we present a detailed analysis of the computational complexity for the proposed CNLDD method. At a given timestep t, the number of newly received examples (namely, $\widetilde{\mathcal{S}}_t$) is n_t, while the feature dimension of each example and the number of classes are d and C, respectively. In Algorithm 2, step 2 (*i.e.*, estimate the transition matrix for each example), step 6 (*i.e.*, estimate the distribution discrepancy for each cluster), and steps 10∼12 (*i.e.*, obtain the optimal parameters and weights) all require solving optimization problems iteratively by using gradient-based methods. For conciseness, we use a single notation I to denote the number of iterations required to solve each of these optimization problems. In the following, we analyze the computational complexity of each step in our CNLDD method, after which the overall complexity is presented. Specifically, the computational complexity of each step is as follows:

1) In step 2 of Algorithm 2, there are U disjoint subsets, and the examples in each subset share a transition matrix. Let $K_i < n_t$ denote the number of examples in the i-th subset. For 2-NN identification within the i-th subset, the computational complexity is $\mathcal{O}(d \cdot K_i \log K_i)$. Therefore, for the U subsets, the 2-NN identification requires $\mathcal{O}(d \cdot \sum_{i=1}^{U} K_i \log K_i) \le \mathcal{O}(d \cdot \sum_{i=1}^{U} K_i \log n_t) = \mathcal{O}(d \cdot n_t \log n_t)$ computations. Moreover, in each iteration, the computational complexity of calculating the expected quantities (namely, Eq. (3)) is $\mathcal{O}(C^2)$, which arises from the matrix-vector products between $\mathbf{T}$ and $\mathbf{p}$. Since 2-NN identification is only performed once, the computational complexity of Step 2 is $\mathcal{O}\left(dn_t \log(n_t/U) + UI \cdot C^2\right)$.
2) In step 3 of Algorithm 2, the calculation of the matrix-vector product between each pair of $\mathbf{T}(\mathbf{x})$ and $\widehat{\mathbf{p}}(Y|X=\mathbf{x})$ requires $\mathcal{O}(C^2)$ computations. Therefore, by considering all n_t training examples at timestep t, the computational complexity is $\mathcal{O}(n_t \cdot C^2)$.
3) In step 4 of Algorithm 2, $\mathcal{O}(KMd)$ computations are required to calculate the distances between data points and cluster centers. Therefore, the computational complexity of K-Means clustering is $\mathcal{O}(IMKd)$, where M denotes the size of memory buffer, and I is the total number of updates for cluster centers.
4) In steps 5∼7 of Algorithm 2, CCCP is employed to estimate each discrepancy $\widehat{disc}_{\mathcal{F}_{\Theta}^{\text{lin}}}(\widetilde{\mathbb{P}}_n, \widetilde{\mathbb{Q}}_m)$ (as shown in Section C). Therefore, the total number of gradient updates is $\mathcal{O}(KI^2)$. As shown in Eq. (49), the calculation of gradient requires $\mathcal{O}(C \times d)$ computations. Therefore, the computational complexity of steps 5∼7 in CNLDD is $\mathcal{O}(KI^2Cd)$.
5) In steps 8∼12 of Algorithm 2, updates of the parameter $\boldsymbol{\theta}$ and the weight $\mathbf{q}$ require $\mathcal{O}(dC)$ and $\mathcal{O}(n_t)$ computations, respectively (see Eq. (18)). Therefore, the computational complexity is $\mathcal{O}(I \max\{d \times C, n_t\})$.
6) In steps 13∼14 of Algorithm 2, we invoke Algorithm 1 twice according to our two-step buffer update strategy. In the first invocation (namely, step 13), the number of data points is n_t, and the procedure cover$(\widetilde{\mathcal{S}}_t, \rho \cdot |\widetilde{\mathcal{S}}_t|)$ selects ρn_t examples from $\widetilde{\mathcal{S}}_t$, which correspond to the covering centers. To implement this, we use a vector of size n_t to record the minimal distance of each example to the centers and select the example with the maximal minimal distance as the next covering center. This process requires $\mathcal{O}(n_t d)$ computations. Since we must identify ρn_t centers, the first invocation of Algorithm 1 requires $\mathcal{O}(n_t \times d \times \rho n_t)$ computations. Similarly, step 14 requires $\mathcal{O}((M + \rho n_t) \times d \times M)$ computations. Therefore, the computational complexity is $\mathcal{O}(n_t \times d \times \rho n_t + (M + \rho n_t) \times d \times M) = \mathcal{O}(\rho n_t^2 d + M^2 d + \rho n_t M d)$.

Therefore, by considering the computational complexity of each step in CNLDD, the overall complexity is given by $\mathcal{O}(dn_t \log n_t + n_t C^2 + IMKd + KI^2Cd + M^2d + n_t Md)$. Here, the typical range of the parameter I is $1 \le I \le 40$, and it is set to 20 in our implementation. Moreover, K is set to a small value in our experiments, such as 5 or 6. The size of memory buffer (namely, M) is not large in practice, and we set it to 1,000 or 2,000 in our experiments. Additionally, the number of examples at a specific timestep is generally in the magnitude of 1,000. The number of classes C is typically less than 100, and the feature dimension produced by the ResNet-18 [8] adopted in our paper is typically 512. Therefore, considering the ranges of these parameters, the overall complexity is generally acceptable.

E Runtime Analysis

In this section, we present detailed runtime analyses of the proposed CNLDD method. Furthermore, we compare CNLDD with other representative continual noisy label learning approaches in terms of the computational time incurred during memory update and model learning within a single timestep.

First, we provide the per-step runtime analysis of the proposed Algorithm 2 in Tab. 1. From Tab. 1, it can be observed that the majority of runtime is spent on the optimization of hypothesis $f_{\boldsymbol{\theta}}$, which involves iterative gradient-based updates of the network parameters. In contrast, the optimization of $\mathbf{q}$ only takes a small fraction of the overall runtime, indicating its relatively low computational cost. The estimation of the distribution discrepancy (steps 5–7) is extremely fast, mainly because we implement it through efficient tensor multiplication with `PyTorch`. Moreover, due to GPU-accelerated distance computations, the proposed two-step buffer update strategy (steps 13 and 14) exhibits high efficiency in practice.

Subsequently, we compare our CNLDD method with four representative continual noisy label learning methods, namely, ContinualCRUST, SPR, PuriDivER, and CNLL, in terms of computational cost incurred during memory update and model training. Specifically, the experimental results are shown in Tab. 2. It can be observed that the proposed two-step buffer update strategy in CNLDD achieves significantly less runtime when compared with other methods across all the datasets. Regarding the overall runtime, CNLDD remains within the same magnitude as other approaches, being slightly higher than CNLL and PuriDivER but substantially lower than SPR.

In summary, Tab. 1 and Tab. 2 show that although there are several optimization steps in the proposed CNLDD method at the first glance, its overall runtime remains within a practically acceptable range.

TABLE 1
Runtime (in seconds) of each step in Algorithm 2 (per timestep). Experiments are conducted on *PACS*, *Digits*, *Yearbook*, and *FMoW* datasets under the "inst. 40%" noise case.

Step	***PACS***	***Digits***	***Yearbook***	***FMoW***
step 2 ($\mathbf{T}(\mathbf{x})$ estimation)	3.77	6.19	2.12	15.60
step 3 (density calculation)	4.36	1.88	3.36	51.75
step 4 (clustering)	1.16	2.13	2.23	2.87
steps 5–7 (discrepancy estimation)	0.10	0.09	0.05	0.14
step 6 (single estimation)	0.02	0.02	0.01	0.02
steps 10–12 (optimization over $\boldsymbol{\theta}$)	43.98	20.15	40.54	263.65
steps 10–12 (optimization over $\mathbf{q}$)	6.24	4.54	6.07	55.42
step 13 (feature extraction)	0.29	0.10	0.78	7.22
step 13 (first update)	0.87	0.25	0.85	0.23
step 14 (second update)	0.79	0.21	0.91	0.27
overall runtime	**59.45**	**38.21**	**56.80**	**352.31**

TABLE 2
Runtime comparison (in seconds) of various continual noisy-label learning methods. The upper panel reports the time cost for memory buffer updates, while the lower panel presents the overall runtime in a single timestep under the "inst. 40%" noise case.

Method	***PACS***	***Digits***	***Yearbook***	***FMoW***
Runtime of buffer update				
ContinualCRUST	2.43	1.38	4.46	18.64
SPR	4.17	4.31	11.68	372.36
PuriDivER	2.62	3.59	8.20	80.46
CNLL	2.85	0.91	3.10	15.64
CNLDD (ours)	0.42	0.29	0.61	9.13
Overall runtime				
ContinualCRUST	45.75	37.28	56.18	316.69
SPR	123.56	47.87	61.76	987.88
PuriDivER	48.51	27.73	53.18	312.37
CNLL	44.74	23.77	39.88	212.67
CNLDD (ours)	59.45	38.21	56.80	352.31

References

[1] A. Agarwal and T. Zhang, "Minimax regret optimization for robust machine learning under distribution shift," in *Conference on Learning Theory*. PMLR, 2022, pp. 2704–2729.

[2] P. Awasthi, C. Cortes, and C. Mohri, "Theory and algorithm for batch distribution drift problems," in *International Conference on Artificial Intelligence and Statistics*, 2023, pp. 9826–9851.

[3] A. Blum and T. Mitchell, "Combining labeled and unlabeled data with co-training," in *Annual Conference on Computational Learning Theory*, 1998, pp. 92–100.

[4] J. Cheng, T. Liu, K. Ramamohanarao, and D. Tao, "Learning with bounded instance and label-dependent label noise," in *International Conference on Machine Learning*. PMLR, 2020, pp. 1789–1799.

[5] N. Golowich, A. Rakhlin, and O. Shamir, "Size-independent sample complexity of neural networks," in *Conference On Learning Theory*, 2018, pp. 297–299.

[6] C. Gong, Y. Ding, B. Han, G. Niu, J. Yang, J. You, D. Tao, and M. Sugiyama, "Class-wise denoising for robust learning under label noise," *IEEE Transactions on Pattern Analysis and Machine Intelligence*, vol. 45, no. 3, pp. 2835–2848, 2023.

[7] C. Gong, T. Liu, Y. Tang, J. Yang, J. Yang, and D. Tao, "A regularization approach for instance-based superset label learning," *IEEE Transactions on Cybernetics*, vol. 48, no. 3, pp. 967–978, 2017.

[8] K. He, X. Zhang, S. Ren, and J. Sun, "Deep residual learning for image recognition," in *IEEE Conference on Computer Vision and Pattern Recognition*, 2016, pp. 770–778.

[9] G. Lanckriet and B. K. Sriperumbudur, "On the convergence of the concave-convex procedure," in *Advances in Neural Information Processing Systems*, vol. 22, 2009.

[10] X. Li, T. Liu, B. Han, G. Niu, and M. Sugiyama, "Provably end-to-end label-noise learning without anchor points," in *International Conference on Machine Learning*. PMLR, 2021, pp. 6403–6413.

[11] Y. Liu, "Understanding instance-level label noise: Disparate impacts and treatments," in *International Conference on Machine Learning*. PMLR, 2021, pp. 6725–6735.

[12] A. Maurer, "A vector-contraction inequality for rademacher complexities," in *Algorithmic Learning Theory*, 2016, pp. 3–17.

[13] M. Mohri, A. Rostamizadeh, and A. Talwalkar, *Foundations of Machine Learning*. MIT press, 2018.

[14] C. Scott, G. Blanchard, and G. Handy, "Classification with asymmetric label noise: Consistency and maximal denoising," in *Conference on Learning Theory*. PMLR, 2013, pp. 489–511.

[15] H. Wei, H. Zhuang, R. Xie, L. Feng, G. Niu, B. An, and Y. Li, "Mitigating memorization of noisy labels by clipping the model prediction," in *International Conference on Machine Learning*. PMLR, 2023, pp. 36 868–36 886.

[16] A. L. Yuille and A. Rangarajan, "The concave-convex procedure," *Neural Computation*, vol. 15, no. 4, pp. 915–936, 2003.